IMMUNOSUPPRESSION AND NEUROTOXICITY: HOW IDO CONTRIBUTES TO PATHOGENESIS OF SIV INFECTION

by
Julia L. Drewes

A dissertation submitted to Johns Hopkins University in conformity with the requirements for the degree of Doctor of Philosophy

Baltimore, Maryland
March, 2014

ABSTRACT

In the thirty years since the discovery of human immunodeficiency virus (HIV) as the causative agent of acquired immune deficiency syndrome (AIDS), the world has witnessed one of the most triumphant advances in modern medicine: the transformation of HIV infection from being a death sentence to being a treatable, chronic condition with the advent of combination antiretroviral therapy (cART). However, as the HIV-infected population ages, the face of the epidemic continues to evolve. For example, HIV-infected individuals have an increased rate and earlier onset of a variety of medical complications, particularly in the central nervous system, compared to their peers. The neurological manifestations include neurocognitive impairments as well as neuropsychological disorders such as depression. Understanding the pathogenic mechanisms that persist with and without cART is a critical step towards improving the lives of the aging, HIV-infected population.

The kynurenine pathway of tryptophan catabolism has both immunosuppressive and neurotoxic potential and is therefore uniquely positioned to affect a wide range of comorbidities in HIV/SIV infection. In this dissertation, we examined whether this pathway was elevated to pathogenic levels in the periphery and in the central nervous system of SIV-infected pigtailed macaques, utilizing gas chromatography mass spectrometry for the analysis of pathway metabolites and transcriptional assays for the analysis of pathway enzymes. We found evidence for toxic elevations in kynurenine pathway metabolites in all tissues examined and identified specific kynurenine metabolites in the plasma and CSF as predictive biomarkers of disease in the periphery and in the brain. We also tested the efficacy of two drug therapies, a four-drug

combination antiretroviral therapy and the tetracycline derivative minocycline, on attenuation of kynurenine pathway activation in SIV-infected macaques. Results from these drug studies revealed that neither cART nor minocycline was able to normalize kynurenine pathway activation.

This dissertation provides insights into several unanswered questions regarding the kynurenine pathway during HIV/SIV infection. Additionally, our findings of kynurenine pathway metabolites as predictive biomarkers of disease may translate into useful prognostic indicators in patients.

Thesis advisor: M. Christine Zink, DVM, PhD

Thesis reader: David R. Graham, PhD

ACKNOWLEDGMENTS

As my time as a grad student at Hopkins comes to a close, I look back to when I was a bright-eyed first year, and I am amazed at the changes that have occurred. From my research experiences in undergrad at Stanford I knew pursuing a PhD would take perseverance, a desire to learn, and long hours. What I didn't know was how much I would come to depend on others for guidance and support. There truly is no comparison to a PhD in biological sciences. So much of what we learn is not in textbooks, but rather is passed down by mentors that surround us, from our PI's to technicians, post-docs, and fellow grad students. In my case, I was also lucky enough to have parents who had also been through the PhD process. I wanted to take this time to acknowledge those who have unequivocally made a difference both in my research and in my personal life during the PhD process.

I would first like to thank my thesis advisor, Chris Zink. Chris has unwavering support for her graduate students, and has always been a firm advocate for work/life balance, something that is too often forgotten in science. Her ability to take a complex subject and distill it down to the most salient points, and her artistic eye and perfectionism in creating figures, has greatly informed the way I write and present. Additionally, her background as a veterinarian has been instrumental in teaching me the privileges and responsibilities that go along with performing animal research. Most importantly, while guiding me along the main trajectory of my thesis, Chris has also allowed me to pursue my own research hypotheses, and in so doing has fostered my growth as a scientist.

I'd next like to thank David Graham, who has truly been a co-mentor to me along with Chris. His excitement for science is infectious, and his continual search for the next big thing is inspiring. Dave was also the one who convinced me to learn the intricacies of GCMS so that I could run samples myself, rather than merely shipping samples off to a foreign collaborator. Though I had my doubts, Dave was steadfast in his belief that I could do this, and that I would be good at it, and for that I am truly grateful. My experience with GCMS has also opened the door to several collaborations with outside labs, which will likely result in multiple coauthor publications.

Rounding out my thesis committee were Gene Shearer, Joel Blankson, and Joe Steiner. I had the privilege of writing a paper with Gene, and benefited from his encyclopedic knowledge of the literature and decades of experience in the field of immunology. As for Joel, he was always truly interested in how my experiments were going and how my papers were coming along, but also in how I was doing personally. He kept me motivated even when I couldn't bear to look at a rejected manuscript one more time. To Joe Steiner, I must thank for making science fun, engaging, and transparent. For two years Joe sponsored an orange seed collecting operation through the NeuroAIDS seminar in order to harvest neuroprotective compounds naturally. I will never again look at an orange the same way! Joe has also always been very open about sharing ideas and data, something that I hope to emulate.

I'd also like to thank the other faculty in the Retrovirus group, including Janice Clements, Joe Mankowski, Lucio Gama, Ken Witwer, and Kelly Pate. Their input at lab meetings as well as their open door policies have greatly enhanced my research experiences. I am also grateful to all of the Retrovirus faculty for instilling in me a

willingness to try new methods and techniques. The Retrovirus lab continues to have some of the most elegant and sensitive techniques available, thanks to the fearlessness of the faculty and their ongoing commitment to be a part of cutting edge science.

To my fellow grad students, both within the CMM program and within the Retrovirus laboratory, I owe a huge debt of gratitude. From helping each other get through the first year of classes, lab rotations, and orals, it would not have been the same without you all! The Retrovirus lab crew of Susan Trow, Angela Brice, Juliene Co, Steve Page, Shruthi Ravimohan, Luna Zaritsky, Jeanne Sisk, Katie Kelly Brennan, Sarah Beck, Lisa Mangus, Julia Russell, Josh Croteau, Claudia Avalos, and Ravi Tharakan have made these years not only endurable but actually enjoyable and downright fun.

I am most indebted to two former students in particular, Kelly Meulendyke and Greg Szeto. Kelly was a former graduate student of Chris's who stayed on as a post-doc in the Retrovirus lab. As a result, I have been privileged to have her mentorship throughout the entire PhD process. Kelly taught me to never take the shortcut – always do an experiment up to publication quality standards, and always include negative and positive controls because controls are the most important part of an experiment. Overall, she has been a constant steadying force in the lab and is my go-to person for brainstorming and troubleshooting.

Likewise, Greg has been an incredible mentor to me throughout these past six years. Greg was instrumental in the recent acceptance of our minocycline paper, for which he was a co-author. Despite our manuscript getting rejected from journals three times (although one was *Science*, so that doesn't really count), Greg kept a positive attitude and convinced me that our work was important and publication-worthy. Through

each round of reviews, during which I felt increasingly defensive and frustrated, he kept reminding me that the changes were for the better. I am so grateful now to not only Greg and the other coauthors on the manuscript for their thoughtful suggestions, but also to the numerous reviewers whose critiques made our final, accepted manuscript vastly superior to the initial drafts.

To the mass spec folks – David Colquhoun, Alexey Lyashkov, and Veronica Aquino of the Graham lab, and Francesca Notarangelo and Kyle Horning from Robby Schwarcz's group at UMD – I must also give heartfelt thanks. Francesca and Kyle trained me on the GCMS, while David, Alexey, and Veronica were instrumental in teaching me how to handle the day-to-day problems associated with mass spec and sample preparation. I must particularly thank David whose calmness in the face of instrument failure was always reassuring.

I must also thank a number of other members of the Retrovirus Laboratory for their direct assistance with experiments. Dr. Liao carried out the influenza experiments for the minocycline paper and also assisted with serotonin ELISAs for the CNS chapter of my dissertation. Erin Shirk, our resident expert in flow cytometry, patiently assisted with FACS experiments and helped transition our lab over from the basic 3-color system to state-of-the-art 12 color analyses, bringing new possibilities and dimensions to both my project and the projects of others. Brandon Bullock, the ultimate lab manager, kept things running smoothly in the P3 at all times. Chris Bartizal helped me with several of the less fun aspects of my thesis such as searching for polycons in the -80C freezers, but he managed to make even these mundane tasks enjoyable. Josh Croteau assisted with the *in vitro* macrophage experiments on tryptophan depletion. Kelly Meulendyke assisted

with the running and analysis of CSF metabolites on the GCMS. Ken Witwer, Lucio Gama, Kelly Meulendyke, Elizabeth Engle, Suzanne Queen, and Ceereena Ubaida Mohien were all instrumental in the development and execution of the Nanostring assays that became such a huge part of my thesis.

I would also like to thank the administrative staff who worked tirelessly behind the scenes to make sure the academic programs, departments, and labs ran smoothly: Colleen Graham and Leslie Lichter of the CMM program; and Cathy Rada, Woodland Pomeroy, Sharon Molander, Wendy Elza, Emma Ey, Zipporah Gilchrist, and Nancy Nath of MCP.

Finally, I would like to thank my family for their continued love and support. My parents are both PhD chemists, and while they have always instilled in me a love for science, they have also always encouraged me to follow my own path… even when it took me out to California and back. Sharing stories of the trials and tribulations of the PhD process is a new, shared bond that I am so grateful to have with them. To my sister, whom I have always looked up to, I thank for stretching boundaries and leading the way. Life isn't nearly as scary when someone else goes first. Lastly, I must thank my boyfriend, Mark, who has been a travel companion, a teammate, and a shoulder to cry on, but most of all is my most staunch supporter. Thank you, for all that you do for me, and all that you put up with. I could not have done this without you!

TABLE OF CONTENTS

LIST OF TABLES

LIST OF FIGURES

CHAPTER I.

Introduction

HIV infection in the cART era

Despite the ability of combination antiretroviral therapy (cART) to potently suppress viral loads in HIV-infected patients, there is evidence of ongoing residual viral replication and reactivation from latency in both peripheral (1, 2) and central (3) tissue compartments of patients on cART. While treatment intensification (i.e., adding a 4th or 5th drug) can further decrease the incidence of viral "blips", intensification does not completely ablate residual viremia (4). Suboptimal drug penetration in tissues such as the brain may also result in incomplete suppression of viral replication (5). Even in suppressed tissue sites, the inability of antiretrovirals to prevent production of early transcriptional products from integrated virus in long-lived reservoirs (e.g., macrophages and memory T cells) may contribute to lingering immune activation, apoptosis, and dysfunction. For example, patients on cART have small but persistent elevations in genes such as TRAIL (6-8), DR4 (8, 9), DR5 (6), Fas (6), FasL (6), caspase-3 (10), and IDO activity (11) in peripheral cells and tissues. Additionally, up to a quarter of patients (10 - 27%) are "immunologic nonresponders" who suppress viremia with cART but do not exhibit recovery of CD4+ T cell counts (12).

In the central nervous system (CNS), HIV-infected individuals may experience a host of neurocognitive and neuropsychological complications as a result of the early and sustained replication of virus in the brain. Although HIV/SIV does not directly infect neurons, the release of toxic viral proteins (e.g., Tat, gp120) and a host of inflammatory cytokines and neuromodulatory factors (e.g., IL-6, glutamate, quinolinic acid, reactive oxygen species) from glial cells perpetuates inflammation, reduces the synaptic-dendritic density of neurons, and eventually can cause neuronal loss (13, 14). The neurocognitive

manifestations of these changes range from asymptomatic neurocognitive impairment (ANI), in which patients have deficits in at least two cognitive domains but are not yet impacted in their day to day activities, to minor neurocognitive disorder (MND) in which daily life is noticeably impacted, to the severely debilitating HIV-associated dementia (HAD) (15). While the prevalence of HAD has been greatly diminished in the cART era, occurrence of ANI and MND have actually risen (13, 16, 17). HIV-infected patients also have a two-fold higher risk of developing depression (18), which is associated with a decreased adherence to cART, worsening of cognitive status, and faster progression to AIDS (19, 20).

With the inability of cART to normalize the immunological and neurological complications of HIV, and development of a vaccine and/or agents to purge latent virus still out of reach, efforts to improve the quality of life of the aging HIV-infected population in the short-term must focus on a better understanding of viral and immunological dynamics in peripheral and central tissue sites. These findings can then inform drug discovery in the identification of adjunct therapeutics for cART.

Indoleamine 2,3-dioxygenase: gatekeeper of the kynurenine pathway of tryptophan metabolism

One particular area of research with both peripheral and central implications during HIV infection is the kynurenine (KYN) pathway of tryptophan (TRP) metabolism. TRP is the most limiting of the essential amino acids, and most of it is bound by albumin in bodily fluids (~90%) or is incorporated into proteins. Of the remaining free TRP, the vast majority (99%) is catabolized down the KYN pathway, serving as an important

source of the cellular cofactor nicotinamide (NAD+) (21). Three enzymes act as gatekeepers of this pathway, performing the initial rate-limiting step of breaking the indole ring of TRP to form N-formyl-L-kynurenine: tryptophan 2,3-dioxygenase (TDO2), indoleamine 2,3-dioxygenase 1 (IDO1), and indoleamine 2,3-dioxygenase 2 (IDO2).

Despite performing identical reactions, the induction and regulation of these three enzymes are very different. TDO2 is constitutively expressed in the liver, is induced by glucocorticoids, and likely serves as the primary TRP catabolizing enzyme during homeostasis (22). In contrast, IDO1 is predominantly expressed in immune privileged sites such as the eye, testes, and placenta, but its expression is rapidly induced during inflammation in a myriad of cell types primarily by interferon (IFN) γ stimulation of the Jak/STAT pathway. To a lesser extent, IDO1 can be induced by IFNα, IFNβ, tumor necrosis factor (TNF) α, IL-6, viral proteins (Tat, Nef, and gp120), platelet-activating factor, and cellular interactions such as CD40/CD40L and B7/CTLA-4 (23-29). More recently, it was discovered that the cytokine transforming growth factor (TGF) β is critical in the maintenance of long-term IDO induction in tolerogenic dendritic cells (DCs) and regulatory T cells (Tregs) (30). This mechanism appears to involve activation of the noncanonical NFκB pathway following TGFβ-mediated phosphorylation of specific ITIMs on IDO1, resulting in tonic, stable upregulation of IDO1 and TGFβ gene expression in DCs and Tregs (31). IDO2 was only recently discovered, and an important role of IDO2 in biology has not yet been established. Thus, the predominant gate-keeper of the KYN pathway during viral infections such as HIV/SIV appears to be IDO1.

Neuro- and immunomodulatory functions of tryptophan and its metabolites

The effects of chronic upregulation of the KYN pathway are incredibly damaging in both the periphery and the CNS because TRP is a rare amino acid, only available in a limiting supply via food intake or breakdown of proteins. Aside from NAD+ production, TRP is also a precursor for the neurotransmitters serotonin and melatonin. Reductions in available free TRP may lead to reduced synthesis of serotonin, which is a risk factor for the development of depression (32, 33). HIV-infected patients have been documented to have decreased levels of serotonin in CSF (34) and brain tissue (35), and are twice as likely to develop depression compared to uninfected cohorts (18). Because TRP is also a building block for proteins, reducing extracellular TRP levels suppresses proliferation of actively dividing cells. This was first shown to be a protective mechanism against the proliferation of parasites such as *Toxoplasma gondii* (36), but has since been extended to expansion of T cells, in which low levels of TRP causes accumulation of uncharged TRP-tRNAs and activates the GCN2 stress kinase pathway (37).

In addition to the consequences of TRP depletion, increased turnover down the KYN pathway also leads to generation of higher-than-normal levels of KYN metabolites that have neurotoxic and immunosuppressive capabilities. In the brain, quinolinic acid (QUIN), 3-hydroxkynurenine (3HK), and 3-hydroxyanthranilic acid (3HANA) all have the potential to generate reactive oxygen species (38-40). QUIN exacerbates inflammation by promoting astrocyte production of several cytokines and chemokines, including IL-1β, CCL2 (MCP-1), IL-8, and CCL5 (RANTES), and also mediates upregulation of the HIV coreceptors CCR5 and CXCR4 on astrocytes (41). QUIN is also a well-established mediator of NMDA receptor excitotoxicity (42), causing phenotypic

cytoskeletal changes in striatal neurons exposed *in vitro* to sub-micromolar concentrations of QUIN (43, 44) and also inducing axon-sparing lesions in the brain upon direct injection of QUIN (45). Kynurenic acid (KYNA), on the other hand, can counteract QUIN's excitotoxicity via inhibition of not only NMDA receptor excitotoxicity but also via inhibition of the other ionotropic subtypes of glutamate receptors (46). However, excessive KYNA can also lead to learning deficits in mice due to a decrease in synaptic glutamate release and subsequent changes in glutamate-mediated dopamine signaling at the α7nAChR (47). Given the decreases in brain tissue dopamine levels during HIV/SIV infection, this additional activity of KYNA could exacerbate neurocognitive changes associated with dopamine dysregulation (48). Thus, the neurotoxic potential of KYN metabolites is thought to outweigh the protective benefits during HIV infection.

In addition to neuromodulatory effects, KYN metabolites also have several important functions in the immune system. Landmark studies showing that induction of the KYN pathway is critical for the maintenance of tolerance in the context of pregnancy (49), transplant immunology (50), and tumor immune evasion (51) have led to the generalized theory that elevations in KYN metabolites as well as reductions in TRP levels are immunosuppressive. More specifically, metabolites in this pathway can inhibit proliferation in a TRP-independent manner (KYN, picolinic acid [PIC]) (52); can convert naïve T cells or proinflammatory Th17 cells into regulatory T cells (Tregs) following interactions at the aryl hydrocarbon receptor (KYN, 3HANA) (53, 54); can directly cause apoptosis of activated T cells (3HANA, cinnabarinic acid [which is dimerized 3HANA]) (55, 56); and can stimulate production of anti-inflammatory cytokines such as TGFβ from DCs, potentiating IDO induction (3HANA) (57). KYN's recently discovered activity as a

ligand of the cytosolic aryl hydrocarbon receptor (AHR) further helps to explain the potentiation of tolerogenic activity between DCs and Tregs (54, 58).

Project overview

The immunosuppressive and neurotoxic metabolites generated by the KYN pathway during HIV/SIV infection could be major contributors to HIV pathogenesis, even in the setting of cART. Several groups have proposed targeting the KYN pathway with inhibitors in order to restore immune balance in the periphery, relieve neurotoxic stress in the CNS, and improve overall patient outcomes. However, several key questions remain regarding KYN pathway activation during HIV/SIV infection. First, it is currently unknown whether the levels of KYN metabolites in plasma and CSF during HIV/SIV infection are representative of drainage from tissues or represent distinct compartments. Secondly, tissue levels of serotonin, TRP, and KYN pathway metabolites have never before been concurrently examined in the brain during HIV/SIV infection, so current generalizations in the field regarding a link between KYN pathway activation and risk of depression have been largely speculative. Thirdly, while CSF and plasma levels of KYN metabolites following cART have been reported by several groups, it is unknown whether these metabolites remain elevated in tissue sites following cART. Finally, while expression of the rate-limiting enzyme IDO1 has been repeatedly examined in the context of HIV/SIV infection, the expression levels of downstream enzymes of the KYN pathway have not been thoroughly examined, despite their potential utility as targets for adjunct therapies.

To explore these questions, we utilized the pigtailed macaque model of HIV infection, wherein animals are dually inoculated with an immunosuppressive swarm and a neurovirulent clone and consistently develop symptoms of AIDS and SIV-associated neurological disease by three months post inoculation (59). Given that there is still no alternative animal model system for the study of HIV infection that recapitulates all the major features of pathogenesis, the macaque model has been invaluable in elucidating mechanisms of pathogenesis and has also been a boon in the testing of novel neuroprotective therapies such as minocycline (60-62). Additionally, treating these animals with a 4-drug cART regimen has been shown to recapitulate the dynamics of virus suppression and CD4+ T cell recovery seen in patients on cART (63).

In Chapter II of this thesis, we describe the longitudinal kinetics of the KYN pathway metabolites as well as TRP and serotonin in the CSF and striatum of SIV-infected pigtailed macaques. In order to accomplish this, we developed a multiple reaction monitoring (MRM) gas chromatography mass spectrometry (GCMS) method with our collaborators Francesca Notarangelo and Robert Schwarcz at the University of Maryland Psychiatric Research Center to measure levels of TRP and its metabolites in a variety of tissue specimens. We found that the KYN pathway was induced in a biphasic manner in both CSF and brain. Although we could not rule out the potential for intrathecal production of metabolites, we found that terminal CSF QUIN and KYN/TRP ratios positively correlated with levels in corresponding brain tissue, suggesting that CSF measures can approximate brain IDO activation. KYN/TRP and QUIN/TRP ratios were also early predictive markers of the development of encephalitis, with both KYN/TRP and QUIN/TRP ratios significantly distinguishing between animals that would develop

encephalitis and those that would not as early as day 28 p.i. We also confirmed in matched brain tissue that induction of the IDO pathway occurs concurrently with serotonin loss in striatum. Finally, we observed that while a non-CNS-penetrant 4-drug cART regimen is efficacious at suppressing active viral replication in the brain, the KYN metabolic pathway remains elevated above uninfected controls. Sustained elevations in neurotoxic KYN metabolites could provide a mechanism for the ongoing neurocognitive and neuropsychiatric complications of HIV infection.

In Chapter III, we show that KYN pathway induction in the spleens of SIV-infected animals was also biphasic, although in contrast to the brain where chronic induction of metabolites was higher than during the acute phase, in the spleen we saw the opposite. Plasma levels mirrored the dynamics occurring in the spleen. Additionally, we show that the acute peak in *IDO1* expression in the spleen was rapidly downregulated despite continued elevations in IFNγ. In fact, the rapid up- and downregulation of *IDO1* expression more closely mimicked trends in type I IFN responses. We hypothesize that this may be a result of induction of suppressor of cytokine signaling (SOCS) proteins that can downregulate both IDO1 and type I IFN at the transcriptional and post-transcriptional level. Thus, although type II IFN (i.e., IFNγ) has consistently been shown to be the most robust inducer of IDO1, the downregulation of IDO1 appears to be more tightly linked to type I IFN responses. Interestingly, in both the spleen and brain, we found that only upstream enzymes in the KYN pathway were transcriptionally upregulated during infection, suggesting that they might be better pharmacologic targets than downstream enzymes.

Finally, in Chapter IV, we examine the potential for minocycline to act as an adjunct therapy in HIV/SIV infection. We focused on the potential for minocycline to antagonize plasmacytoid DC (pDC) responses because pDCs have been shown to be key regulators of type I IFN responses, IDO induction, and maintenance of Tregs, which are responsible for maintaining immune tolerance. We found that while minocycline potently suppressed IFN and IDO responses in pDCs and PBMCs *in vitro*, minocycline did not alter IFN or IDO responses in *in vivo* SIV-infected spleens. However, we did find that minocycline suppressed activation-induced cell death responses, demonstrated via suppression of CD25, Fas, and caspase-3 expression. These data suggest that minocycline may still be of use in attenuating the pervasive activation-induced apoptosis in the context of HIV infection, even if the *in vivo* doses are not sufficient to alter IDO responses.

CHAPTER II.

Extensive analysis of serotonin, tryptophan, and the kynurenine pathway in the CNS of SIV-infected pigtailed macaques and the effect of cART treatment

Abstract

Kynurenine pathway activation may contribute to HIV-associated neurological disorders. However, changes in serotonin and kynurenine metabolites in brain tissue have been understudied, particularly in the context of combination antiretroviral therapy (cART). In this study, tryptophan, serotonin, kynurenine, 3-hydroxykynurenine, and quinolinic acid were measured in longitudinal CSF from SIV-infected macaques and striatum from macaques with or without cART. Additionally, kynurenine pathway enzyme mRNA levels were measured in striatum from macaques throughout infection. We found that kynurenine metabolites increased significantly in both CSF and striatum during acute and chronic infection. Tryptophan decreased significantly in CSF while serotonin decreased significantly in brain. CSF kynurenine and quinolinic acid were early predictors of encephalitis. Transcriptionally, only upstream kynurenine pathway enzymes *IDO1*, *KMO*, and *KYNU* were significantly upregulated during acute or chronic infection. Elevations in striatal kynurenine metabolites during chronic infection correlated with *IFNβ*, *MxA*, and SIV *Gag* RNA, as well as protein measures of MHC class II, CD68, and APP. Finally, a non-CNS penetrating cART regimen restored CSF but not striatal levels of kynurenine metabolites to control levels. Overall these data show that activation of the kynurenine pathway in the CNS is biphasic and only partially resolved with non-CNS penetrant cART. Additionally, we identified CSF kynurenine and quinolinic acid as predictive biomarkers of CNS disease.

Introduction

Neurocognitive and neuropsychiatric disorders can be caused by or exacerbated by HIV infection and can impact the quality of life of HIV-infected patients, even in those who have suppressed virus with combination anti-retroviral therapy (cART). While occurrence of the most severe neurological complication, HIV-associated dementia, has been significantly reduced in the cART era to 2 – 7% of HIV-infected individuals (64, 65), the lifetime prevalence of "milder" neurological disorders persists: roughly 1/3 of HIV-infected individuals experience major depression or depressive symptoms (19, 20, 64, 66), and 28 – 52% develop mild motor/cognitive deficits despite the availability of cART (20, 64, 65, 67). Furthermore, HIV-associated depression is associated with an increased risk of developing neurological disease (20), and the greater the severity of depression, the greater the decline in cognitive function (19), suggesting that the two mechanisms may be linked. The insidious impact of these "mild" versions of neurological disorders is evident in the negative effect on cART adherence rates and a faster progression to AIDS (68, 69) and earlier mortality (68). Understanding the driving forces behind the neurocognitive and neuropsychiatric complications of HIV infection and finding therapeutics to combat these two axes of HIV neuropathogenesis could improve the quality of life of the aging HIV-infected population.

Results from a meta-analysis of studies on depression and HIV suggest that HIV-infected individuals are nearly twice as likely to develop depression as compared to uninfected individuals (18). While the etiology of depression or major depressive disorder even outside the context of HIV infection is complex, one of the prevailing theories is that there is a deficiency in the synaptic levels of the monoamines serotonin,

dopamine, and/or norepinephrine. However, only 30% of depressed patients respond to therapies targeting these pathways (32). Furthermore, experimental acute depletion of monoamines such as serotonin worsens mood in patients with a previous history of depression but does not affect healthy controls (33). Thus, while acute depletion of serotonin and other monoamines does not cause depression *per se*, at the very least such depletion is a risk factor in susceptible individuals. As a result, alterations in levels of serotonin during the course of a variety of syndromes, including HIV infection, may have significant psychiatric health implications.

In HIV, researchers have documented losses as great as 50% of serotonin in serum and plasma from patients who had progressed to AIDS (70, 71). In asymptomatic patients in earlier stages of HIV infection, serotonin deficits in CSF and/or plasma have also been reported (34), although the deficits were not typically as severe as those seen in AIDS patients (70). Stressful life events and reduced social support networks are well-documented phenomena seen in HIV infected cohorts that may contribute to the development of depression (69). However, there is also a direct molecular explanation for reduced serotonin levels in HIV infection and therefore an increased risk of developing depression: depletion of serotonin's amino acid precursor, tryptophan (TRP) (70, 72-74), due to induction of the kynurenine (KYN) pathway of TRP catabolism (72, 73). Indoleamine 2,3-dioxygenase (IDO1) is the rate-limiting enzyme of this pathway, controlling the initial breakdown of TRP into L-formylkynurenine. IDO1 is induced by interferon (IFN) γ and to a lesser extent by IFNα, IFNβ, tumor necrosis factor (TNF) α, CD40-CD40L interactions, platelet-activating factor, and viral proteins Tat, Nef, and gp120 (23-28). Many of these factors likely act in concert to induce the high levels of

IDO1 found in brain tissue during HIV/SIV infection and may provide a mechanism for the development of depression in patients (75, 76).

In addition to having a role in depletion of serotonin levels leading to depression susceptibility, activation of the KYN pathway is also implicated in neurocognitive deficits in HIV infection. The downstream KYN pathway metabolite quinolinic acid (QUIN) in particular has long been associated with NMDA receptor excitotoxicity (42). Heyes and Markey were the first to establish that QUIN is elevated in the CSF of HIV infected individuals (77) and that levels of QUIN in the CSF correlate with the severity of HAND (78). Since that time, other KYN pathway metabolites have also been shown to have neuromodulatory potential in the brain. For example, 3HK, 3HANA, and QUIN can all generate reactive oxygen species (ROS) (38-40), although paradoxically they also have some ability to scavenge ROS (79). Kynurenic acid (KYNA), a neuroprotective metabolite of the kynurenine pathway generated primarily in astrocytes, is also an antioxidant (80, 81). More importantly, KYNA ameliorates glutamate excitotoxicity by interfering with glutamate release via α7nAChR as well as by antagonizing all three ionotropic glutamate receptors (NMDA, kainate, and AMPA receptors) (46). However, KYNA's blockade of glutamate release also results in reductions in glutamate-mediated dopamine release (47), potentially exacerbating the dopamine dysfunction that is well established in HIV/SIV infection (48). Cumulatively, the neurotoxic potential of KYN metabolites is thought to outweigh any protective effects in HIV infection.

Thus, the two axes of the IDO pathway, 1) a reduction in serotonin and its precursor TRP and 2) an increase in neurotoxic KYN metabolites, converge to form a double hit on neuropsychiatric function and motor/cognitive function in HIV infection.

Despite the cumulative knowledge gained over the years on the impacts of HIV and SIV on serotonin/TRP metabolism, no comprehensive study has looked at all of the various components longitudinally in actual brain tissue. In particular, there is a dearth of knowledge on changes in tissue serotonin. Additionally, while several groups have examined changes in KYN/TRP metabolism in plasma and CSF following cART therapy (82, 83), no reports as of yet have documented the effects of cART on these pathways in brain tissue, despite calls for testing of specific IDO pathway inhibitors for the treatment of HAND.

To contribute knowledge to this area, we analyzed the levels of 5 pertinent molecules in the serotonin/KYN pathways (serotonin, TRP, KYN, 3HK, and QUIN) and the expression of 9 serotonin/KYN pathway genes (*TPH1*, *TPH2*, *IDO1*, *IDO2*, *TDO2*, *KMO*, *KYNU*, *HAAO*, and *QPRT*) in longitudinally sampled striatal brain from SIV-infected pigtailed macaques as well as macaques treated with cART. The striatal region was chosen because it is a hot spot for viral replication (84), demonstrates pronounced neuropathological changes during HIV/SIV infection (85), and is highly susceptible to both QUIN-mediated excitotoxicity (45, 86-88) and 3HK-mediated oxidative stress (39). In addition to striatum, we also measured the serotonin/KYN pathway metabolites in CSF to directly compare changes in the CSF to changes in brain tissue. We hypothesized that changes in serotonin and KYN metabolites in CSF would be reflective of changes occurring in brain tissue, and that a cART regimen not capable of effectively crossing the blood-brain barrier would allow for ongoing immune activation and lingering elevation of KYN pathway metabolites in the CNS.

Results

CSF QUIN and KYN/TRP ratios are early predictors of encephalitis

Levels of QUIN in CSF have been shown to correlate with the severity of HIV-associated neurocognitive disorders (HAND) in HIV-infected individuals as well as with the severity of encephalitis in SIV-infected macaques (78, 89). However, it is unclear whether QUIN or other TRP metabolites are *predictive* markers that could be used to identify patients at risk of developing neurological disease prior to the onset of actual clinical symptoms. To answer this question, we examined the levels of serotonin, TRP, KYN, 3HK, QUIN, and KYN/TRP ratios in longitudinally sampled, archived CSF samples from eight SIV-infected pigtailed macaques with known encephalitis outcomes at euthanasia.

Animals that went on to develop moderate to severe encephalitis displayed a much wider range of variability in CSF serotonin levels compared to animals that developed no or mild encephalitis, but there were no statistically significant differences in serotonin levels between the two groups as measured by two-way ANOVA (Fig. 1A). Furthermore, CSF serotonin levels amongst all animals, regardless of encephalitis scores, were not statistically different at any timepoint during infection as compared to pre-infection values.

In contrast, TRP levels were significantly decreased in CSF at all timepoints between days 7 and 42 p.i. (Fig. 1B; $p = 0.008$ for days 7, 10, and 14 p.i.; $p = 0.016$ for days 21 and 28 p.i.; $p = 0.039$ for day 42 p.i.). Terminally (55-T), TRP was no longer significantly below pre-infection values because the animals with no or mild encephalitis recovered back to pre-infection levels even though TRP levels in moderate to severe

animals remained low. In general, the more severe animals consistently had lower levels of TRP in CSF than none/mild animals, but none of these differences were significant.

KYN showed a biphasic induction pattern in the CSF, with significant elevations at both day 7 p.i. and terminally (55-T) in infected animals (Fig. 1C; $p = 0.016$, $p = 0.039$, respectively). The induction chronically was primarily due to the moderate/severe encephalitic animals, which had significantly more CSF KYN than animals with no or mild encephalitis from day 28 p.i. onwards (Fig. 1C; $p < 0.050$ for day 28 p.i. none/mild versus moderate/severe animals; $p < 0.001$ for day 42 p.i.; $p < 0.001$ for 55-T). The animals that developed no or mild encephalitis had completely normalized levels of KYN during chronic infection (day 35 p.i. onwards), timepoints at which encephalitis begins to develop in this model.

3HK spiked acutely at day 7 p.i. (Fig. 1D; $p = 0.039$) and returned to baseline by day 14 p.i. 3HK then stayed at low levels throughout chronic infection in all eight animals. The more severe encephalitic animals tended to have slightly higher levels of 3HK in the CSF chronically, but these differences were not statistically significant.

QUIN was significantly elevated in the CSF of all animals at all timepoints post-infection compared to pre-infection values (Fig. 1E; $p = 0.008$ for all timepoints). Animals that developed moderate or severe encephalitis had even higher values of CSF QUIN at day 42 p.i. and terminally (55-T) compared to animals that did not develop severe encephalitis (Fig. 1E; $p < 0.010$ and $p < 0.0001$, respectively).

Finally, KYN/TRP ratios, which are a well-established representation of IDO enzyme activity and typically are more sensitive than KYN or TRP alone, were also upregulated at all timepoints post-infection in the CSF of infected animals (Fig. 1F; $p =$

0.008, $p = 0.016$, $p = 0.008$, $p = 0.039$, $p = 0.023$, $p = 0.023$, and $p = 0.039$ for the longitudinal timepoints). Importantly, KYN/TRP ratios significantly distinguished between none/mild and moderate/severe encephalitic animals as early as day 28 p.i., when KYN/TRP returned to baseline in the none/milds but resurged in the moderate/severe animals (Fig. 1F; $p < 0.001$ for none/milds versus moderate/severes at day 28 p.i., $p < 0.001$ at day 42 p.i., $p < 0.0001$ terminally).

Although metabolites downstream of KYN are not typically normalized to TRP levels and are not a direct measure of an enzyme's activity, we found that normalizing QUIN to TRP increased QUIN's diagnostic potential as QUIN/TRP ratios significantly differentiated between animals with none or mild encephalitis versus animals with moderate to severe encephalitis as early as day 28 p.i. (graph not shown; $p < 0.01$ by two-way ANOVA for day 28 p.i. none/mild vs. moderate/severe.; $p < 0.0001$ for day 42 p.i. and terminally none/mild vs. moderate/severe). These data suggest that KYN/TRP and QUIN/TRP ratios in the CSF are sensitive, early predictors of which animals will go on to develop encephalitis.

Serotonin decreases while KYN metabolites increase in brain tissue during SIV infection

We next wanted to determine whether our findings in CSF were representative of what was occurring in brain tissue during infection. To this end, striatal samples were taken from perfused, frozen brain tissue from animals euthanized at various points throughout infection and analyzed for TRP and TRP metabolites. While we had not found changes in CSF serotonin (Fig. 1A), we did find that striatal serotonin was significantly decreased at both acute (day 14) and terminal (T) timepoints (Fig. 2A; $p < 0.010$ and $p <$

0.050, respectively). Conversely, whereas we had seen profound reductions in CSF TRP, we did not find evidence for TRP loss in striatal tissue (Fig. 2B).

KYN metabolites in striatum behaved similarly to their CSF counterparts, with KYN, 3HK, QUIN, and KYN/TRP ratios significantly induced in a biphasic manner at both acute (day 7, 10, and/or 14 p.i.) and chronic stages of infection (day 35, 42, 56, and/or terminally) (Fig. 2C-F; see Supp. Table 3 for specific *p*-values). Likewise, when segregated according to encephalitis severity, the animals with more severe encephalitis consistently had higher levels of KYN, 3HK, QUIN, and KYN/TRP ratios in striatum compared to animals with less severe encephalitis, as was seen in the CSF.

These data suggest that CSF levels of KYN metabolites reflect changes occurring in striatal brain tissue, while CSF levels of serotonin and TRP may not be directly comparable to striatal tissue levels. However, the CSF draws were taken longitudinally in eight animals while striatal samples were collected from a much larger cohort of animals euthanized at various points throughout infection. To truly understand the relationship between CSF levels and brain tissue levels, we next compared the terminal CSF draws from the eight animals shown in Figure 1 to their corresponding terminal striatal levels from Figure 2.

Terminal CSF QUIN and KYN/TRP ratios, but not serotonin, TRP, KYN, or 3HK, correlate with concentrations in matched terminal brain

The matched terminal CSF and brain concentrations of TRP and its metabolites in eight SIV-infected macaques are shown in Figure 3. Prior to infection, the baseline levels of serotonin, TRP, KYN, 3HK, and QUIN were all higher in striatum than in CSF (see

Supp. Fig. 1 for CSF μM values prior to infection, and Figure 2 for striatal μM values in uninfected animals). Terminally, this trend remained for serotonin, TRP, KYN, and 3HK, with those analytes remaining higher in striatum than CSF (Fig. 3A-D). However, QUIN and KYN/TRP ratios increased more in CSF than in striatum, with terminal levels in none/mild encephalitic animals being comparable between CSF and brain, and moderate/severe encephalitic animals actually having higher levels of QUIN and KYN/TRP ratios in the CSF as compared to brain (Fig. 3E, 3F). Terminal CSF QUIN and KYN/TRP ratios were also the only two markers that significantly correlated with their respective terminal brain values as determined by Spearman's rank correlation test (QUIN: r = 0.833, $p = 0.015$; KYN/TRP ratio: r = 0.738, $p = 0.046$). These data suggest that the best CSF markers of concurrent brain IDO pathway activation are KYN/TRP ratios and QUIN.

mRNA expression of upstream KYN pathway enzymes IDO1, KMO, and KYNU increases during SIV infection

The KYN/TRP ratio is a well-established marker for indoleamine 2,3-dioxygenase (IDO) activity. We hypothesized that the increase in IDO activity, as measured by KYN/TRP ratios in striatum of our SIV-infected pigtailed macaques, was at least partially due to an increase in *IDO1* mRNA expression because IDO1 is highly regulated at the transcriptional level by cytokines such as interferon (IFN) gamma, IFN beta, and tumor necrosis factor (TNF) alpha that are upregulated in the brain during SIV infection (76, 90). We hypothesized that other KYN pathway enzymes would also be transcriptionally upregulated during infection. To test this, mRNA was isolated from

striatal sections adjacent to the samples from which metabolites were analyzed, and the transcript levels of 7 KYN pathway genes (*IDO1*, *IDO2*, *TDO2*, *KMO*, *KYNU*, *HAAO*, *QPRT*) and the tryptophan hydroxlase enzymes *TPH1* and *TPH2* that convert TRP to serotonin were measured.

Expression of *IDO1*, the KYN pathway enzyme responsible for the first and rate-limiting step involving the oxidation of TRP to L-formyl-kynurenine, was significantly upregulated at both acute (day 4 p.i.) and chronic (day 56 p.i. and terminal) timepoints in striatum (Fig. 4A; $p < 0.01$, $p < 0.01$, and $p < 0.001$, respectively). The majority of expression values for *indoleamine 2,3-dioxygenase 2* (*IDO2*) and *tryptophan dioxygenase* (*TDO2*) at all timepoints throughout infection were below the threshold for quantitation and were excluded from further analysis (data not shown). *TPH1* and *TPH2* expression levels in striatum were similarly low and were subsequently confirmed by qRT-PCR to be unchanged in uninfected animals versus terminally infected animals (data not shown). These data suggest that *IDO1* is the primary dioxygenase in the striatum responsible for conversion of KYN to TRP, and that the loss of serotonin in terminal striatum as reported in Figure 2 is not due to a deficiency in transcriptional expression of the rate-limiting enzymes of serotonin synthesis, *TPH1* and *TPH2*.

Expression of *kynurenine 3-monooxygenase* (*KMO*), which converts KYN to 3HK, was significantly upregulated terminally (Fig. 4B; $p < 0.05$). Expression of *kynureninase* (*KYNU*), which converts KYN to anthranilic acid and 3HK to 3-hydroxy athranilic acid (3HANA), was also significantly upregulated chronically (day 56 p.i. and terminally) (Fig. 4C; $p < 0.05$ and $p < 0.001$, respectively). However, *3-hydroxyanthranilate 3,4-dioxygenase* (*HAAO*) and *quinolinate phosphoribosyltransferase*

(*QPRT*), which mediate downstream events leading to conversion of 3HANA to QUIN and finally breakdown of QUIN into NAD+, were both unchanged during infection (Fig. 4D, 4E).

Overall, the mRNA expression data suggest that the upstream KYN pathway genes *IDO1*, *KMO*, and *KYNU* are highly regulated at the transcriptional level during SIV infection, while downstream enzymes such as *HAAO* and *QPRT* are maintained at a static level. This is further supported by evidence that animals that had moderate to severe encephalitis tended to have higher expression of *IDO1*, *KMO*, and *KYNU* mRNA than animals with no or mild encephalitis, while the expression of downstream enzymes *HAAO* and *QPRT* did not segregate by severity of encephalitis (Fig. 4A-E).

Striatal KYN pathway metabolites correlate with markers of neuropathogenesis in chronically infected animals

Encephalitis scoring in our model is a semi-quantitative measure of inflammation as determined by the presence of perivascular macrophage-rich cuffs, multi-nucleated giant cells, and gliosis (59). Given the strong associations between encephalitis severity and levels of CSF metabolites, brain metabolites, and brain KYN pathway enzyme expression, we hypothesized that striatal KYN metabolites would correlate with more quantitative measures of inflammation in chronically infected animals (day 35 p.i. onwards).

IDO1 transcriptional activity is known to be upregulated by both type I and type II interferons as well as several other cytokines. Given the upregulation of *IFNβ* and the interferon-stimulated gene *MxA* in the CNS of infected macaques (90), we first compared

the expression of these two interferon-related genes versus KYN/TRP ratios in striatum. KYN/TRP ratios significantly correlated with both *IFNβ* (Fig. 5A; r = 0.492, $p = 0.006$) and *MxA* (Fig. 5B; r = 0.882, $p < 0.0001$).

While many cell types in the brain can upregulate *IDO1* in response to IFN treatment and thus can initiate the KYN pathway of TRP metabolism, only macrophages and microglia are thought to express the full cohort of enzymes required for conversion of TRP to QUIN (91). Because of the critical role of these two cell types in the KYN pathway, we next wanted to determine whether generation of QUIN correlated with markers of macrophage/microglial activation. We found that levels of QUIN in striatum significantly correlated with both MHC class II (Fig. 5C; r = 0.493, $p = 0.027$) and CD68 protein expression (Fig. 5D; r = 0.774, $p < 0.001$) as determined by immunohistochemistry in subcortical white matter adjacent to striatum.

QUIN levels in striatum also significantly correlated with SIV *Gag* RNA in striatum (Fig. 5E; r = 0.903, $p < 0.0001$). The relationship between QUIN and viral load was biphasic, with viral loads less than 10^6 copy equivalents corresponding to small changes in QUIN, while viral loads above 10^6 led to a much sharper increase in QUIN production. Notably, a significant correlation between QUIN and SIV remained even when only viral loads < 10^6 were examined (statistic not shown on graph; r = 0.638, $p = 0.003$).

Finally, since QUIN and other KYN pathway metabolites are known to be neurotoxic, we also compared QUIN to corpus callosum levels of amyloid precursor protein (APP), a measure of neuron axonal damage and predictor of motor deficits in SIV infection (59). Despite the small sample size, QUIN significantly correlated with changes

in APP (Fig. 5F; r = 0.782, $p = 0.011$). Thus overall, KYN pathway metabolites correlated with inflammatory cytokine responses, macrophage/microglial activation, viral load, and neuronal damage.

cART reduces, but does not completely normalize, KYN pathway activation in striatum

The strong correlative relationship between KYN pathway activation and severity of neurological disorders, and the persistence of these disorders in the HIV-infected population despite the use of cART, has led to calls for the testing of specific IDO pathway inhibitors such as 1-methyl tryptophan for the prevention and treatment of these ailments. cART has certainly reduced the severity of these diseases, but *IDO1* mRNA (92) and CSF and plasma levels of KYN metabolites have consistently been shown to be incompletely resolved by cART in patients and in animal models of HIV infection (11, 83). However, to the best of our knowledge, levels of KYN metabolites in brain tissue following cART treatment have not been previously demonstrated. To determine whether lingering markers of immune activation in the CSF such as KYN/TRP ratios are truly reflective of ongoing activation in brain tissue, we examined the levels of TRP and its metabolites in the striatum of animals whose viral loads had been suppressed for 100 days with a 4-drug, predominantly non-CNS penetrating cART regimen consisting of 2 protease inhibitors (saquinavir and atazanavir), an integrase inhibitor (L-870812), and a nucleotide reverse transcriptase inhibitor (PMPA) (Fig. 6A-F). In this model, cART-treated animals have no detectable viral RNA (a measure of active viral replication) in striatum at euthanasia, but integrated viral DNA is still present (92).

We previously showed that serotonin levels were significantly decreased in terminally infected striatal tissue samples compared to uninfected controls (Fig. 2A). cART did not significantly raise striatal serotonin levels compared to terminally infected animals (Fig. 6A, $p = 0.552$), although serotonin levels in cART-treated animals were no longer significantly below uninfected animals ($p = 0.096$). cART also did not have a significant effect on TRP levels in striatum (Fig. 6B, $p = 0.921$); however, TRP levels in striatum were never significantly below controls at any timepoint during infection in infected, untreated animals (Fig. 2B).

Although upstream KYN metabolites in striatum showed a downward trend with cART treatment, levels of KYN (Fig. 6C, $p = 0.111$), 3HK (Fig. 6D, $p = 0.135$), and the KYN/TRP ratio (Fig. 6F, $p = 0.072$) in striatum were not significantly different in cART treated animals compared to infected, untreated macaques. Additionally, all three markers were still significantly higher in cART treated animals compared to uninfected controls (KYN, $p = 0.0007$; 3HK, $p = 0.028$; KYN/TRP ratio, $p = 0.0007$). The only metabolite that cART significantly downregulated was QUIN (Fig. 6E, $p = 0.004$, SIVT vs. cART). However, even QUIN remained significantly elevated above uninfected controls ($p = 0.003$, Uninf vs. cART). Thus, KYN pathway metabolites in cART-treated animals most closely mimic the trends seen in infected, untreated animals with no or mild encephalitis (Fig. 2), who consistently had metabolite levels that were above uninfected control levels but were not as high as the levels found in moderately or severely encephalitic animals.

Discussion

Key findings from our study are that 1) CSF KYN/TRP and QUIN/TRP ratios are sensitive, early predictive markers of inflammation in the brain during infection, 2) KYN pathway activation in the brain is biphasic and is followed by serotonin loss in the brain at both acute and chronic timepoints, and 3) cART does not fully restore KYN pathway activation in the brain to control levels despite viral suppression. These results suggest that the KYN pathway of TRP metabolism may indeed be contributing to ongoing neurocognitive and neuropsychiatric disorders seen in HIV-infected individuals despite successful viral suppression with cART.

The utility of QUIN as not just a biomarker for encephalitis but also as an early predictor of encephalitis before the onset of overt pathology extends upon the previous findings of Heyes and Markey, who established the associations between increasing QUIN levels with increasing inflammation and worsening of cognitive status in the brain and CSF during HIV/SIV infection (77, 78, 93). In the CSF of our animals, QUIN predicted which animals would go on to develop moderate to severe encephalitis by day 42 p.i., but the KYN/TRP ratio significantly distinguished this even earlier at day 28 p.i.. Given the robustness of QUIN alone, we hypothesized that an analogous QUIN/TRP ratio would be of diagnostic use in a similar manner to the KYN/TRP ratio, and indeed the QUIN/TRP ratio discriminated between the two encephalitis groups by day 28 p.i. as well. These data make the QUIN/TRP and KYN/TRP ratios in the CSF among the most powerful diagnostic predictors of encephalitis development in our model, with MCP-1 being the only other marker that we have found that can predict future encephalitis development this early (94).

Furthermore, while the brain levels of all KYN pathway metabolites (KYN, 3HK, QUIN, and KYN/TRP ratios) in virtually every SIV infected animal were elevated above the median of uninfected controls during infection, QUIN was the only metabolite that was consistently elevated in the CSF of all animals, including those that developed no or mild encephalitis. This provides impetus for the study of QUIN as a biomarker for not only distinguishing between mild and severe forms of encephalitis, but also for making the subtle - but important - distinction between mild and no encephalitis. As most HIV-infected patients in the cART era are unlikely to have severe CNS disease as a result of the efficacy of cART, biomarkers that can distinguish between milder forms of disease will become increasingly relevant.

In both striatum and CSF of our animals, QUIN values above 1 μM were associated with more severe neurological disease and more severe inflammation as determined by pathology examination as well as more quantitative measures such as IFN responses (*IFNβ1*, *MxA* mRNA expression), macrophage/microglial activation (MHC II, CD68 protein expression), viral load, and neuronal damage (APP protein). These QUIN values are similar to those reported by Heyes and Markey (89). The concentrations of QUIN in striatum at terminal timepoints in the animals with no or mild encephalitis (median = 410 nM) and in the cART treated animals (median = 277 nM) are not in the upper μM or mM range necessary to induce acute toxicity to neurons (44). However, chronic exposure of striatal neurons to low levels of QUIN in the 100 nM – 350 nM range can cause cytoskeletal changes indicative of NMDA excitotoxicity (43, 44). While levels of brain QUIN in our model are derived from perfused tissue, given the similarly high levels of QUIN in CSF, it is highly likely that in foci of viral replication or

macrophage/microglial activation neurons would be exposed to chronic levels of QUIN well above this range of 100 nM - 350 nM needed for excitotoxic changes. The importance of even small increases of QUIN in the striatal region is further substantiated by the fact that the forebrain region (which includes the striatum) is more susceptible to QUIN-mediated NMDA receptor excitotoxicity than other brain regions such as the cerebellum (86), likely because of increased expression of the QUIN-responsive NR2B subunit of NMDA receptors in the forebrain (87). Thus even the relatively small elevations in QUIN in the cART treated animals compared to uninfected controls could contribute to ongoing neuropathogenesis.

In addition to elevations in KYN metabolites in the brain, we also found that upstream enzymes in the KYN pathway, *IDO1*, *KMO*, and *KYNU*, were transcriptionally upregulated during infection in striatum. The local increase in expression of these enzymes in concert with increased levels of the metabolites themselves strongly suggests that the striatum is an active site of KYN metabolite production, rather than merely a site of accumulation of KYN metabolites from plasma or from other sources in the brain.

In the serotonin arm of TRP catabolism, we found that serotonin was significantly decreased at both acute (day 14 p.i.) and terminal timepoints in the striatum, but did not find any reduction in expression of the tryptophan hydroxylases *TPH1* and *TPH2*. These data suggest that the lack of serotonin in brain is more likely a result of shunting of TRP down the KYN pathway via IDO activity rather than a deficiency in the activity of serotonin-synthesizing enzymes.

To our knowledge, only one other report has been published on serotonin levels in brain tissue during HIV or SIV infection. In that report, post-mortem serotonin levels in

the caudate nucleus were found to be significantly reduced in patients who had progressed to AIDS as compared to healthy controls (35). However, that study was confounded by the presence of secondary infections (cytomegalovirus, toxoplasmosis, and progressive multiple leukoencephalopathy) in nearly 1/3 of the subjects and a post-mortem delay of 0.5-5 days which could have affected measurement of this extremely labile analyte. Other evidence of serotonergic dysfunction in the setting of HIV infection comes from an imaging study in which HIV-infected patients had lower levels of serotonin transporter (5HTT) binding potential, which the authors suggested might be indicative of overt serotonergic loss (95). While such imaging studies are certainly valuable, they nonetheless are indirect measurements of serotonin levels.

Our pigtailed macaque model is a carefully controlled, consistent model of HIV infection that is devoid of confounding factors seen in patients that could influence serotonin levels or cause depression, including secondary opportunistic infections, drug use, socioeconomic status, and dietary intake of tryptophan (82). Thus, our finding that serotonin was significantly decreased in perfused striatum of SIV-infected macaques at both acute and terminal timepoints provides strong evidence that serotonin stores are depleted in brain tissue as a result of SIV/HIV infection and not due to confounding factors. Importantly, the fact that serotonin levels during acute infection recovered by day 21 p.i., as well as the fact that cART treated animals did not have significantly lower levels of serotonin terminally compared to uninfected controls, suggests that the loss in serotonin is at least partially reversible.

Our finding that TRP was not significantly downregulated in brain tissue at any stage of SIV infection does not necessarily negate the hypothesis that serotonin loss is

due to a decrease in the pool of available TRP in the brain. Because our measurements were all performed on perfused brain tissue, we were essentially measuring intracellular levels of TRP and TRP metabolites. The extent of intracellular TRP depletion compared to extracellular depletion could be drastically different. An exact measurement of TRP in the extracellular milieu would have to be done using microdialysis. As a surrogate, drainage into the CSF may approximate the sum total of extracellular fluid draining from the brain, and in our macaques TRP was depleted in CSF at virtually every timepoint throughout infection. Similar findings have been reported in a mouse model of inflammation-driven depression, where peripheral injection of LPS resulted in decreased plasma levels of TRP, an increase in KYN both peripherally and in the brain, and an increase in serotonin turnover in the brain, but no loss of TRP in the brain (96). That study, in conjunction with our findings, perhaps indicates that during periods of low TRP availability stemming from immune activation, the cells within the brain 1) prioritize TRP for KYN generation rather than serotonin synthesis, and 2) maintain their intracellular TRP levels at all costs, depleting extracellular stores of TRP levels as represented by reduced TRP drainage into the CSF.

In addition to the risk of serotonin depletion as a result of KYN pathway activation, the neurotoxic potential of the metabolites in this pathway have been well described, from the generation of ROS to NMDA excitoxicity (46). While some metabolites also have neuroprotective abilities, such as KYNA's antagonism of NMDA excitotoxicity, long-term exposure of even KYNA can result in neuronal dysfunction as seen in learning deficits and reductions in extracellular glutamate and dopamine in mice upon exposure to KYNA (97, 98). Thus overall the KYN pathway is thought to be

neurotoxic or at least neuromodulatory in the long-term. Two hypotheses have been proposed as to why the brain would shunt TRP down the KYN pathway during inflammation, risking serotonin loss and neuronal dysfunction. The first is that a reduction in extracellular TRP via IDO induction is an evolutionary adaptation of the immune system to prevent replication of invading bacteria, although this theory has been more firmly established in peripheral organs (99). The second theory is that the generation of NAD+ at the end of the KYN pathway is cytoprotective in the context of neuroinflammation and also provides a source of energy for cells (100). While a shift from serotonin synthesis to KYN/NAD+ synthesis during the acute phase response of a viral or bacterial infection may be neuroprotective initially, chronic induction of KYN pathway metabolites and chronic depletion of TRP appears to counteract any protective effects .

These supposed neuroprotective aspects of KYN pathway activation during neuroinflammation may become more important as the development of KYN pathway inhibitors progresses. However, in the meantime the main focus should be to develop therapeutics that can fully restore metabolites in the brain during HIV/SIV infection to control levels. We found that, despite cART treatment suppressing active viral replication in the brain to undetectable levels, all of the KYN metabolites (KYN, 3HK, QUIN, and KYN/TRP ratios) remained significantly elevated above uninfected controls. While there was a decreasing trend in all the metabolite levels with cART treatment, QUIN was the only metabolite that was significantly changed by cART therapy.

Importantly, the 4-drug cART regimen that we used was primarily non-CNS penetrating. If CSF levels of these metabolites remain elevated above controls as well,

this would provide a mechanism by which patients on cART therapy could be monitored for risk of developing neurological impairments prior to the development of fulminant symptoms. Such patients could be switched to CNS-penetrant therapies or could be given adjunct immunotherapies that target the IDO pathway such as 1-methyl tryptophan. Additionally, because the current clinical guidelines do not recommend initiating cART until a patient's CD4+ T cell count is below 350, QUIN or QUIN/TRP levels in the CSF might also be of use in identifying patients who should be administered cART earlier to prevent or slow neurological changes. Overall, our findings support the continued study of serotonin, QUIN, and other KYN pathway metabolites as biomarkers of HIV associated neuropsychiatric and neurocognitive disorders, and our findings in cART treated macaques suggest the need for targeted inhibition of the IDO pathway during HIV/SIV infection to prevent chronic, low-level exposure of neurons to neurotoxic and neuromodulatory metabolites in the context of viral suppression.

Materials & Methods

Animal studies

Archived samples from 84 juvenile pigtailed macaques (Macaca nemestrina) were studied. Of the 84 animals, 10 were uninfected controls and 74 were inoculated intravenously with SIV/DeltaB670 and SIV/17E-Fr, as previously described (59). Sixty-nine of the SIV-infected macaques received no drug treatment. Beginning at day 12 p.i., 5 of the SIV-infected macaques received combination antiretroviral therapy (cART) which suppressed plasma viremia to <100 SIV RNA copy eq./mL by day 70 p.i. (63). The 4-drug cART regimen consisted of 270 mg/kg of the protease inhibitor atazanavir (Bristol-Myers Squibb), 10 mg/kg of the integrase inhibitor L-870812 (Merck), and 205 mg/kg of the protease inhibitor saquinavir (Roche) administered orally twice/day; as well as 30 mg/kg of the nucleotide reverse transcriptase inhibitor PMPA (Gilead) administered subcutaneously once daily. The 5 cART-treated animals were euthanized 161-175 days p.i. after approximately 100 days of plasma viremia suppression. Infected, untreated macaques were euthanized during various stages of disease (4, 7, 10, 14, 21, 35, 42, 56, and 84 days p.i.). Some animals were euthanized prior to their planned euthanasia date due to presentation of clinical symptoms that met euthanasia criteria as described previously (101). These animals are grouped with 84-day animals as SIV terminal (T or SIVT in figures). All animals had longitudinal CSF draws performed at the following timepoints: at least 3 pre-infection draws, then on days 7, 10, 14, 21, 28, and every two weeks thereafter. CSF was centrifuged at 1300 rpm for 15 min to remove any cells before being frozen at -80°C. All animals were euthanized in accordance with federal guidelines and institutional policies. Macaques were perfused with sterile PBS while under deep

anesthesia, and tissues were collected and either frozen until use or fixed. All animal studies were approved by the Johns Hopkins Animal Care and Use Committee; all animals were humanely treated in accordance with federal guidelines and institutional policies.

Immunohistochemisry, histopathology, and encephalitis scoring

Immunohistochemical staining for MHC II and CD68 in subcortical white matter adjacent to striatum and APP in corpus callosum was quantitated as previously described (92, 102).

For encephalitis scoring, six regions of brain (basal ganglia, frontal cortex, thalamus, parietal cortex, cerebellum, midbrain) were stained with hematoxylin and eosin and examined by two pathologists, who scored the brain regions as none, mild, moderate, or severe based on the presence of perivascular macrophage-rich cuffs, multi-nucleated giant cells and gliosis, as previously described (59, 103).

Brain tissue homogenization

Three millimeter punches were taken from perfused striatum of snap-frozen pigtailed macaque brain tissue. Punches were weighed and diluted 1/20 weight/volume with cold 0.1% ascorbic acid, and sonicated 3 times at 30% amplitude for 3 sec on ice. Samples were processed in batches of 10 to minimize processing time. Residual debris was removed by centrifugation prior to extraction of metabolites.

Metabolite extraction from brain homogenates

On ice, 50 µL of basal ganglia homogenates (of the original 1/20 dilution or diluted further for a final of 1/2000 in 0.1% ascorbic acid) were spiked with 50 µL of a solution containing heavy standards at the following concentrations: [$^{2}H_5$] tryptophan (1 µM, CDN Isotopes, Quebec, Canada), [$^{2}H_6$] kynurenine (5 µM, custom synthesis from Sigma Aldrich Isotec), and [$^{2}H_3$] quinolinic acid (0.2 µM, custom synthesis from Synfine, Ontario, Canada). The following standards were also spiked in but not analyzed for the purposes of this manuscript: [$^{2}H_5$] DOPAC (2 µM), [$^{13}C_6$] dopamine (2 µM), [$^{2}H_5$] glutamate (1 µM), [$^{2}H_5$] glycine (1 µM), [$^{2}H_5$] homovanillic acid (2 µM), [$^{2}H_4$] serotonin (2 µM), and [$^{2}H_2$] tyrosine (1 µM) (all from CDN Isotopes, Quebec, Canada), and [$^{13}C_6$] anthranilic acid (1 µM, Sigma Aldrich). Fifty microliters of -20°C acetone was added to homogenates and samples were centrifuged at 20K *g* for 5 min to precipitate protein. Eighty percent (120/150 µL) of the acetone supernatant was transferred to a new microcentrifuge tube, to which 50 µL of a 2:5 ratio methanol:chloroform mixture was added. Samples were centrifuged at 20K g for 10 min, and 60% (80/134 µL) of the aqueous layer was transferred to a glass vial. The aqueous solution was dried and then derivatized with 120 µL of 2,2,3,3-pentafluoro-1-propanol (Sigma) and 135 µL of pentafluoropropionic anhydride (Sigma) by heating at 75°C for 30 min. Derivatized samples were dried and stored at -80°C.

Metabolite extraction from CSF

CSF was diluted 1/2 in 0.2% ascorbic acid or 1/100 in 0.1% ascorbic acid for metabolite and amino acid analysis, respectively. Fifty microliters of a heavy standard

mixture, identical to the one used in brain sample preparation, were added to CSF samples. Fifty microliters of -20°C acetone were added and samples were centrifuged at 20K g for 10 min to precipitate protein. Eighty percent (120/150 µL) of the acetone supernatant was transferred to a glass vial and dried. No methanol/chloroform extraction was performed on CSF. CSF samples were derivatized identically to brain samples.

GC/MS/MS analysis of metabolites

GC/MS/MS was performed as previously described (104). Briefly, dried samples were resuspended in 50 µL ethyl acetate and 1 µL was injected in pulsed, splitless mode into an Agilent 7890A GC coupled to a 7000 MS/MS equipped with a 7693A autosampler operated in electron capture negative ionization (ECNI) mode. For the CSF samples diluted 1/100, 2 µL were injected. Methane was used as the ECNI reagent gas, nitrogen as the collision gas, and helium as the carrier gas (all Airgas). The 30 m GC capillary column consisted of a 0.5 m precolumn connected to two adjoining 15 m columns, all HP-5ms with 0.25 mm ID x 0.25 µM film (Agilent). The inlet was held at 250°C, the oven temperature initially held at 60°C for 1 min, then ramped 13°C/min to 230°C, for a total run time of 14.08 min.

The multiple reaction monitoring (MRM) transitions used in this study were based off of transitions initially described by Eckstein *et al* (105) and have been subsequently optimized. The transitions (Q1, Q3), collision energies (CE), and retention times (RT) for the derivatized compounds were as follows: **TRP** Q1 = 608.2, Q3 = 270, CE = 5, RT = 13.1 min; **[$^{2}H_{5}$] TRP** Q1 = 613.2, Q3 = 351, CE = 20, RT = 13.1 min; **TYR** Q1 = 585.2, Q3 = 268, CE = 20, RT = 10.9 min; **[$^{2}H_{2}$] TYR** Q1 = 587.2, Q3 =

436.9, CE = 20, RT = 10.9; **KYN** Q1 = 612, Q3 = 442, CE = 10, RT = 13.0 min; **[^{2}H$_6$] KYN** Q1 = 618, Q3 = 447, CE = 10, RT = 13.0 min; **QUIN** Q1 = 431.0, Q3 = 298.0, CE = 10V, RT = 9.4 min; **[^{2}H$_3$] QUIN** Q1 = 434.0, Q3 = 301.0, CE = 10V, RT = 9.4 min; **3HK** Q1 = 630, Q3 = 219, CE = 15, RT = 12.9 min.

Data were analyzed with Agilent MassHunter software, Build B.04. Samples were injected in a randomized order to minimize experimental bias. Each sample was injected at least twice. The average of the peak areas from replicate injections were normalized to the average of the heavy standards for each respective compound. 3HK was the only compound for which we did not have a matching heavy standard; thus we normalized 3HK to [^{2}H$_6$] KYN because of their similar ionization properties. These values were fit to the matrix-spiked light standard curves for each compound based on the standard addition method.

Serotonin ELISA

Due to its highly labile nature, serotonin was measured by ELISA (Eagle Biosciences) in brain homogenates in 0.1% ascorbic acid or in longitudinal CSF samples from pigtailed macaques, including 3 pre-infection CSF draws that were averaged to constitute the 0 dpi timepoint. CSF samples were diluted 1/2 in 0.2% ascorbic acid before being assayed according to the manufacturer's instructions. Samples were read on a microplate reader (BioRad) at the recommended wavelength.

RNA extraction from macaque brain

Three or four millimeter punches weighing roughly 50 mg were taken from perfused striatum of snap-frozen macaque brain tissue, adjacent to the punch taken for GCMS. One mL of RNA STAT-60 (Isotex Diagnostics) was added and samples were homogenized in a Fast Prep Machine 1 x 6.0 for 20 sec. Two hundred µL of chloroform were added and samples were shaken and incubated at room temperature for 2-3 min. Samples were centrifuged at 18K *g* for 15 min at 4°C. Roughly 600 µL of the aqueous layer were transferred to a new tube, and 500 µL -20°C isopropanol was added. Samples were vortexed and incubated overnight at -20°C. RNA was pelleted by centrifugation at 18K *g* for 15 min at 4°C. Isopropanol was discarded and pellet was washed once with 1 mL -20°C 70% ethanol and centrifuged at 8K *g* for 5 min. Ethanol was poured off and the pellet was air-dried for 15-30 min at room temperature. The pellet was resuspended in 100 µL of RQ1 DNase solution (85 µL water, 10 µL RQ1 Buffer [Qiagen], 3 µL RNase Out [Invitrogen], 2 µL RQ1 DNase [Qiagen]) and incubated for 1 hr at 37°C. Samples were then additionally purified with a miRVana Kit (Invitrogen). RNA concentration was determined by NanoDrop (ThermoFisher) and subsequently diluted to 20 ng/µL for Nanostring nCounter gene expression analysis.

Nanostring nCounter gene expression analysis

Nanostring analysis allows for the highly sensitive and reproducible detection of mRNA transcripts without conversion to cDNA or enzymatic amplification (106). As part of a collaborative project analyzing multiple research questions, a codeset of 260 genes (including 11 putative housekeeping genes) was designed based on rhesus macaque

(*Macaca mulata*) and human sequences according to NanoString specifications. For the purposes of this manuscript, only genes involved in TRP metabolism and genes needed for housekeeping normalization were included in the analysis (9 genes of interest + 11 housekeeping genes = 20 genes). One hundred nanograms of each RNA sample were assayed using the custom Nanostring CodeSet according to the manufacturer's nCounter Gene Expression Assay Protocol. Samples were run in a randomized order to minimize experimental bias. Data was analyzed according to the Nanostring nCounter Expression Data Analysis Guide, with minor modifications. Any samples that were outside Nanostring's acceptable quality control range for binding density (0.05 – 2.25) or positive control normalization (0.3 – 3) were rerun. A value of "1" was added to each value to eliminate any "0" values which could interfere with downstream analysis. Data were then normalized by the geometric mean of six spiked positive controls within each well to correct for assay efficiency. Positive control normalization factors ranged between (0.5 – 1.6). Positive control corrected data were then subjected to housekeeping gene normalization. As no single housekeeping gene has been proven to be consistently expressed across different cell types, cell maturation states, tissue types, or disease models (107-111), we implemented the Kruskal-Wallis non-parametric analysis of variance (ANOVA) test and measured the coefficient of variance (cv) on all 11 putative housekeeping genes to find the three most stably expressed genes across the brain samples (107, 112). The geometric mean of these three genes (ACTB, GAPDH, and TBP) was used to normalize the positive control corrected data (111). Housekeeping normalization factors ranged from (0.7 – 3.8). Gene-specific background for each probe was assessed as the average + 2 SD of 3 MS2 phage RNA samples (Roche) which were

run at various points throughout the assay and should not have cross-hybridized with any of the probe sequences. These gene-specific background threshold levels are represented in the data graphs as the grey shaded areas. Trends in IDO1 mRNA expression in brain have been independently verified for subsets of the animals by qRT-PCR (data not shown). Note that while the Nanostring nCounter system counts the actual number of transcripts bound to each gene-specific probe in a given area, overall one cannot compare the expression level of one gene versus another due to the possibility of differences in probe binding efficiencies.

qRT-PCR

IFNβ, MxA, and SIV RNA for correlation studies were analyzed by qRT-PCR as previously described (90). Validation of TPH1 and TPH2 Nanostring expression data was accomplished by performing qRT-PCR with the following Taqman primer/probe assays designed against rhesus macaque (*Macaca mulatta*) sequences: TPH1: Rh02863703_m1 FAM; TPH2: Rh00998774_m1 FAM; GAPDH: Rh02621745_g1 VIC primer limited; ACTB: Rh03043379_gH VIC primer limited (all Life Technologies). qRT-PCR reagents other than the primer/probes were identical to those previously described (90). TPH assays were run on a BioRad CFX96 thermal cycler.

Statistics

For longitudinal CSF analytes, one of the severe animals was missing the day 21 p.i. and day 42 p.i. timepoints due to hemolysis of the CSF. The “last value carried forward” imputation for longitudinal data (113) was used to replace these missing values;

i.e., values from day 14 p.i. were used for the day 21 p.i. timepoint, and values from day 28 p.i. were used for the day 42 p.i. timepoint. For comparison of CSF from animals that developed mild encephalitis versus those that developed severe encephalitis, we performed a 2-way repeated measures ANOVA comparing CSF fold change values between the two groups of animals at each timepoint. In a second analysis the Wilcoxon signed rank test comparing values to a theoretical value of "1" was used to examine whether there were changes in CSF analytes post-infection versus pre-infection regardless of encephalitis status. All CSF statistics were performed on the fold change data.

For striatal metabolite levels in longitudinal samples the Kruskal-Wallis (non-parametric ANOVA) with Dunn's post-test was used to analyze changes throughout infection compared to uninfected controls. For striatal Nanostring nCounter mRNA expression data, the Benjamini-Hochberg false discovery rate (FDR) test was applied to Kruskal-Wallis *p*-values to correct for multiple comparisons based on the simultaneous analysis of 9 TRP/KYN pathway genes in this study. For any genes for which a significant Benjamini-Hochberg corrected *p*-value was obtained ($p < 0.05$), Dunn's post-test was performed comparing all time points to the values for uninfected controls.

For correlation studies a Spearman's rank correlation was used to compare metabolites with markers of inflammation and neuronal injury.

For cART metabolite data in striatum a Mann-Whitney test was performed to compare SIVT vs cART and Uninf vs cART.

Figure 1. KYN metabolites are induced biphasically in CSF and predict encephalitis outcomes. CSF from 8 animals, 3 with no or mild encephalitis at euthanasia (grey squares) and 5 with moderate or severe encephalitis at euthanasia (black circles), were followed longitudinally. Serotonin (**A**) was measured by ELISA, while tryptophan (TRP) (**B**), kynurenine (KYN) (**C**), 3-hydroxykynurenine (3HK) (**D**), and quinolinic acid (QUIN) (**E**) were measured by GCMS. KYN/TRP ratios (**F**) represent IDO enzyme activity. Data are plotted as the median fold changes over the average of 2 or 3 pre-infection CSF draws from each animal. The dotted line represents the median of pre-infection values. "T" represents terminal infection. Error bars denote interquartile ranges. Asterisks (*) represent timepoints that were significantly different ($p < 0.05$) from pre-infection values. Crosses (†) represent timepoints that were significantly different ($p < 0.05$) between the two encephalitis groups. For exact *p*-values, see Supplementary Tables 1 and 2. All axes are linear with the exception of serotonin and QUIN, which are in $\log_2$ scale.

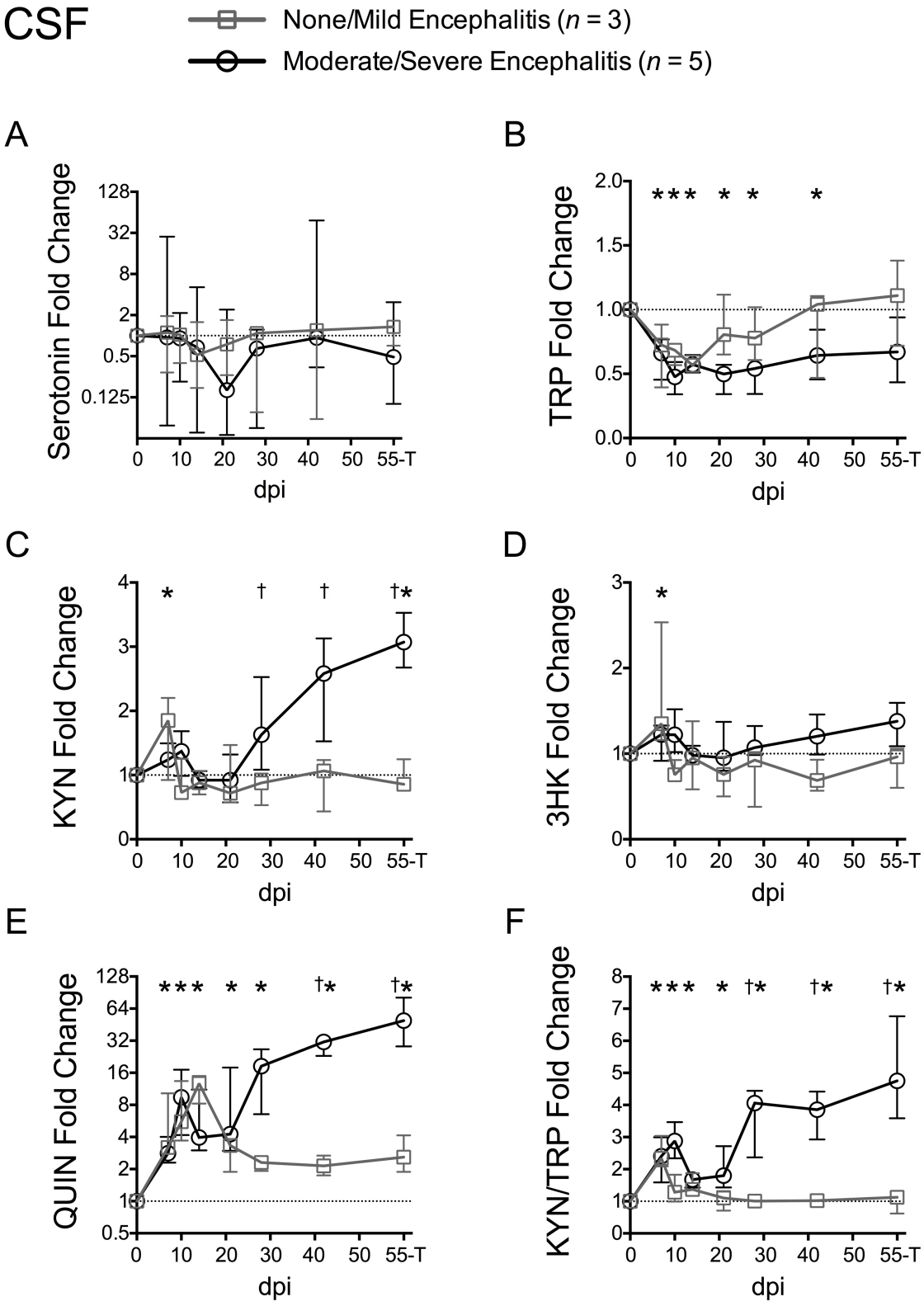
CSF
None/Mild Encephalitis (n = 3)
Moderate/Severe Encephalitis (n = 5)
A
Serotonin Fold Change
128
32
8
2
0.5
0.125
0 10 20 30 40 50 55-T
dpi
B
TRP Fold Change
2.0
1.5
1.0
0.5
0.0
***
*
*
*
0 10 20 30 40 50 55-T
dpi
C
KYN Fold Change
4
3
2
1
0
*
†
†
†*
0 10 20 30 40 50 55-T
dpi
D
3HK Fold Change
3
2
1
0
*
0 10 20 30 40 50 55-T
dpi
E
QUIN Fold Change
128
64
32
16
8
4
2
1
0.5
***
*
*
†*
†*
0 10 20 30 40 50 55-T
dpi
F
KYN/TRP Fold Change
8
7
6
5
4
3
2
1
0
***
*
†*
†*
†*
0 10 20 30 40 50 55-T
dpi

Figure 2. Serotonin decreases while KYN metabolites increase in the brain during SIV infection. Serotonin (**A**), TRP (**B**), KYN (**C**), 3HK (**D**), QUIN (**E**), and KYN/TRP ratios (**F**) were measured in striatum from 79 animals euthanized at various timepoints throughout infection (6 – 13 animals per timepoint). "Un" represents uninfected animals that were mock inoculated and euthanized approximately 84 days post mock inoculation. "T" represents SIV-infected animals that were euthanized due to terminal disease criteria or animals that reached the end of an 84-day study period. Animals are grouped according to their encephalitis scores at euthanasia (grey squares for none/mild encephalitis; black circles for moderate/severe encephalitis); medians and interquartile ranges are depicted for both encephalitis outcomes. The dotted line represents the median of uninfected animals. Asterisks (*) represent timepoints that were significantly different ($p < 0.05$) from uninfected controls by Kruskal-Wallis analysis, encompassing all animals at each timepoint regardless of encephalitis outcomes. For exact *p*-values, see Supplementary Table 3. TRP is shown in linear scale; all others are shown on a $\log_2$ scale.

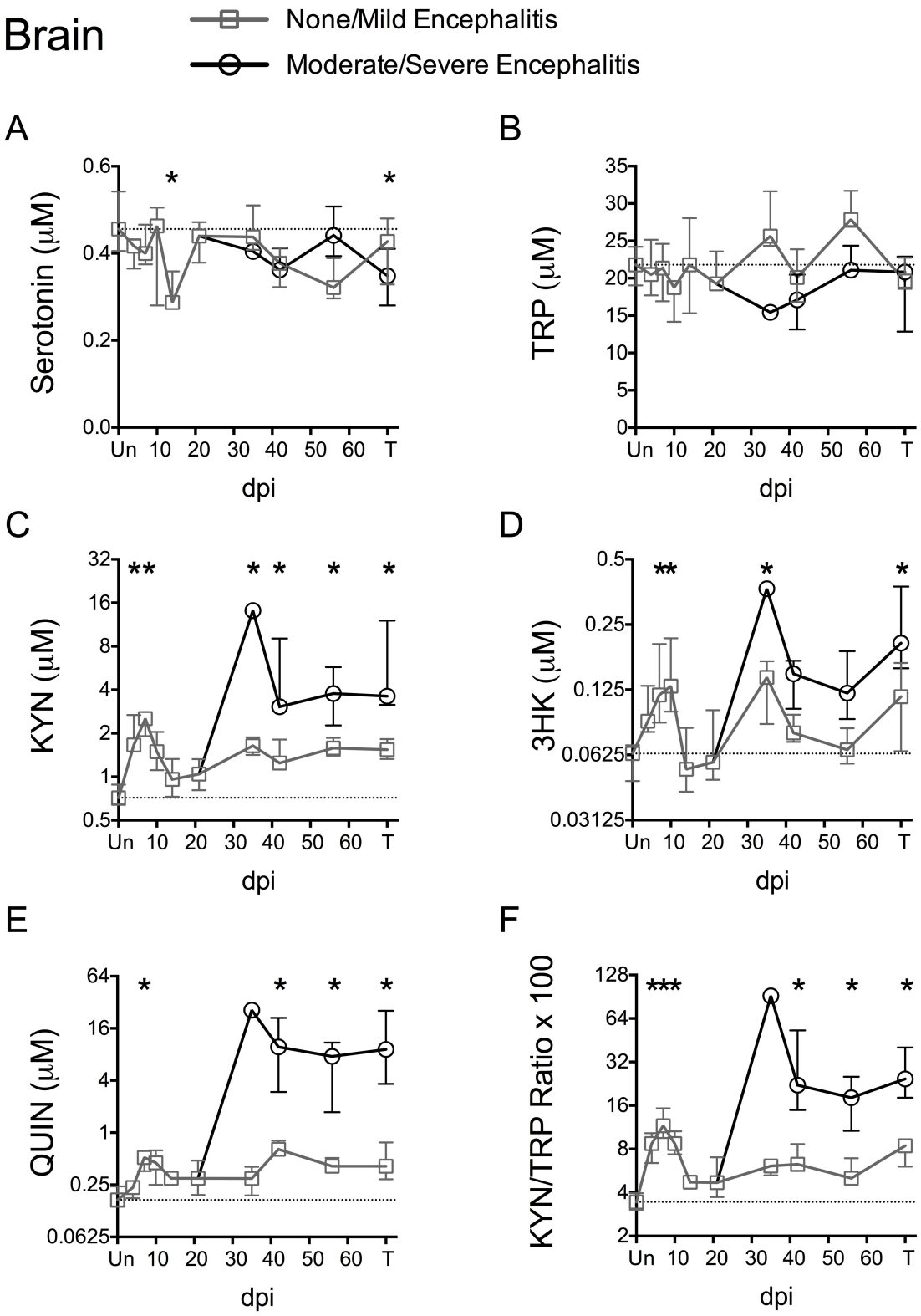
Brain
None/Mild Encephalitis
Moderate/Severe Encephalitis
A
Serotonin (μM)
0.6
0.4
0.2
0.0
Un 10 20 30 40 50 60 T
dpi
B
TRP (μM)
35
30
25
20
15
10
5
0
Un 10 20 30 40 50 60 T
dpi
C
KYN (μM)
32
16
8
4
2
1
0.5
Un 10 20 30 40 50 60 T
dpi
D
3HK (μM)
0.5
0.25
0.125
0.0625
0.03125
Un 10 20 30 40 50 60 T
dpi
E
QUIN (μM)
64
16
4
1
0.25
0.0625
Un 10 20 30 40 50 60 T
dpi
F
KYN/TRP Ratio x 100
128
64
32
16
8
4
2
Un 10 20 30 40 50 60 T
dpi

Figure 3. Terminal CSF KYN, QUIN, and KYN/TRP ratios reflect changes occurring in brain during SIV infection. (**A**-**F**) The relationship between terminal CSF TRP metabolite levels and terminal striatal brain TRP metabolite levels were examined in 8 SIV-infected pigtailed macaques. (**G**, **H**) Spearman's rank correlations between terminal brain and terminal CSF for QUIN and KYN/TRP ratios are shown. Animals with none or mild encephalitis are depicted as small black circles, and animals with moderate to severe encephalitis are depicted as large, open circles.

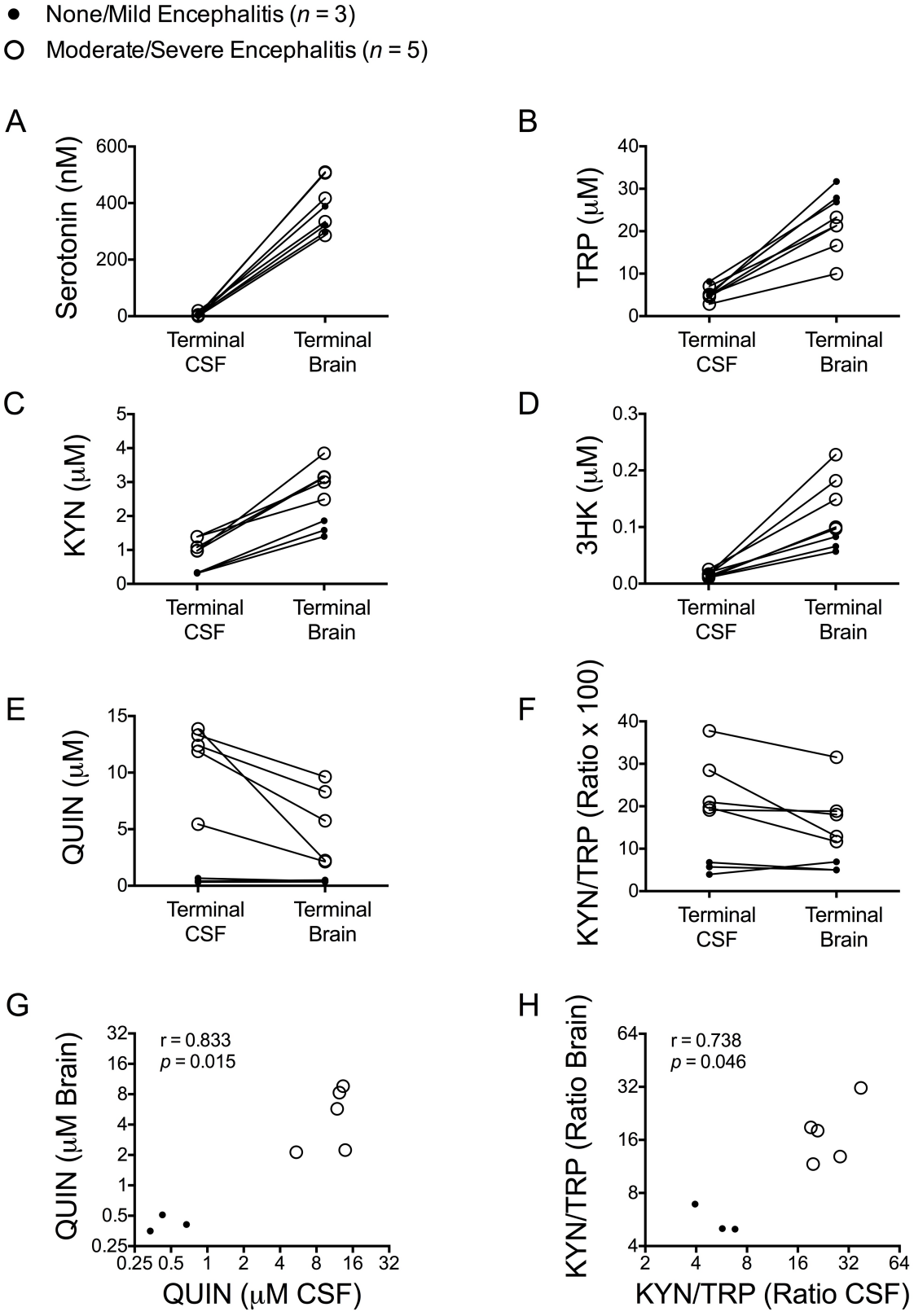
● None/Mild Encephalitis (n = 3)
○ Moderate/Severe Encephalitis (n = 5)
A
Serotonin (nM)
600
400
200
0
Terminal CSF
Terminal Brain
B
TRP (μM)
40
30
20
10
0
Terminal CSF
Terminal Brain
C
KYN (μM)
5
4
3
2
1
0
Terminal CSF
Terminal Brain
D
3HK (μM)
0.3
0.2
0.1
0.0
Terminal CSF
Terminal Brain
E
QUIN (μM)
15
10
5
0
Terminal CSF
Terminal Brain
F
KYN/TRP (Ratio x 100)
40
30
20
10
0
Terminal CSF
Terminal Brain
G
QUIN (μM Brain)
r = 0.833
p = 0.015
32
16
8
4
2
1
0.5
0.25
0.25 0.5 1 2 4 8 16 32
QUIN (μM CSF)
H
KYN/TRP (Ratio Brain)
r = 0.738
p = 0.046
64
32
16
8
4
2 4 8 16 32 64
KYN/TRP (Ratio CSF)

Figure 4. Expression of upstream KYN pathway enzymes increases during acute and chronic infection. (**A**-**E**) The mRNA expression of 5 KYN pathway enzymes involved in the catabolism of TRP to QUIN and eventually clearance through generation of NAD were analyzed in striatum from 79 animals using the Nanostring nCounter system. "Un" represents uninfected animals that were mock inoculated and euthanized approximately 84 days post mock inoculation. "T" represents SIV-infected animals that were euthanized due to terminal disease criteria or animals that reached the end of an 84-day study period. Animals are grouped according to their encephalitis scores at euthanasia (grey squares for none/mild encephalitis; black circles for moderate/severe encephalitis); medians and interquartile ranges are depicted for both encephalitis outcomes. The dotted lines designate the medians of uninfected controls. The black arrow on each graph represents the gene-specific, low-confidence thresholds as determined by the average plus 2 standard deviations of bacteriophage RNA that should not cross-hybridize with Nanostring probes. Asterisks (*) represent timepoints that were significantly different ($p < 0.05$) from uninfected controls, encompassing all animals regardless of encephalitis outcomes. For exact *p*-values, see Supplementary Table 4. *IDO1*, *KMO*, and *KYNU* are shown on a $\log_2$ axis.

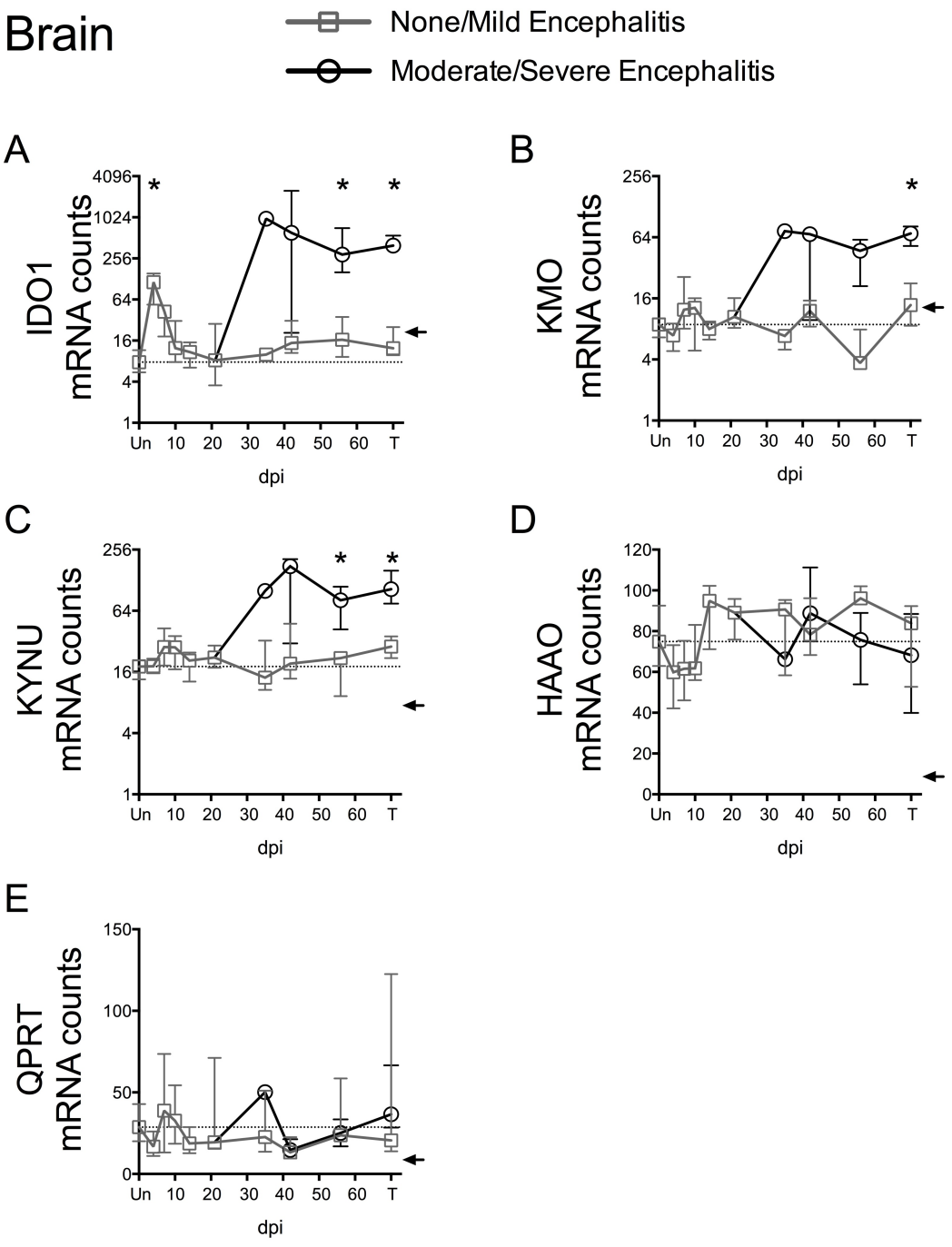
Brain
None/Mild Encephalitis
Moderate/Severe Encephalitis
A
IDO1
mRNA counts
4096
1024
256
64
16
4
1
Un 10 20 30 40 50 60 T
dpi
B
KMO
mRNA counts
256
64
16
4
1
Un 10 20 30 40 50 60 T
dpi
C
KYNU
mRNA counts
256
64
16
4
1
Un 10 20 30 40 50 60 T
dpi
D
HAAO
mRNA counts
120
100
80
60
40
20
0
Un 10 20 30 40 50 60 T
dpi
E
QPRT
mRNA counts
150
100
50
0
Un 10 20 30 40 50 60 T
dpi

Figure 5. Striatal KYN pathway metabolites correlate with markers of neuropathogenesis in chronically-infected animals. KYN/TRP ratios and QUIN levels in striatum from chronically-infected animals (35 days p.i. and onwards) were compared against markers and inducers of neuropathogenesis that have been previously measured in our lab. (**A**, **B**) Correlations of KYN/TRP ratios versus striatal type 1 interferon responses as measured by qRT-PCR (*IFNβ1*, $n = 30$ animals; *MxA*, $n = 25$ animals). (**C**, **D**) Correlations of QUIN versus markers of macrophage/microglial activation (MHC II, CD68) as measured by immunohistochemistry in subcortical white matter adjacent to striatum ($n = 20$ animals). (**E**) Correlation of QUIN versus SIV viral RNA as measured by qRT-PCR in striatum ($n = 37$ animals). (**F**) Correlation of QUIN versus amyloid precursor protein (APP), a marker of neuronal axon damage, as measured by immunohistochemistry in corpus callosum ($n = 10$ animals). All statistical analyses are Spearman's rank correlations.

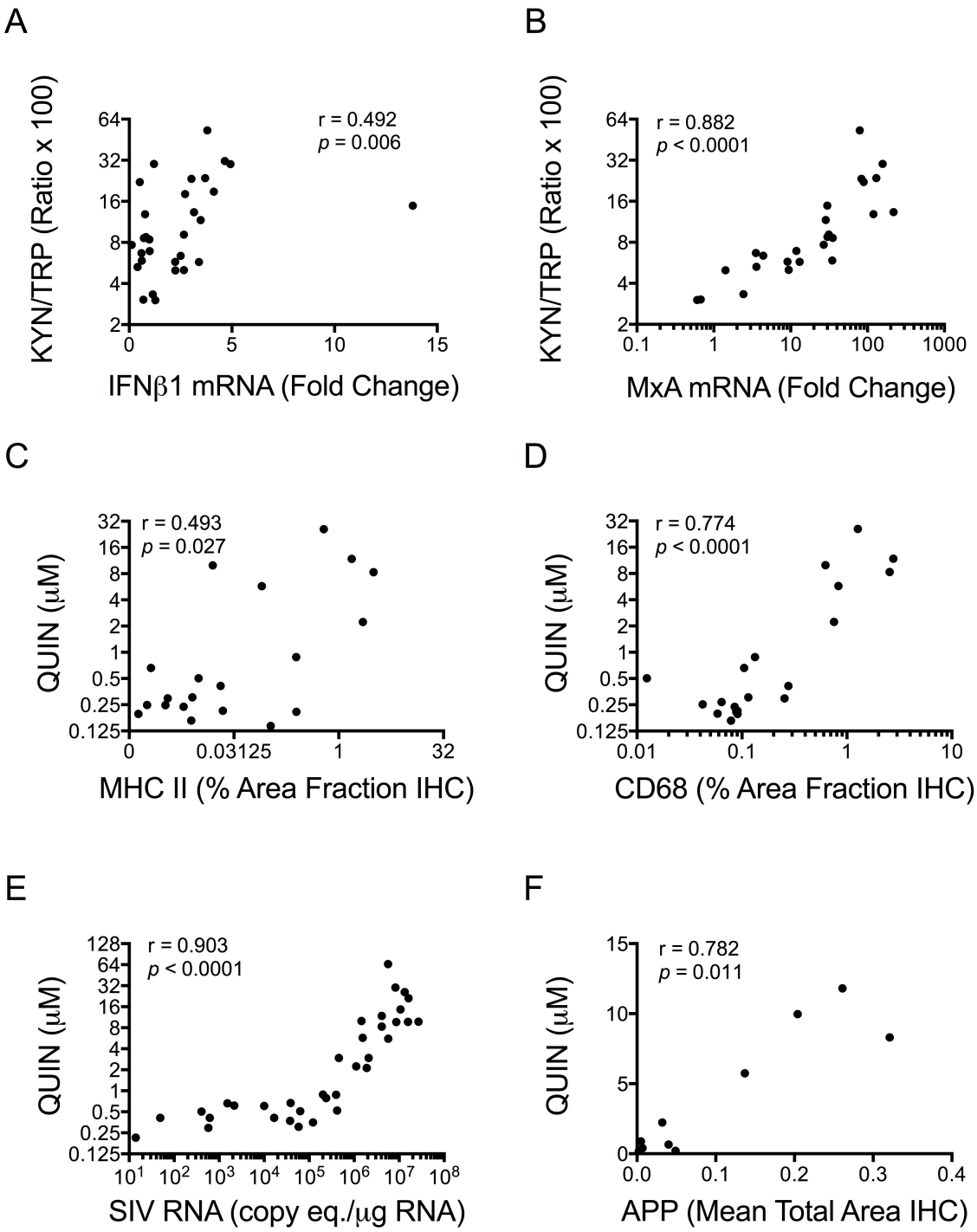
A
KYN/TRP (Ratio x 100)
r = 0.492
p = 0.006
IFNβ1 mRNA (Fold Change)
B
KYN/TRP (Ratio x 100)
r = 0.882
p < 0.0001
MxA mRNA (Fold Change)
C
QUIN (μM)
r = 0.493
p = 0.027
MHC II (% Area Fraction IHC)
D
QUIN (μM)
r = 0.774
p < 0.0001
CD68 (% Area Fraction IHC)
E
QUIN (μM)
r = 0.903
p < 0.0001
SIV RNA (copy eq./μg RNA)
F
QUIN (μM)
r = 0.782
p = 0.011
APP (Mean Total Area IHC)

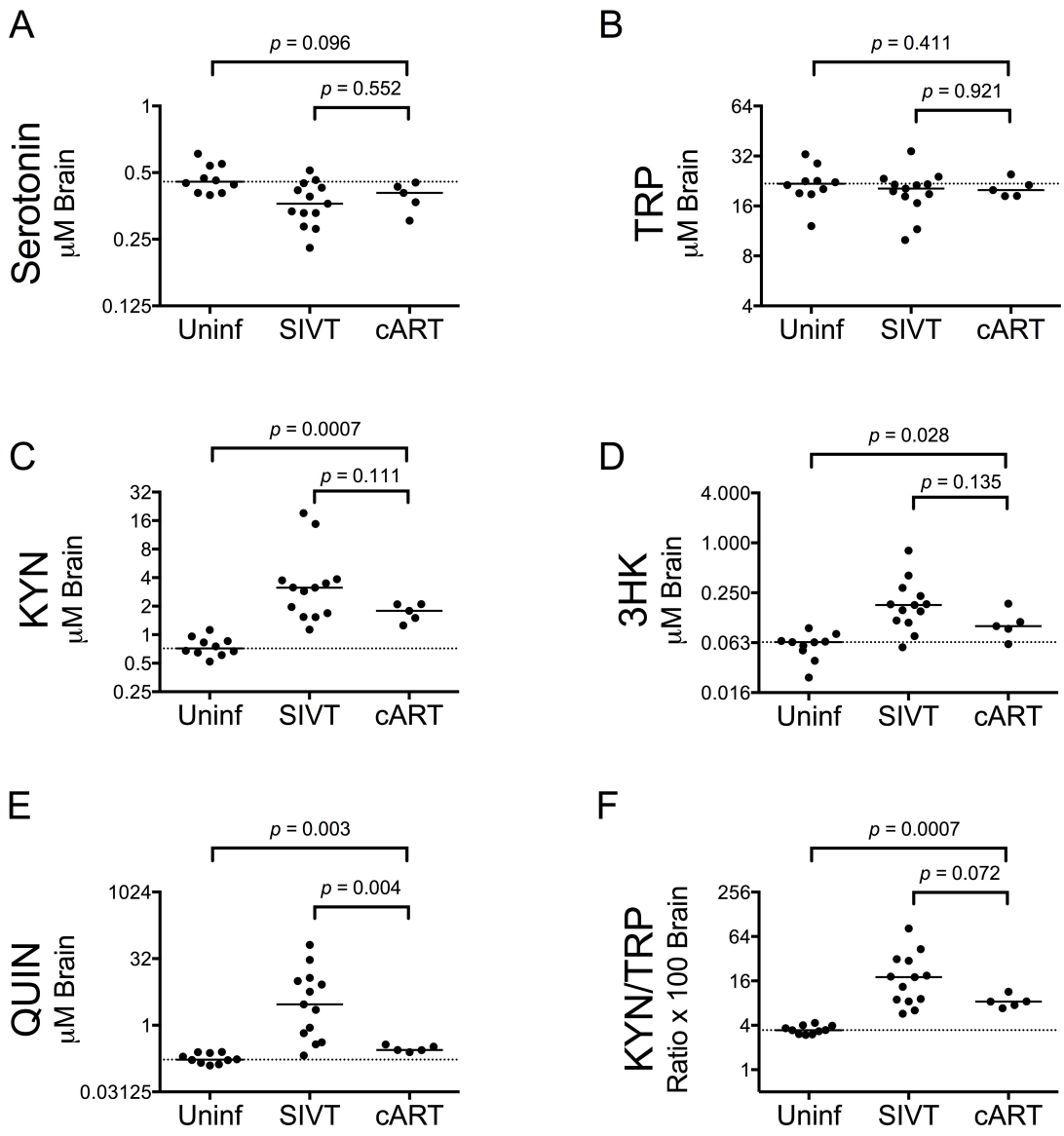

Figure 6. cART does not fully protect against elevated KYN pathway metabolites in brain. (**A-F**) Levels of serotonin, TRP, and KYN metabolites in striatum from 5 cART-treated animals are compared against 13 uninfected controls and 13 SIV-infected, untreated animals that were euthanized with terminal disease (SIVT). Data were analyzed by Mann-Whitney non-parametric *t*-tests. All graphs are shown on $\log_2$ axes.

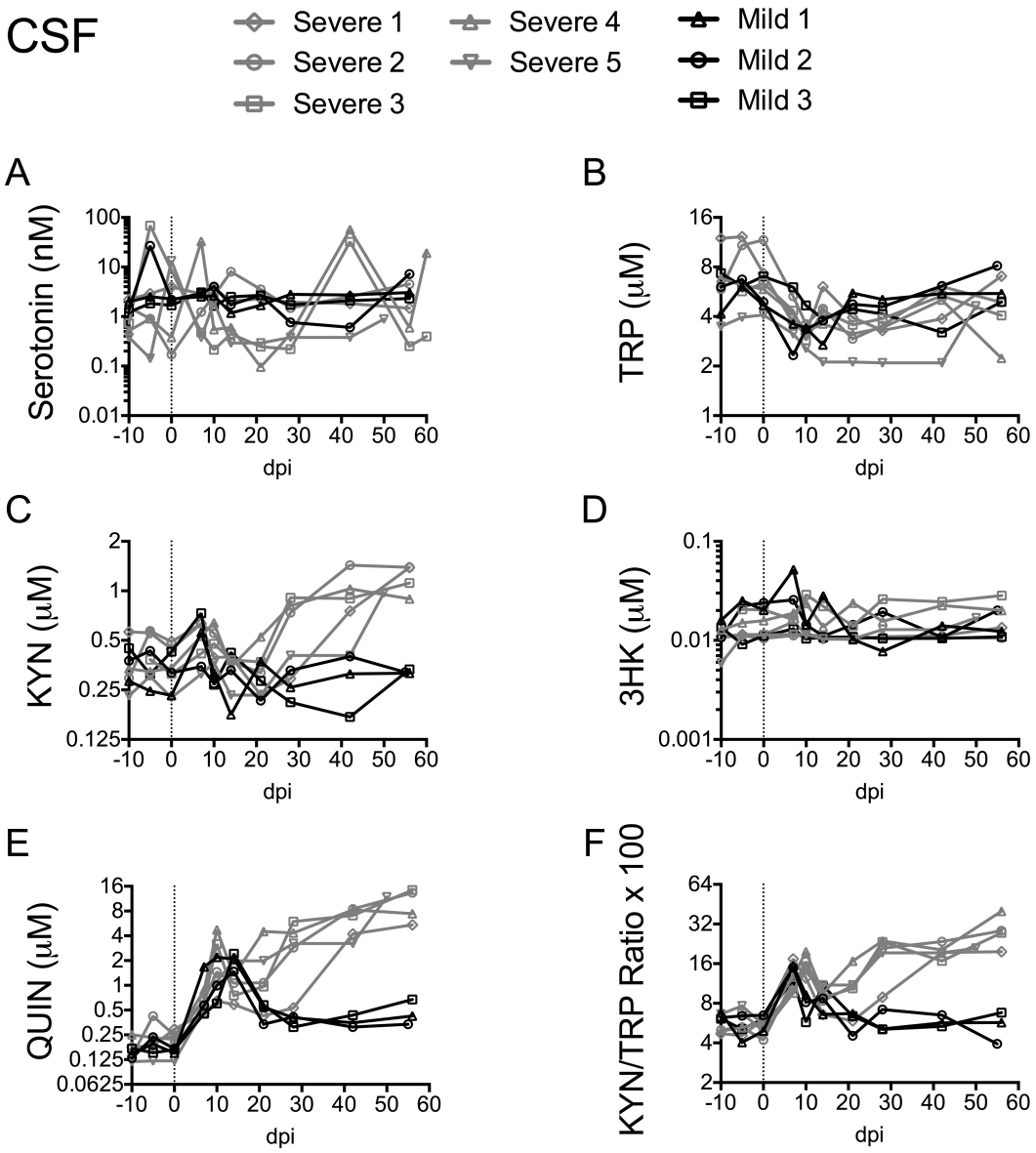

Supplementary Figure 1. Raw CSF metabolite data. CSF from 5 animals with severe encephalitis at euthanasia (grey symbols and lines) and 3 animals with mild encephalitis at euthanasia (black symbols and lines) were followed longitudinally. Two or three pre-infection draws were taken for each animal and are represented at the -10, -5, and 0 days p.i., although actual pre-infection draws were taken roughly 50-100 days prior to infection. The vertical dashed line represents the initiation of viral infection.

	Uninfected versus:						
Analyte	7 dpi	10 dpi	14 dpi	21 dpi	28 dpi	42 dpi	56 dpi
Serotonin	ns	ns	ns	ns	ns	ns	ns
TRP	**0.008**	**0.008**	**0.008**	**0.016**	**0.016**	**0.039**	ns
KYN	**0.016**	ns	ns	ns	ns	0.055	**0.039**
3HK	**0.039**	ns	ns	ns	ns	ns	ns
QUIN	**0.008**	**0.008**	**0.008**	**0.008**	**0.008**	**0.008**	**0.008**
KYN/TRP Ratio	**0.008**	**0.016**	**0.008**	**0.039**	**0.023**	**0.023**	**0.039**

Supplementary Table 1. Wilcoxon signed rank test of longitudinal CSF metabolites.

	Milds vs. Severes:						
Analyte	7 dpi	10 dpi	14 dpi	21 dpi	28 dpi	42 dpi	56 dpi
Serotonin	ns	ns	ns	ns	ns	ns	ns
TRP	ns	ns	ns	ns	ns	ns	ns
KYN	ns	ns	ns	ns	**≤ 0.050**	**≤ 0.001**	**≤ 0.0001**
3HK	ns	ns	ns	ns	ns	ns	ns
QUIN	ns	ns	ns	ns	ns	**≤ 0.01**	**≤ 0.0001**
KYN/TRP Ratio	ns	ns	ns	ns	**≤ 0.001**	**≤ 0.001**	**≤ 0.0001**

Supplementary Table 2. Two-way ANOVA of longitudinal CSF metabolites.

	Uninfected versus:								
Analyte	4 dpi	7 dpi	10 dpi	14 dpi	21 dpi	35 dpi	42 dpi	56 dpi	SIVT
Serotonin	ns	ns	ns	**≤ 0.01**	ns	ns	ns	ns	**≤ 0.05**
TRP	ns	ns	ns	ns	ns	ns	ns	ns	ns
KYN	**≤ 0.01**	**≤ 0.001**	ns	ns	ns	**≤ 0.01**	**≤ 0.01**	**≤ 0.0001**	**≤ 0.0001**
3HK	ns	**≤ 0.05**	**≤ 0.05**	ns	ns	**≤ 0.01**	ns	ns	**≤ 0.0001**
QUIN	ns	**≤ 0.05**	ns	ns	ns	ns	**≤ 0.0001**	**≤ 0.0001**	**≤ 0.0001**
KYN/TRP Ratio	**≤ 0.01**	**≤ 0.001**	**≤ 0.01**	ns	ns	ns	**≤ 0.01**	**≤ 0.001**	**≤ 0.0001**

Supplementary Table 3. Kruskal-Wallis with Dunn's post-test of striatal metabolites.

Gene	B-H *p*-value	Uninfected versus: 4 dpi	7 dpi	10 dpi	14 dpi	21 dpi	35 dpi	42 dpi	56 dpi	SIVT
IDO1	**≤ 0.001**	**≤ 0.01**	ns	ns	ns	ns	ns	ns	**≤ 0.01**	**≤ 0.001**
KMO	**≤ 0.01**	ns	ns	ns	ns	ns	ns	ns	ns	**≤ 0.05**
KYNU	**≤ 0.01**	ns	ns	ns	ns	ns	ns	ns	**≤ 0.05**	**≤ 0.001**
HAAO	ns	ns	ns	ns	ns	ns	ns	ns	ns	ns
QPRT	ns	ns	ns	ns	ns	ns	ns	ns	ns	ns

Supplementary Table 4. Benjamini-Hochberg (B-H) corrected Kruskal-Wallis with Dunn's post-test of KYN pathway enzymes in striatum.

CHAPTER III.

Maintenance of tissue tryptophan levels despite kynurenine pathway activation in the spleens of SIV-infected pigtailed macaques

Abstract

Induction of the indoleamine 2,3-dioxygenase (IDO) pathway of tryptophan catabolism may contribute to the dysfunction of T cells during HIV/SIV infection via depletion of local tryptophan levels and production of immunomodulatory kynurenine metabolites. Changes in tryptophan and kynurenine levels have been observed in plasma, but their levels in actual lymphoid tissues have been relatively unexplored in the context of HIV/SIV infection. Additionally, it is unknown whether enzymes downstream of IDO1 in the pathway are differentially regulated during infection. We explored these questions in our SIV-infected pigtailed macaque model by comparing longitudinal changes in metabolites and expression of enzymes in plasma, PBMCs, and spleen tissue taken from animals euthanized at various points during infection. Despite elevations in KYN metabolites, we did not find evidence for significant depletion of TRP in either the plasma or spleen, though our N was small ($N \geq 5$). We also found that monocyte-derived macrophages stimulated with IFNγ *in vitro* maintained their intracellular levels of TRP while depleting extracellular levels. Upstream enzymes in the KYN pathway *IDO1*, *KMO*, *KYNU* and the kynurenine aminotransferase *KAT III* (*CCBL2*) were significantly upregulated during infection in the spleen. *KAT II* (*AADAT*) was downregulated during infection, while *KAT I* (*CCBL1*) and *HAAO* remained unchanged. Finally, we found that mDCs, followed by macrophages, expressed the highest levels of IDO1 in the spleens of terminally infected animals. Overall, our findings shed light on how cells and tissues prioritize tryptophan use in the face of kynurenine pathway activation.

Introduction

Despite the ability of combination antiretroviral therapy (cART) to potently suppress viral loads in HIV-infected patients, there is evidence of residual immune dysfunction in patients on cART. Patients with a low CD4+ T cell count at the time of therapy initiation are more at risk for incomplete CD4+ T cell recovery (114), and up to a quarter of patients are "immunologic nonresponders" who do not exhibit recovery of CD4+ T cell counts despite successful suppression of viremia with cART (12). Persistent elevations in pro-apoptotic and immunosuppressive pathways likely contribute to the continued T cell dysfunction seen in patients on cART (6-8, 11). In the absence of an effective HIV vaccine or agents clinically proven to purge latent virus, further understanding of pathways involved in T cell dysfunction is necessary in order to restore immune balance in many HIV-infected individuals.

One particular area of research with potentially far-reaching implications for immune function is the kynurenine (KYN) pathway of tryptophan (TRP) catabolism. TRP is an essential amino acid that, in humans, can only be harvested from food intake or breakdown of proteins. The vast majority (~90%) of TRP during homeostasis is catabolized in the liver down the KYN pathway by tryptophan 2,3-dioxygenase (TDO2) (21), which serves as an important generator of the cellular cofactor NAD+. During HIV/SIV infection, levels of a second TRP catabolizing enzyme, indoleamine 2,3-dioxygenase (IDO1) are induced in tissues and circulating cells by interferon (IFN) γ and, to a lesser extent, by IFNα, IFNβ, tumor necrosis factor (TNF) α, IL-6, viral proteins (Tat, Nef, and gp120), platelet-activating factor, and cellular interactions such as CD40/CD40L and B7/CTLA-4 (23-29). More recently, it was discovered that the

cytokine transforming growth factor (TGF) β is critical in the maintenance of long-term IDO induction in tolerogenic dendritic cells (DCs) and regulatory T cells (Tregs) (30). A third TRP-catabolizing enzyme, IDO2, may be required for IDO1-mediated generation of regulatory T cells (115), but a prominent role of this enzyme in disease processes has yet to be fully established. Thus, the predominant gatekeeper of the KYN pathway during inflammatory processes such as infection with HIV/SIV is thought to be IDO1.

While the KYN pathway is an important source of NAD+, TRP is a rare essential amino acid, and small changes in TRP metabolism can have major consequences. For example, reducing extracellular TRP levels suppresses proliferation of actively dividing cells via accumulation of uncharged TRP-tRNAs and subsequent activation of the GCN2 stress kinase pathway (37). This mechanism could suppress the ability of a patient's T cells to respond to either HIV itself or to secondary opportunistic infections. In addition to the consequences of TRP depletion, increased turnover down the KYN pathway also leads to generation of KYN metabolites that have immunomodulatory capabilities. For example, KYN and picolinic acid (PIC) prevent T cell proliferation in a non-TRP-dependent manner (52). KYN and 3-hydroxy anthranilic acid (3HANA) can convert naïve T cells or proinflammatory Th17 cells into regulatory T cells (Tregs) following interactions at the aryl hydrocarbon receptor, which may increase susceptibility to opportunistic infections at mucosal surfaces (53, 54). 3HANA and its dimerized form, cinnabarinic acid, can directly cause apoptosis of activated T cells (55, 56). 3HANA can also directly stimulate production of anti-inflammatory cytokines such as TGFβ from DCs, potentiating IDO induction (57). KYN's recently discovered activity as a ligand of

the cytosolic aryl hydrocarbon receptor (AHR) further helps to explain the cooperative induction of tolerogenic activity between DCs and Tregs (54, 58)

Immunosuppressive metabolites generated by the KYN pathway during HIV/SIV infection could be major contributors to peripheral HIV pathogenesis, even in the setting of cART. However, several key questions remain unanswered in the field. For example, in the context of TRP depletion, do cells deplete intracellular levels of TRP in addition to extracellular levels, or do they maintain intracellular levels at all costs? Secondly, while non-invasive measurements of KYN metabolites in plasma and PBMCs of HIV-infected patients have been invaluable in the study of KYN pathway activation, do these measurements in the circulation accurately reflect changes occurring in lymphoid tissues? Thirdly, while expression of the rate-limiting enzyme IDO1 has been repeatedly examined in the context of HIV/SIV infection, are the expression levels of downstream enzymes of the KYN pathway similarly regulated? Finally, while a wide range of cell types can express IDO following *in vitro* stimuli with cytokines, which of these cell types are most responsible for IDO expression during chronic infection in actual tissue sites?

To explore these questions, we used the pigtailed macaque model of HIV infection, wherein animals are dually inoculated with an immunosuppressive swarm and a neurovirulent clone and consistently develop clinical symptoms of AIDS by three months post inoculation. We focused on the spleen as a representative immune organ. Using high throughput nanostring technology and multiplexed GC/MS assays, we characterized the kinetics of the major enzymes and metabolites in the IDO pathway in both the spleen and in plasma/PBMCs at various timepoints throughout infection. We found that both *in vitro* (in macrophages) and *in vivo* (in chronically infected spleen

tissue), cells and tissues actively maintained internal TRP levels despite ongoing KYN pathway activation. Longitudinal changes in KYN pathway metabolites and enzyme expression were actually greater in plasma and PBMCs than changes seen in spleen tissue, but still maintained some diagnostic value for pathogenesis in tissue. Finally, we found that in chronically infected spleens, mDCs and monocyte/macrophages expressed higher levels of *IDO1* as compared to pDCs and T cells. These data suggest that antigen-presenting cells continue to be at the forefront of ongoing KYN pathway activation in the spleen even during terminal infection and therefore are uniquely situated to contribute to T cell dysfunction.

Materials & Methods

Animal studies

Juvenile pigtailed macaques were inoculated intravenously with two strains of SIV, the neurotropic swarm SIV/DeltaB670 and the immunosuppressive clone SIV/17E-Fr, as previously described (59). Animals were euthanized during various stages of disease (7, 10, 14, 21, 35, 42, 56, and 84 days p.i.). Some animals were euthanized prior to their planned euthanasia date due to presentation of clinical symptoms that met euthanasia criteria as described previously (101). These animals are grouped with 84-day animals as SIV terminal ("T" in figures). All animals had longitudinal blood draws performed at the following timepoints: at least 3 pre-infection draws, then on days 7, 10, 14, 21, 28, and every two weeks thereafter. PBMCs were frozen viably, while plasma was frozen at -80°C. All animals were euthanized in accordance with federal guidelines and institutional policies. Macaques were perfused with sterile PBS while under deep anesthesia, and tissues were collected and either flash frozen until use or fixed. All animal studies were approved by the Johns Hopkins Animal Care and Use Committee; all animals were humanely treated in accordance with federal guidelines and institutional policies.

Isolation of PBMCs and plasma from pigtailed macaques

Whole blood was centrifuged at 2500 rpm for 15 min to separate plasma. Plasma was frozen back at -80°C. Blood was then diluted 1:3 with 1 x HBSS with EDTA without Ca^{2+} or Mg^{2+} and layered on top of 15 mL Percoll working solution (53% Percoll from Amersham Biosciences, 10% 10X HBSS without Ca^{2+} or Mg^{2+}, 37% sterile water) in a

50 mL conical tube. The Percoll/blood gradient was centrifuged for 30 min at 2000 rpm, brake off, at room temp. The top aqueous layer was discarded and the white blood cell layer was moved to a new conical and washed twice with HBSS with EDTA, centrifuging 10 min at 1600 rpm. White blood cells were then incubated with 15 mL red blood cell lysis buffer (1X solution of the following 10X buffer: 4.15g NH_4Cl, 0.5g $KHCO_3$, 0.15 g EDTA dissolved in water and adjusted to pH 7.2-7.3 in a final volume of 500 mL) for 15 min at 37°C. PBMCs were washed with HBSS with EDTA and centrifuged for 10 min at 1600 rpm and either plated immediately for cell culture experiments or frozen at -80°C.

Macrophage cell culture stimulation with IFNγ and IFNβ

PBMCs from 3 pigtailed macaques were plated at a density of $4x10^6$ cells per well in 12-well plates in 2 mL of macrophage differentiation media (Dulbecco's DMEM with 20% human AB serum, 1% macrophage colony stimulating factor, 0.2% sodium pyruvate, 2 mM L-glutamine, 1 mM HEPES buffer, and 2 mg/mL gentamicin). After 3-4 days in culture, 1 mL of media was removed and replaced with fresh media. After 7 days in culture, mature macrophages were visible in culture wells and were washed 3x with PBS to remove any remaining lymphocytes. One mL of macrophage differentiation media with 10% human AB serum instead of 20% was then added to each well. To some wells, either 25 ng/mL of rhesus IFNγ (R&D Systems) or 100 units/mL human IFNβ1a (PBL Interferon Source) were added to induce IDO. Because of low induction of IDO expression with IFNβ, cells from one animal were stimulated with 4x as much IFNβ (400 units/mL). For all 3 animals, two wells were immediately harvested for the 0 hr

timepoint; additional wells were harvested 24, 48, and 72 hr later in duplicate for each condition as well as for unstimulated controls for each timepoint. To harvest samples, supernatants were first pulled off and spun down to remove residual cellular debris. Adherent macrophages were then washed with PBS before removal with gentle scraping. Cells were partitioned into 2 aliquots, one for qRT-PCR and one for metabolites, before being spun down and frozen at -80°C.

Spleen tissue homogenization for metabolite extraction

Three millimeter punches were taken from perfused, snap-frozen spleen tissue from SIV-infected pigtailed macaques. Punches were weighed and diluted 1/20 weight/volume with cold 0.1% ascorbic acid, and sonicated with a tip sonicator 3-5 times at 70% amplitude for 5 sec each, all while on ice. Ten samples were processed at a time to minimize thaw time. Residual debris was removed by centrifugation prior to extraction of metabolites.

Metabolite extraction from spleen

On ice, 50 μL of spleen homogenates (of the original 1/20 homogenates for metabolites or diluted further for a final of 1/2000 in 0.1% ascorbic acid for amino acids) were spiked with 50 μL of a solution containing the following heavy standards: [$^2H_5$] tryptophan (1 μM, CDN Isotopes, Quebec, Canada), [$^2H_2$] tyrosine (1 μM, CDN Isotopes, Quebec, Canada), [$^2H_6$] kynurenine (5 μM, custom synthesis from Sigma Aldrich Isotec), and [$^2H_3$] quinolinic acid (0.05 μM, custom synthesis from Synfine, Ontario, Canada). The following standards were also spiked into some samples but not analyzed for the

purposes of this manuscript: [$^{2}H_5$] glutamate (1 μM, CDN Isotopes, Quebec, Canada), [$^{13}C_6$] anthranilic acid (0.5 μM, Sigma Aldrich), and [$^{2}H_4$] serotonin (2 μM, CDN Isotopes, Quebec, Canada). Fifty μL ice cold acetone was added to homogenates and samples were centrifuged at 20K *g* for 5 min to precipitate protein. Eighty percent (120/150 μL) of the acetone supernatant was transferred to a new microcentrifuge tube, to which 50 μL of a 2:5 ratio methanol:chloroform was added. Samples were centrifuged at 20K *g* for 10 min, and 60% (80/134 μL) of the aqueous layers were transferred to glass vials. The aqueous solution was dried and then derivatized with 120 μL of 2,2,3,3-pentafluoro-1-propanol (Sigma Aldrich) and 135 μL of pentafluoropropionic anhydride (Sigma Aldrich) by heating at 75°C for 30 min. Derivatized samples were dried and stored at -80°C.

Metabolite extractions from plasma and macrophage cell culture supernatants

Metabolite extractions from plasma and cell culture supernatants were identical to spleen with the following modifications: samples were diluted 1/2 in 0.2% ascorbic acid for metabolites (a 1/100 dilution in 0.1% ascorbic acid was still used for amino acids), and no methanol/chloroform extraction was performed. Acetone extraction supernatants were dried down by centrifugation under vacuum and then derivatized as above. The heavy standard mixture for plasma and cell culture supernatants required higher concentrations for two metabolites: 15 μM instead of 5 μM for [$^{2}H_6$] kynurenine, and 0.2 μM instead of 0.05 μM for [$^{2}H_3$] quinolinic acid. All other heavy standards were kept at 1 μM.

Metabolite extraction from in vitro *macrophage cells*

Macrophage cell pellets were resuspended in 80 – 120 µL of 0.1% ascorbic acid and sonicated 2x for 3 sec each at 30% amplitude in a tip sonicator on ice. Fifty microliters of this homogenate was used as the starting material for intracellular amino acid and metabolite measurements. The heavy standard concentrations were identical to those used for plasma and cell culture supernatant samples. The acetone precipitation, methanol/chloroform extraction, and derivatization for the macrophage cell pellets were otherwise performed in an identical manner to the protocol used for spleen homogenates.

GC/MS/MS analysis of amino acids and KYN pathway metabolites

Dried samples were resuspended in 50 µL ethyl acetate, with the exception of the *in vitro* macrophage lysates which were resuspended in a smaller volume of 25 µl to maximize signal. One µL, or 2 µL for the *in vitro* macrophage lysates, was injected in pulsed, splitless mode into an Agilent 7890A GC coupled to a 7000 MS/MS equipped with an Agilent 7693A autosampler operated in electron capture negative ionization (ECNI) mode as previously described (104). The multiple reaction monitoring (MRM) transitions used in this study were based on transitions initially described by Eckstein *et al* (105) and have been subsequently optimized. The transitions for the derivatized compounds were as follows: **TRP** Q1 = 608.2, Q3 = 270, CE = 5, RT = 13.1 min; **[$^2H_5$] TRP** Q1 = 613.2, Q3 = 351, CE = 20, RT = 13.1 min; **TYR** Q1 = 585.2, Q3 = 268, CE = 20, RT = 10.9 min; **[$^2H_2$] TYR** Q1 = 587.2, Q3 = 436.9, CE = 20, RT = 10.9; **KYN** Q1 = 612, Q3 = 442, CE = 10, RT = 13.0 min; **[$^2H_6$] KYN** Q1 = 618, Q3 = 447, CE = 10, RT = 13.0 min; **QUIN** Q1 = 431.0, Q3 = 298.0, collision energy (CE) = 10V, retention time

(RT) = 9.4 min; **[$^2H_3$] QUIN** Q1 = 434.0, Q3 = 301.0, CE = 10V, RT = 9.4 min; **3HK** Q1 = 630, Q3 = 219, CE = 15, RT = 12.9 min.

Data were analyzed with Agilent MassHunter software, Build B.04. Samples were injected in a randomized order to minimize experimental bias. Each sample was injected at least twice. The average of the peak areas from replicate injections were normalized to the average of the heavy standards for each respective compound. 3HK was the only compound for which we did not have a matching heavy standard; thus we normalized 3HK to [$^2H_6$] KYN because of their similar ionization properties. These values were fit to the matrix-spiked light standard curves for each compound based on the standard addition method.

FACS sorting of spleen cells

Cells were mechanically teased from spleen tissue at euthanasia. Cells were then stained with two panels, one to isolate pDCs, mDCs, and CD14+ cells, and the other to isolate CD4+ and CD8+ T cells. The DC panel was as follows: BDCA-2 APC (clone AC144; Miltenyi Biotec), BDCA-1 PE (clone AD5-8E7; Miltenyi Biotec), CD123 PerCP-Cy5.5 (clone 7G3; BD Biosciences), CD20 PE-Cy7 (clone 2H7; BD Biosciences), CD3 PacBlue (clone SP34-2; BD Biosciences), CD14 FITC (clone M5E2; BD Biosciences), and Live/Dead Aqua (Invitrogen Life Technologies). The T cell panel was as follows: CD3 FITC (clone SP34-2; BD Biosciences), CD8 PE (clone RPA-T8; BD Biosciences), CD4 PerCP-Cy5.5 (clone L200; BD Biosciences), and Live/Dead Aqua (Invitrogen Life Technologies).

RNA extraction and qRT-PCR of FACS-sorted spleen cells

After cell isolation by FACS, mRNA was extracted from cells using the RNeasy Plus Mini kit (Qiagen). RNA was reverse transcribed in duplicate using the High Capacity cDNA Kit (Invitrogen Life Technologies, PN#4375575). A no reverse transcription control was run for each RNA sample. Reverse transcription was carried out on a thermal cycler under the following conditions: 25°C for 10 min, 27°C for 120°C min, 85°C for 5 min, and then cooled to 4°C. Because of the small amount of starting material, cDNA was then pre-amplified using the TaqMan PreAmp Master Mix (Applied Biosystems/Life Technologies) with a pooled assay of 0.2X primers for GAPDH, IDO1, and Mx (preamplification of 18S was not recommended by the manufacturer because it is already highly abundant). Preamplification conditions were run on a thermal cycler: 95°C for 10 min, 95°C for 15 sec, 60°C for 4 min, with steps 2-3 repeated 14 times. Preamplified cDNA was then diluted 1/20 and amplified again in a thermal cycler, this time using the TaqMan Gene Expression Assay (Life Technologies). Two separate plates were run: the first plate included primer/probe mixes for 18S Cy5, IDO1 TXR, and Mx FAM. The second plate included primer/probe mixes for 18S Cy5 and GAPDH VIC (Taqman). qRT-PCR conditions were as follows: 50°C for 2 min, 95°C for 10 min, 95°C for 15 sec, 60°C for 1 min, with steps 3-4 repeated 40 times. 18S Cy5 values between the two plates were virtually identical, with a Pearson's correlation $r = 0.998$ and a p-value < 0.0001, enabling the normalization of IDO1 and Mx to both GAPDH and 18S housekeeping genes. GAPDH VIC primer/probe was obtained from Life Technologies (Rh02621745_g1). 18S, Mx, and IDO1 primer/probes were custom synthesized from Integrated DNA Technologies: IDO1 (5'- TGCTTTGACGTCCTGCTGG, 5'-

TTCCTGTGAGCTGGTGGCA, and 5'- TXR - ATGCTGCTCAGTTCCTCCAGGACA - IAbRQs); Mx (5'- AGGAGTTGCCCTTCCCAGA, 5'- TCGTTCACAAGTTTCTTCAGTTTCA, and 5'- FAM - ACCAGCGGGCATCTGGTCACGA - BHQ1); 18S rRNA (5'- TAGAGGGACAAGTGGCGTTC, 5'- CGCTGAGCCAGTCAGTGT, and 5'- Cy5 - AGCAATAACAGGTCTGTGATG - BHQ2).

RNA extraction and qRT-PCR of in vitro *macrophages*

Frozen macrophage cell pellets were resuspended in 350 µl RLT Plus lysis buffer (Qiagen) supplemented with 10 µL/mL β-mercaptoethanol and vortexed. RNA was extracted with the Qiagen RNeasy Plus Mini Kit according to the manufacturer's instructions, and mRNA was eluted in 50 µL of RNase-free water. mRNA was then treated with RQ1 DNase (Promega) for 30 min at 37°C, followed by inactivation with Stop Solution (Promega) for 10 min at 65°C. For qRT-PCR for IDO1 mRNA, roughly 200 ng RNA were reverse transcribed into cDNA with SuperScript III enzyme (Invitrogen). PCR amplification of cDNA was performed in a CFX96 thermal cycler (BioRad) with Multiplex NoRox PCR Mix (Qiagen) and identical GAPDH, 18S, and IDO primer/probes as those used for the FACS sorted spleen cells. Results were analyzed via the ΔΔ Ct method with normalization to the GAPDH housekeeping gene and subsequent normalization to the unstimulated controls for each timepoint. Similar results were obtained whether normalized to 18s or GAPDH.

RNA extraction and qRT-PCR of longitudinal PBMCs

RNA was extracted from archived, longitudinally sampled PBMCs from 5 pigtailed macaques using the RNeasy Mini Kit (Qiagen) according to the manufacturer's instructions. Reverse transcription and PCR amplification of cDNA for Mx, IDO1, and 18s were performed identically to the protocol used for the *in vitro* macrophages above.

RNA extraction and Nanostring nCounter gene expression analysis of spleen samples

As part of a larger collaborative project, a custom CodeSet for 116 macaque genes (including the 8 transcripts analyzed in this manuscript as well as 11 putative housekeeping genes) for 96 samples were designed according to NanoString specifications based on rhesus macaque (*Macaca mulata*) and human sequences. Two hundred ng of each RNA sample were hybridized for 16 hours with the CodeSet, and genes were quantitated using the nCounter Digital Analyzer. Sixty-two of the 96 samples were examined in this study; the rest were excluded from the present analysis. Data were analyzed according to the Nanostring nCounter Expression Data Analysis Guide, with minor modifications. A value of "1" was added to each value to eliminate any "0" values which could interfere with downstream analysis. Data were then normalized by the geometric mean of six spiked positive controls to correct for assay efficiency. Background for each sample was assessed as the average of 8 spiked negative controls plus 2 standard deviations following positive control correction. The highest background value obtained was applied as the cut-off for the entire data set. Any genes with a majority of values below this threshold of 43 counts were excluded from the present analysis, with the exception of SIV/17E-Fr for which below threshold values were

expected and obtained for uninfected animals. As no single housekeeping gene has been proven to be consistently expressed across different cell types, cell maturation states, tissue types, or disease models (107-111), we used the Kruskal-Wallis non-parametric analysis of variance (ANOVA) on all positive control normalized genes to find the 4 most stably expressed genes across the spleen samples (107, 112). We found that the markers CD19, GEM, STK25, and CCS were the least varying genes between infection groups (Kruskal-Wallis p-values = 0.203, 0.170, 0.121, and 0.111, respectively). The geometric mean of these 4 genes was used to normalize the positive control corrected data (111). Alternative normalization to lymphocyte genes such as CD4 in HIV/SIV infected lymphoid tissue has been used in other studies as well (116-118). All traditional housekeeping genes in our panel (ACTB, B2M, GAPDH, HPRT1, HMBS, RPL13A, RPS9, SDHA, TBP, UBC, and YWHAZ) had Kruskal-Wallis p-values < 0.05 despite the loading of equal amounts of RNA in each well. Trends in SIV viral load and IDO1 mRNA expression in spleen have been independently verified for subsets of the animals by qRT-PCR (data not shown).

Statistical analyses

Spleen metabolite data were analyzed by the Kruskal-Wallis test (non-parametric ANOVA). Metabolites with a significant overall Kruskal-Wallis p-value < 0.05 were subjected to Dunn's multiple comparisons test to compare post-infection timepoints to values from uninfected animals.

Plasma metabolites and PBMC qRT-PCR data were analyzed by the Friedman test (paired, non-parametric ANOVA). Analytes with a significant overall Friedman p-

value < 0.05 were subjected to Dunn's multiple comparisons test to compare post-infection timepoints to the matched animals' pre-infection values.

Longitudinal spleen Nanostring mRNA data were analyzed by Kruskal-Wallis followed by multiple comparisons correction with Benjamini Hochberg. Transcripts that had a significant overall Kruskal-Wallis p-value < 0.05 following Benjamini Hochberg correction underwent Dunn's multiple comparisons test to examine post-infection values versus uninfected values.

Results

Preservation of intracellular TRP levels in macrophages undergoing KYN pathway activation

In chapter II, we reported that TRP levels in brain tissue during chronic SIV infection were not depleted despite robust induction of KYN pathway metabolites in the brain and significant loss of TRP in CSF. Others have reported similar findings in a mouse model of inflammation, where injection of LPS resulted in increases in KYN metabolites both peripherally and in the brain, but TRP depletion only occurred in plasma and not in the brain itself (96). To test the hypothesis that cells prioritize maintenance of intracellular TRP levels at the expense of external levels, we grew mononuclear cells in the presence of MCSF and human serum for 7 days to differentiate them into mature macrophages. Macrophages were then stimulated with 25 ng/mL IFNγ for 0, 24, 48, and 72 hrs. At these timepoints, supernatants were harvested for KYN metabolite analysis, and cell lysates were harvested for both KYN metabolites and transcriptional analysis of *IDO1* expression. Metabolites from IFNγ-stimulated macrophages were normalized to metabolite levels in unstimulated controls at each timepoint to control for metabolic turnover over time as well as to tyrosine (TYR), which does not change during HIV infection (119), in the supernatants and cell lysates to control for minor variations in cell number that could affect rates of metabolic turnover.

In the supernatants of the IFNγ-stimulated macrophages, TRP levels dropped immediately at 24 hrs and stayed below control levels throughout the experiment (Fig. 1A). Corresponding to the drop in TRP in the supernatant and indicative of IDO activity, levels of the metabolites KYN, 3HK, and QUIN all increased by 24 hrs in the

macrophage supernatants (Fig. 1B). Metabolite levels in the supernatant peaked in the sequential order in which they are generated in the pathway, with KYN peaking at 24 hrs (KYN is the 2nd metabolite in the pathway, after L-formyl-kynurenine), 3HK peaking at 48 hrs (3HK is the 3rd metabolite in the pathway), and the terminal pathway metabolite QUIN peaking at 72 hrs.

In contrast to the immediate and sustained drop in supernatant TRP levels, intracellular TRP remained stable throughout the timecourse, with some donors even displaying slight increases in TRP at 72 hrs post IFNγ stimulation (Fig. 1C). This maintenance of intracellular TRP occurred despite increases in intracellular KYN, 3HK, and QUIN at all timepoints (Fig. 1D). A comparison of KYN/TRP ratios in the supernatant versus intracellular lysates revealed more robust fold changes in the supernatant (Fig. 1E). This difference was due to both larger increases in KYN (5-fold increase above a baseline of 2.8 μM in the supernatant vs. 2-fold increase above 0.1 μM in the cell lysates) and to more drastic declines in TRP in the supernatant as compared to the cell lysates (50% loss from baseline of 60 μM in the supernatant vs. 10% loss from baseline of 6 μM intracellularly). Thus, the cells appeared to actively secrete KYN metabolites as they were being generated at each step in the pathway while maintaining intracellular TRP levels, all at the expense of dramatically altering the extracellular conditions.

As KYN/TRP ratios are an established surrogate for IDO1 activity, we also measured IDO1 transcriptionally to compare whether *IDO1* mRNA levels more closely matched changes in intracellular or extracellular metabolite levels. We found that transcriptional patterns of *IDO1* induction mirrored the changes in KYN/TRP ratios in

the supernatant nearly identically, and did not as closely reflect the intracellular pattern of KYN/TRP ratios (Fig. 1F versus Fig. 1E). Finally, we determined the kinetics of *IDO1* transcriptional expression in response to both IFNγ and a second IDO-inducing cytokine, IFNβ, because chronic stimulation of type I IFN responses by virus is thought to contribute to chronic induction of IDO *in vivo* in HIV/SIV infection (120). We found that IFNγ was a much more potent stimulator of *IDO1* than IFNβ (Fig. 1F) at the concentrations used in this experiment (25 ng/mL IFNγ, 100 units/mL IFNβ). Induction of KYN pathway metabolites was also much less in the IFNβ-stimulated cells as compared to IFNγ (data not shown). One donor was stimulated with four times as much IFNβ (400 units/mL) but still did not induce levels of IDO comparable to IFNγ.

Overall, these data suggest that macrophages are remarkably adept at maintaining homeostatic concentrations of intracellular TRP in the face of robust KYN pathway activation.

Longitudinal kinetics of KYN pathway metabolites in spleens of SIV-infected pigtailed macaques

We next sought to determine the extent to which TRP and KYN metabolites are altered *in vivo* in lymphoid tissue during the course of SIV infection. To this end, we harvested metabolites from archived spleens from 89 animals euthanized at various points throughout infection, with a minimum of 5 animals per timepoint. During acute infection (0-14 days p.i.), TRP levels displayed an immediate drop at day 4 p.i., though this decrease was not statistically significant, then slowly recovered back to uninfected control levels by day 10 p.i. (Fig. 2A). This drop in TRP coincided with an elevation in

KYN levels at day 4 p.i. (Fig. 2B). Similar to TRP, KYN returned to baseline by day 10 p.i. Levels of the downstream KYN metabolites 3HK (Fig. 1C) and QUIN (Fig. 1D) peaked slightly later at day 7 p.i., with QUIN being significantly higher at day 7 p.i. as compared to uninfected controls ($p < 0.01$ by Kruskal-Wallis). During chronic infection (day 35 p.i. and onwards), neither TRP nor any of the KYN metabolites underwent any significant changes, though some animals during terminal infection (T; approximately 84 days p.i.) had higher levels of KYN metabolites than others.

Longitudinal kinetics of KYN metabolites in plasma during SIV infection

Our finding that there was no significant change in KYN pathway metabolites in the chronically infected spleens was surprising. We next sought to determine whether this indicated a lack of KYN metabolite induction as a whole in the periphery. To this end, we measured the KYN metabolites in plasma sampled longitudinally from 5 macaques prior to and during SIV infection. By using paired, longitudinal plasma samples we were able to control for variation in baseline levels of metabolites from animal to animal by normalizing data to values from the average of 3 pre-infection blood draws from each animal. Despite this added level of stringency, we again saw an initial drop in plasma TRP levels during acute infection that was not significantly different from pre-infection values (Fig. 3A), similar to that detected in spleen. We also found no evidence for significant TRP depletion chronically in the plasma. In contrast, KYN levels (Fig. 3B) were significantly elevated both acutely (day 7 p.i., $p < 0.01$) and chronically (day 56 p.i., $p < 0.05$) in the plasma.

3HK levels (Fig. 3C) were actually below pre-infection values throughout infection, significantly so at day 42 p.i. ($p < 0.05$), whereas QUIN levels (Fig. 3D) were elevated throughout infection, reaching significance both acutely (day 7 p.i., $p < 0.001$; day 14 p.i., $p < 0.05$) and chronically (day 56 p.i., $p < 0.05$; day 70 p.i., $p < 0.05$). KYN/TRP ratios (Fig. 3E) were significantly elevated in plasma both acutely (day 7 p.i., $p < 0.0001$; day 10 p.i., $p < 0.001$) and terminally ($p < 0.01$). The paradox between induction of KYN and QUIN but decreases in 3HK could be due to either extremely rapid turnover of 3HK into 3HANA by the enzyme kynureninase (KYNU) in tissues and cells or alternative catabolism of KYN through anthranilic acid (AA). AA can then be converted to 3HANA and therefore rejoin the KYN pathway downstream of 3HK. Overall, the plasma data suggest that there are significant changes occurring in the KYN pathway of TRP catabolism during both acute and chronic infection, despite the paucity of metabolite changes during chronic infection in the spleen.

Systems-wide comparison of KYN metabolite changes during SIV infection

We next wanted to compare the overall flux of metabolites in the peripheral plasma and spleen side by side with our previous data on brain and CSF (Chapter II). Though the same animals were not used across all four tissue sites, the consistency of our model allows us to make reasonable comparisons between different groups of animals. The median fold changes from uninfected controls are represented for metabolites in plasma, CSF, spleen, and brain (Fig. 4A-D). The median micromolar values in the uninfected controls are displayed next to each metabolite in each graph.

For TRP, the largest decreases were found during acute infection, though the four compartments displayed slightly different kinetics: spleen TRP levels dropped to its lowest point at day 4 p.i., whereas the plasma, CSF, and brain all reached their lowest TRP levels later at day 10 p.i., when spleen levels had already normalized. During chronic infection (day 35 p.i. and onwards), CSF was the only compartment that consistently had levels of TRP below baseline. Brain tissue TRP in contrast was extremely stable, while plasma and spleen displayed some bounce but never led to any significant changes.

KYN and QUIN increased both acutely and chronically in all four compartments, with the spleen once again peaking the earliest during acute infection (days 4 and 7 for spleen vs. day 7 and/or 10 p.i. for the other compartments). Interestingly, 3HK was induced in spleen and brain both acutely and chronically, but in the CSF 3HK only displayed a small increase during acute infection and then returned to baseline, while plasma levels of 3HK were actually lower than baseline for much of the infection process.

Overall, despite different kinetics during acute infection and variable statistical significance, KYN and QUIN levels in plasma and CSF appeared to accurately reflect chronic changes occurring in KYN and QUIN levels in the spleen and brain, respectively. Plasma TRP was relatively predictive of spleen TRP changes, whereas CSF TRP was consistently lower than baseline in comparison to brain levels. Finally, 3HK levels were discordant between both plasma and spleen and CSF and brain. This was similarly shown in chapter II, where terminal CSF and terminal brain from matched animals correlated

strongly for KYN and QUIN, but did not correlate for 3HK and only weakly correlated for TRP ($p = 0.040$, r = 0.582).

Biphasic induction of IDO1 mRNA in longitudinal PBMCs correlates with plasma KYN/TRP ratios

Having established levels of TRP and KYN metabolites in longitudinal plasma and spleen, we next wanted to examine whether transcriptional changes in IDO1 matched the changes in metabolites. We therefore measured IDO1 expression in longitudinal PBMCs from the same five animals. *IDO1* was induced biphasically in the PBMCs, reaching levels significantly higher than controls at day 7 p.i. and terminally (both $p < 0.05$ by Friedman analysis). This induction of *IDO1* in the PBMCs positively correlated with KYN/TRP ratios in the plasma ($p < 0.0001$, r = 0.552). These data suggest that circulating PBMCs may contribute to release of metabolites in plasma, or at least accurately reflect secretion of metabolites from tissues into plasma.

Kinetics of IDO pathway enzyme expression during SIV infection in spleen

We next examined the relationship between metabolites and IDO1 in the spleen itself. While upregulation of *IDO1* expression in lymphoid tissues during HIV/SIV infection has been established (53, 116), it is currently unknown as to whether other enzymes in the KYN pathway are similarly regulated. Thus, we employed the Nanostring nCounter expression analysis system to analyze mRNA expression of key enzymes in the KYN pathway. We found that *IDO1* was significantly elevated during acute infection (day 4 p.i., $p < 0.001$; day 7 p.i., $p < 0.01$) but not during chronic infection (Fig. 1A).

Despite no chronic change in *IDO1*, we did find that *KMO* (Fig. 1B) and *KYNU* (Fig. 1C), enzymes that catabolize KYN into 3HK and 3HK into 3HANA, respectively, were significantly elevated both acutely and chronically (day 4 p.i., $p < 0.05$; day 7 p.i., $p < 0.001$; T, $p < 0.05$ for *KMO*) (day 4 p.i., $p < 0.05$; day 7 p.i., $p < 0.0001$; day 10 p.i., $p < 0.05$; T, $p < 0.05$ for *KYNU*). *HAAO*, which is responsible for the breakdown of 3HANA into 2-amino-3-carboxymuconic semialdehyde, the precursor for QUIN, remained unchanged throughout infection (Fig. 6D). We also measured RNA levels of SIV/17E-Fr, one of the two SIV strains used to inoculate the macaques, to determine whether induction of the KYN pathway enzymes followed changes in viral loads. Strikingly, SIV RNA (Fig. 1E) followed the pattern of induction of *KMO* and *KYNU* more so than *IDO1*: SIV RNA peaked at day 7 ($p < 0.0001$) during acute infection, then resurged at day 35 p.i. and remained significantly elevated throughout chronic infection (day 35 p.i., $p < 0.001$; day 42 p.i., $p < 0.01$; T, $p < 0.0001$). The fact that *IDO1* peaked earlier than virus during acute infection and was not upregulated chronically despite significant elevations in virus and other enzymes was surprising. However, *IDO1* expression correlated strongly with IDO activity (KYN/TRP ratios) in the spleen (Fig. 1F, $r = 0.614$, $P < 0.0001$) and in general followed the exact pattern of KYN/TRP induction shown in Fig. 2E, strong evidence that IDO1 is not strongly induced during chronic infection and is regulated transcriptionally in a distinct manner from KMO and KYNU.

Distinct patterns of kynurenine aminotransferase expression during SIV infection

In addition to the QUIN and NAD+ generating arm of the KYN pathway, KYN itself can also be alternatively metabolized in an offshoot of the pathway to kynurenic

acid (KYNA), mediated by several different kynurenine aminotransferases (KATs). We examined expression of three KATs in the spleens of our SIV-infected animals: *CCBL1* (*KAT I*), *AADAT* (*KAT II*), and *CCBL2* (*KAT III*). *KAT I* (Fig. 7A) did not change at all during infection, while *KAT II* (Fig. 7B) was significantly decreased both acutely (day 4 p.i., $p < 0.0001$) and terminally ($p < 0.01$). In contrast, *KAT III* (Fig. 7C) increased both acutely and chronically, with the chronic induction reaching significance at both day 42 p.i. ($p < 0.05$) and terminally ($p < 0.01$). Thus, despite the similar enzymatic roles of these KATs, each KAT displayed its own distinct pattern of regulation.

Relative contributions of various cell types to IDO1 and Mx expression

Our final question was to determine which cell types expressed the highest levels of *IDO1* during chronic infection in the spleen. In a pilot study, cells were teased from spleens taken at euthanasia from two animals with terminal infection, then stained with antibodies and sorted by FACS into five different populations: pDCs, mDCs, CD14+ mononuclear cells, CD4+ T cells, and CD8+ T cells. pDCs were identified as being CD123+/BDCA2+ double positive; mDCs were identified as being CD20-/BDCA1+, and CD14+ monocytes/macrophages were identified as being CD20-/CD3-/BDCA1-/CD14+ (Fig. 8A). T cells were sorted by dual expression of either CD3+/CD4+ or CD3+/CD8+ (Fig. 8B). RNA from these sorted cell types were analyzed for expression of *IDO1* and *Mx* mRNA with normalization to *GAPDH* mRNA.

mDCs were found to express the highest levels of IDO1 (Fig. 8C). The next highest expressers of *IDO1* were the CD14+ monocyte/macrophages, which nevertheless expressed only 10% of the *IDO1* seen in mDCs. pDCs, CD4+ T cells, and CD8+ T cells

had undetectable levels of *IDO1*. mDCs also had the highest expression levels of *Mx* (Fig. 8D), a representative IFN-stimulated gene. CD14+ monocyte/macrophages expressed roughly 50% of the Mx levels seen in mDCs, while CD4+ and CD8+ T cells expressed roughly 20-30% of mDC levels of Mx. pDC expression of Mx from these two macaques were highly variable, with one donor expressing nearly 70% of mDC levels of Mx, while the other donor expressed only 10%. Given that pDCs are typically the highest IFN-producing cells but decline in number and function in many patients during late stage infection (121), it is possible that this second macaque had pDCs with dysfunctional type I IFN responses.

Discussion

The findings presented here are the first to report that peripheral lymphoid tissues maintain TRP levels despite ongoing KYN pathway activation. Spleen concentrations of TRP remained stable, even while QUIN concentrations and *IDO1* enzyme levels significantly increased during acute infection in the spleen. We also did not find any significant changes in TRP in the plasma at any timepoint, even though levels of KYN, QUIN, and KYN/TRP ratios were significantly elevated both acutely and chronically in the plasma. Similar findings in plasma have been reported in a cynomolgus macaque model of HIV infection, where plasma levels of TRP declined slightly during acute infection but actually recovered to pre-infection levels by 3 months p.i. despite persistent, significant elevations in plasma KYN (122). Importantly, while our macaque model is rapidly progressive, the animals are euthanized prior to the onset of AIDS-defining clinical symptoms. In HIV-infected individuals, the dramatic 50% declines of plasma TRP are mostly confined to patients who have progressed to AIDS (123), while during the asymptomatic period of infection average TRP losses are only in the range of 10-15% (124). Thus, our animals may have experienced significant declines in TRP had the studies been carried out longer.

Intriguingly, brain levels of TRP also remained stable despite depletion of TRP levels in CSF and robust production of KYN metabolites in brain and CSF. Similar findings have also been reported in a mouse model of inflammation, where LPS induced depletion of TRP in plasma but not in the brain despite elevated KYN metabolites in both plasma and brain (96). Unfortunately most studies on HIV/SIV infection only report KYN/TRP ratios in plasma or CSF and not in tissues. It is possible that changes in TRP

in the tissues are being masked by their relatively higher concentrations at baseline (roughly 100 μM TRP in spleen, 22 μM in brain, 18 μM in plasma, and 3 μM in CSF in our study). A larger N may therefore be necessary in order to detect significant changes in TRP in the tissues and in plasma given their high starting concentrations in comparison to the CSF.

Alternatively, the lack of change in tissue TRP levels from our findings and from that of others (96) may suggest that cells within these tissues actively strive to maintain their intracellular concentrations of this essential amino acid. Reduced levels of TRP would be allowed to re-enter the circulation as a result. Indeed, we found that macrophages stimulated *in vitro* with IFNγ reduced extracellular levels of TRP from an average of 60 μM down to 30 μM while maintaining an internal TRP concentration of roughly 6 uM throughout the experiment. One possible mechanism for this is that IFNγ is also known to upregulate expression of tryptophanyl-tRNA synthetase (TTS), an enzyme that complexes intracellular TRP with the TRP-tRNA. Thus, cells exposed to IFNγ may simultaneously elevate expression of both *IDO1* and *TTS*, resulting in depletion of extracellular TRP levels while maintaining or even accumulating intracellular levels of TRP-tRNA complexes. Such accumulation of TRP-tRNA complexes could serve as an intracellular reservoir of TRP for protein synthesis (or perhaps other uses), while also protecting the IDO-expressing cells from anergy that occurs when uncharged tRNAs trigger induction of the GCN2 stress kinase pathway (37, 123, 125). Future studies should determine whether cells in tissue sites with active KYN metabolite production also express higher than normal levels of TTS.

Although TRP levels in the plasma and CSF were not good predictors of changes in TRP levels in tissue sites in our study, normalizing KYN to TRP strengthened the statistical significance rather than maintaining or weakening it in plasma, which suggests that even nonsignificant changes in TRP may still be biologically relevant. In general, both KYN and QUIN levels in plasma were good biomarkers for changes occurring in tissue sites. In contrast, changes in plasma 3HK did not predict changes in spleen, and even dipped significantly below pre-infection levels at day 42 p.i. A potential reason for the low levels of 3HK in the plasma may be that 3HK is turned over very rapidly in the tissues. In fact, *KYNU*, which is the enzyme that converts 3HK into 3HANA, was transcriptionally elevated both acutely and chronically in the spleen. Alternatively, KMO, which is the enzyme that synthesizes 3HK from KYN, can also convert KYN into AA in an offshoot of the pathway that sidesteps 3HK and rejoins with the generation of 3HANA. How KMO might selectively synthesize AA instead of 3HK during infection is unclear, although we did find that, like *KYNU*, *KMO* expression was upregulated both acutely and chronically in the spleen. Overall, plasma levels of KYN, QUIN and KYN/TRP ratios were good biomarkers for spleen KYN pathway activation, while TRP and 3HK were poor biomarkers.

In addition to KYN pathway metabolites, our results also shed light on the transcriptional regulation of KYN pathway enzymes during infection. We found that *IDO1* expression in the spleen actually peaked prior to the peak in spleen viral loads (day 4 vs. day 7 p.i.). Others have shown similar findings during acute infection in plasma of SIV-infected macaques, where IDO activity (KYN/TRP ratios) peaked before viral loads during acute infection and coincided with an acute spike in type I IFN levels (122).

However, type I IFN is not as proficient as type II IFN at inducing IDO *in vitro* (126), which we confirmed in monocyte-derived macrophages. Rather than type I IFN being responsible for the induction of IDO during acute infection, it is possible that this early and rapid peak of IDO before the peak in virus instead reflects rapid *downregulation* of IDO by the same mechanisms involved in the contraction of acute type I IFN responses. One such regulator is the suppressor of cytokine signaling (SOCS) family of proteins. SOCS proteins have been shown to inhibit Jak/Stat signaling, which is required for IDO expression, and can also directly target IDO for proteasomal degradation (127). Notably, SOCS proteins have been shown to be elevated in tonsillar tissue of HIV-infected patients (SOCS1, SOCS3) (128) and in the CNS of SIV-infected macaques (SOCS3) (129). Thus, even in the face of continued stimuli, IDO expression may be suppressed via activity of the SOCS proteins and may also help to explain why IDO expression is not significantly upregulated during chronic infection in the spleen.

In contrast, we found that *KMO* and *KYNU* were significantly upregulated both acutely and chronically. Expression of the further downstream enzyme *HAAO* remained stable. We also measured *IDO2*, *TDO2*, and *QPRT*, but expression of these enzymes was below background of our Nanostring assay. Our results are in line with a recent study on expression of KYN pathway enzymes *in vitro*, in which *IDO1*, *KYNU*, and *KMO* levels were highly upregulated in macrophages in response to IFNγ, while expression of *TDO2* and *QPRT* were induced to a lesser degree (130). The one major discrepancy was that in that study *HAAO* (also known as *3-HAO*) was also highly induced in the macrophages, whereas we did not see upregulation of *HAAO* in the spleens of our infected animals. This may have been due to the fact that *HAAO* levels were close to the background levels

of our assay. Given that the regulation of this enzyme is relatively unknown, further validation will be necessary in order to confirm its role in HIV/SIV pathogenesis.

In the offshoot of the KYN pathway that leads to generation of KYNA, we found that expression of three different kynurenine aminotransferases (KATs) displayed three different patterns of regulation during infection: *KAT I* (*CCBL1*) remained stable, *KAT II* (*AADAT*) decreased, and *KAT III* (*CCBL2*) increased during infection. The simultaneous up and downregulation of various KATs may be a reflection of specific cell type expression of these enzymes. Overall, the differential expression of the various enzymes in the KYN pathway suggest that while IDO1 may be the rate-limiting enzyme of this pathway, other enzymes may be strongly influencing the rate of production of particular metabolites.

Finally, we found that mDCs were the cell type in the spleen that expressed the highest levels of IDO1, followed by CD14+ monocyte/macrophages. pDCs, CD4+ T cells, and CD8+ T cells did not express detectable levels of IDO1, although this may have been due to the fact that we were using very small numbers of cells. Our finding that mDCs expressed high levels of IDO1 is in agreement with a previous study in HIV-infected patients in which staining for IDO protein in lymph nodes mostly colocalized with an mDC-specific marker (53). Overall, the fact that mDCs and CD14+ monocyte/macrophages expressed the highest levels of IDO1 in the chronically infected spleens suggests that antigen-presenting cells may continue to influence local T cell dynamics with generation of immunomodulatory KYN metabolites.

Overall, our findings highlight the importance of reporting separate KYN and TRP levels when discussing contributions of KYN pathway activation to the

pathogenesis of immune diseases. Given that extracellular levels of TRP must drop to below 3 μM in order to activate the GCN2 stress pathway in T cells (37), and the fact that we detected levels of TRP in the tissues well above this concentration throughout infection (100 μM for spleen, 20 μM for brain), it seems unlikely that TRP depletion is a major contributor to T cell dysfunction during HIV/SIV infection. However, it is still conceivable that in a tissue microenvironment, perhaps extracellular levels of TRP do reach such nadirs, or that chronic exposure to slightly lower-than-normal levels of TRP may have long-term consequences on T cell function that have not yet been discerned. Future studies will be needed in order to determine whether such microenvironments exist, and whether T cells in such niches are more impacted by TRP starvation or the generation of immunosuppressive KYN metabolites.

Figure 1. Macaque macrophages maintain intracellular TRP levels at the expense of extracellular TRP during KYN pathway activation. Pigtailed macaque macrophages were stimulated with 25 ng/mL IFNγ. After 0, 24, 48, and 72 hr, cell-free supernatants were harvested, and cell cultures were halved into aliquots for measurements of mRNA (IDO1) and metabolites (TRP, KYN, 3HK, and QUIN). To control for minor well-to-well variations in cell number that could affect metabolic turnover, intracellular and extracellular metabolites were normalized to intracellular and extracellular levels of the amino acid tyrosine (TYR), respectively. Data are represented as means +/- SEM of the fold change over unstimulated controls at each timepoint. The average raw micromolar value for each metabolite in the unstimulated controls is shown in parentheses on each graph. The dotted lines represent the unstimulated controls at each timepoint. Results are from 3 independent experiments from 3 different macaques, each with two cell culture technical replicates. (**A**) TRP levels in macrophage supernatants following IFNγ stimulation. (**B**) KYN, 3HK, and QUIN levels in macrophage supernatants following IFNγ stimulation. (**C**) Intracellular TRP from harvested cells following IFNγ stimulation. (**D**) Intracellular metabolites KYN, 3HK, and QUIN from harvested cells following IFNγ stimulation. (**E**) Intracellular and extracellular (supernatant) levels of KYN/TRP ratios, a surrogate for IDO enzyme activity, in macaque macrophages following IFNγ stimulation. (**F**) Intracellular IDO1 mRNA expression levels normalized to GAPDH mRNA in macrophage lysates following IFNγ or IFNβ stimulation as compared to unstimulated cells.

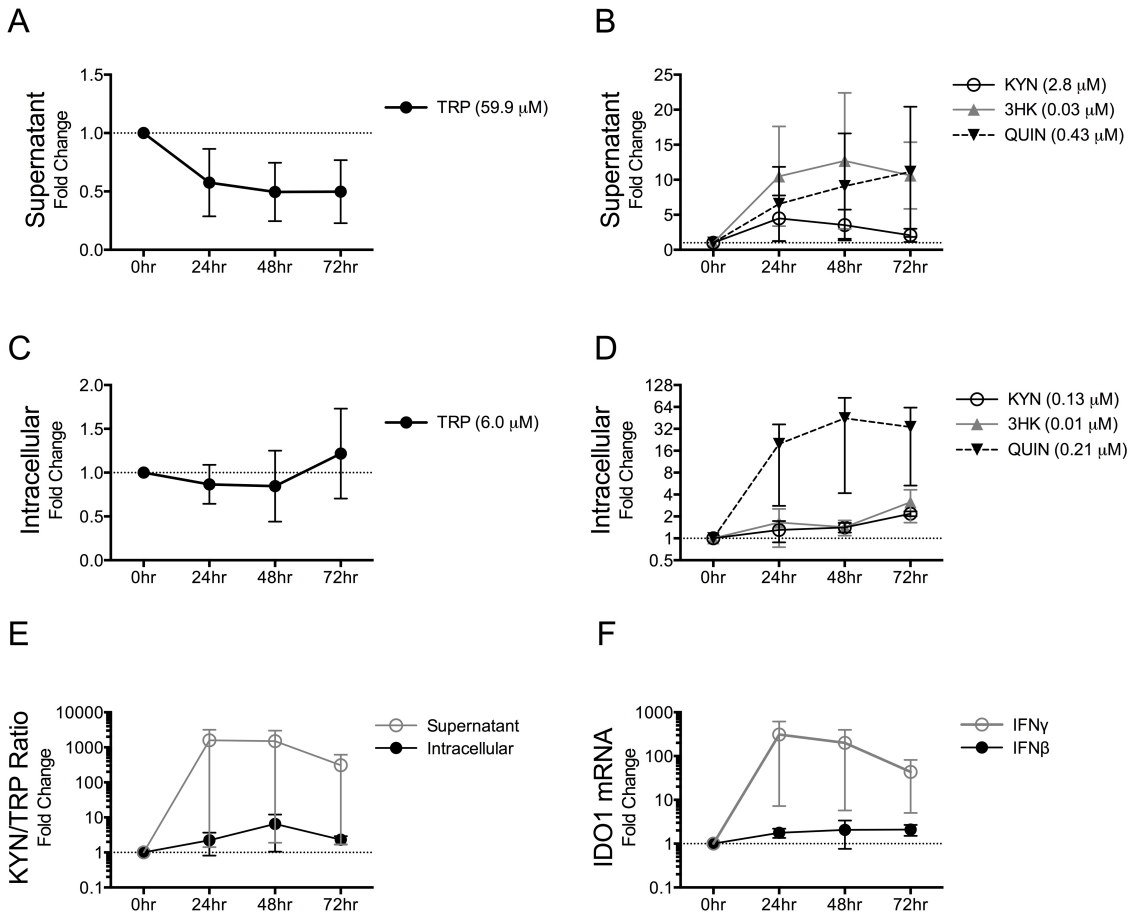
A
Supernatant
Fold Change
1.5
1.0
0.5
0.0
0hr
24hr
48hr
72hr
TRP (59.9 μM)
B
Supernatant
Fold Change
25
20
15
10
5
0
0hr
24hr
48hr
72hr
KYN (2.8 μM)
3HK (0.03 μM)
QUIN (0.43 μM)
C
Intracellular
Fold Change
2.0
1.5
1.0
0.5
0.0
0hr
24hr
48hr
72hr
TRP (6.0 μM)
D
Intracellular
Fold Change
128
64
32
16
8
4
2
1
0.5
0hr
24hr
48hr
72hr
KYN (0.13 μM)
3HK (0.01 μM)
QUIN (0.21 μM)
E
KYN/TRP Ratio
Fold Change
10000
1000
100
10
1
0.1
0hr
24hr
48hr
72hr
Supernatant
Intracellular
F
IDO1 mRNA
Fold Change
1000
100
10
1
0.1
0hr
24hr
48hr
72hr
IFNγ
IFNβ

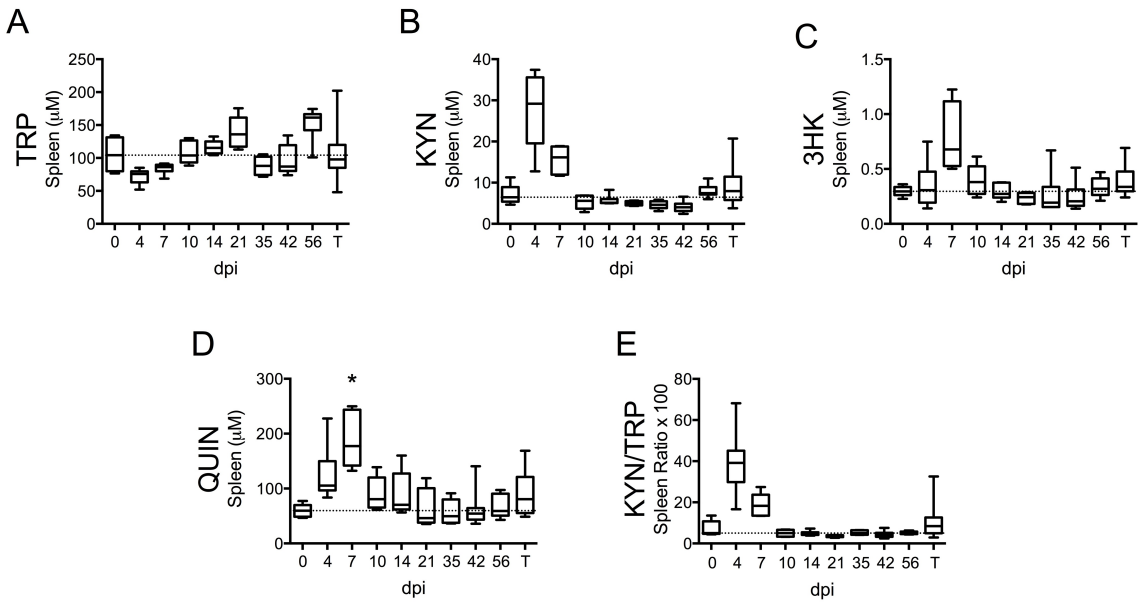

Figure 2. Longitudinal analysis of KYN pathway metabolites in spleens from SIV-infected pigtailed macaques. Archived spleen samples from 89 animals euthanized at various points during infection were analyzed for levels of TRP and KYN metabolites. (**A**) Tryptophan (TRP); (**B**) Kynurenine (KYN); (**C**) 3-hydroxykynurenine (3HK); (**D**) quinolinic acid (QUIN); (**E**) KYN/TRP ratio x 100. Dotted lines represent the medians of uninfected controls for each metabolite. Asterisks (*) represent timepoints that were significantly different ($p < 0.05$) from pre-infection values by Kruskal-Wallis test with Dunn's multiple comparisons correction. For exact *p*-values, see Supplementary Table 1.

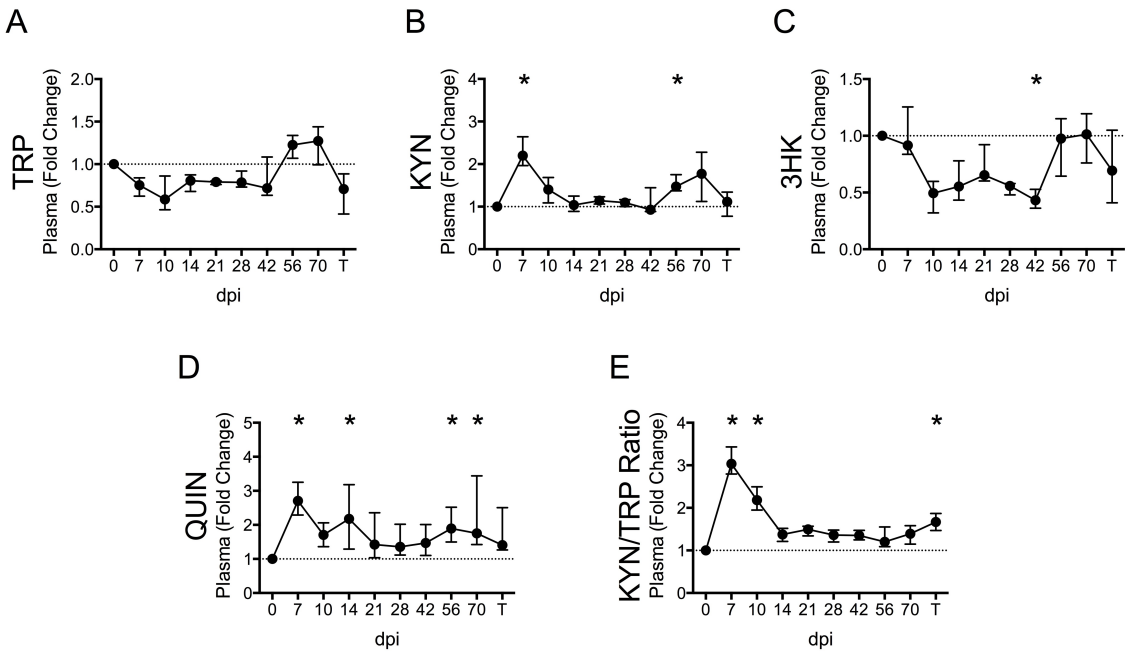

Figure 3. Longitudinal KYN metabolites in plasma during SIV infection of pigtailed macaques. Five pigtailed macaques were followed longitudinally, with 3 plasma samples taken prior to infection and 9 samples taken post infection at days 7, 10, 14, 21, 28, 42, 56, 70, and terminally (approximately 84 dpi). (**A**) Tryptophan (TRP); (**B**) Kynurenine (KYN); (**C**) 3-hydroxykynurenine (3HK); (**D**) quinolinic acid (QUIN); (**E**) KYN/TRP ratio x 100. Data are represented as median fold change over the average of the pre-infection samples for each animal. Error bars represent the interquartile ranges. Dotted lines represent the median of pre-infection values. Asterisks (*) represent timepoints that were significantly different ($p < 0.05$) from pre-infection values by Friedman's test with Dunn's multiple comparisons correction. For exact *p*-values, see Supplementary Table 2.

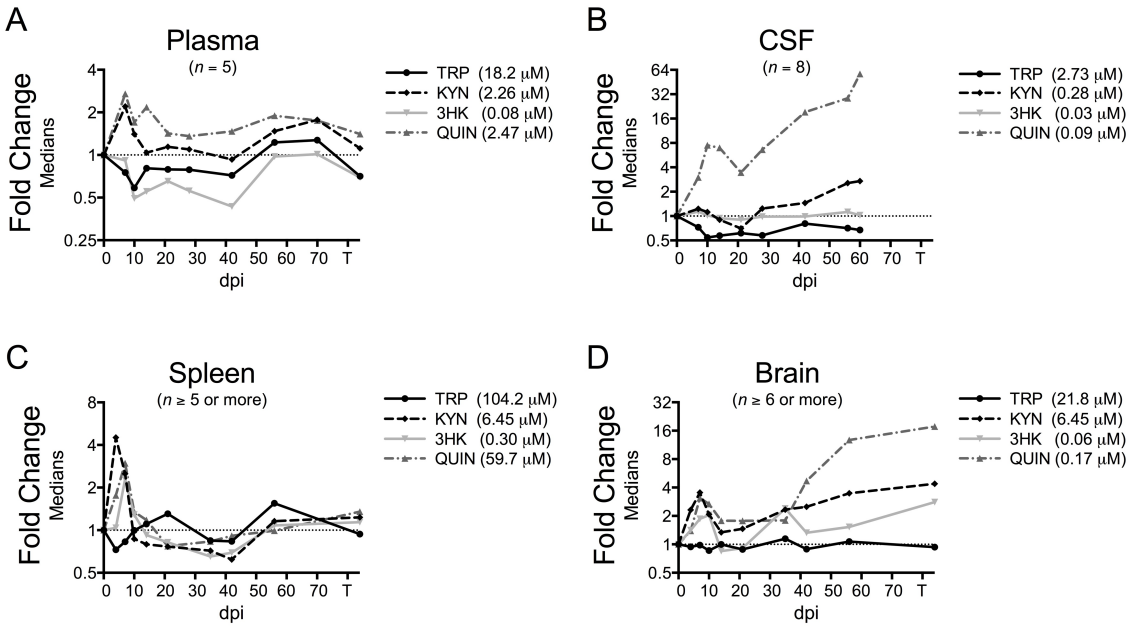

Figure 4. Comparison of changes in KYN pathway metabolites in plasma, spleen, CSF, and brain from SIV-infected pigtailed macaques. The median fold changes of each metabolite are overlaid for plasma (**A**), CSF (**B**), spleen (**C**), and the striatal region of the brain (**D**). The micromolar values in parentheses next to each metabolite in the figure legends represent the median of uninfected animals. The horizontal dotted line represents the median of uninfected animals.

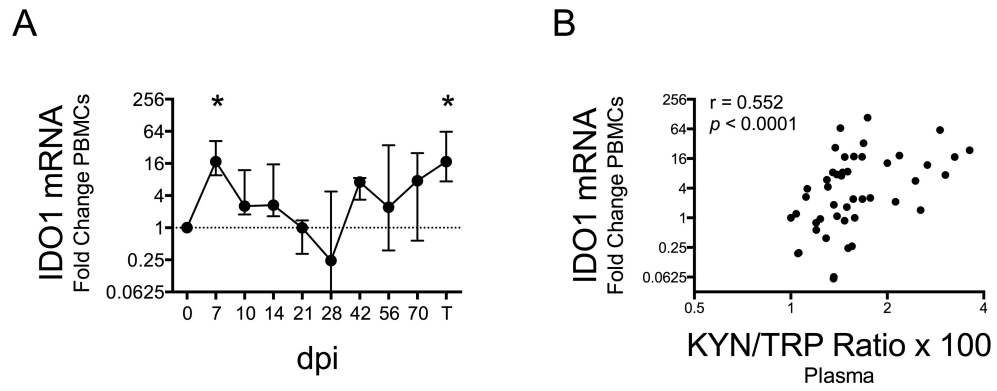

Figure 5. mRNA expression of IDO1 in PBMCs drawn longitudinally from SIV-infected pigtailed macaques. PBMCs drawn from the same 5 animals from which plasma was analyzed were harvested for mRNA expression of IDO1 (**A**). Each animal had 3 blood samples taken prior to infection and 9 samples taken post infection at days 7, 10, 14, 21, 28, 42, 56, 70, and terminally (approximately 84 dpi). Data are represented as median fold change over the average of the pre-infection samples for each animal. Error bars represent the interquartile ranges. Dotted lines represent the median of pre-infection values. Asterisks (*) represent timepoints that were significantly different ($p < 0.05$) from pre-infection values by Friedman's test with Dunn's multiple comparisons correction. For exact *p*-values, see Supplementary Table 3. (**B**) IDO1 expression in PBMCs was correlated to KYN/TRP ratios in matched plasma by Spearman's rank correlation.

Figure 6. Differences in transcriptional regulation of KYN pathway enzymes in spleens of SIV-infected pigtailed macaques. mRNA was harvested from spleens of animals euthanized at various points following SIV infection and analyzed for transcriptional expression of SIV RNA and enzymes in the QUIN/NAD+ producing axis of the IDO pathway of TRP metabolism. (**A**) Expression of *IDO1*, which mediates the oxidative cleavage of the pyrrole ring of TRP to form L-formylkynurenine, the precursor to KYN. (**B**) Expression of *kynurenine 3-monooxygenase* (*KMO*), also known as kynurenine 3-hydroxylase, which adds a hydroxyl group to KYN to generate 3HK. (**C**) Expression of *kynureninase* (*KYNU*), which catalyzes the hydrolytic cleavage of 3HK to form 3HANA and also catalyzes the cleavage of KYN to form anthranilic acid (AA; which then is hydroxylated to form 3HANA as well). In both reactions, the amino acid alanine is generated from the cleaved side product. (**D**) Expression of *3-hydroxyanthranilate-3,4-dioxygenase* (*HAAO*; also known as *3HAO*), which oxidatively cleaves the ring of 3HANA to form 2-amino-3-carboxymuconic semialdehyde, the precursor to QUIN. (**E**) Expression of SIV/17E-Fr *Gag* RNA. The dotted lines in graphs A-E represent the medians of uninfected controls. The shaded regions represent background thresholds of the assay, as determined by the average + 2SD of 8 spiked-in negative controls. Asterisks (*) represent timepoints that are significantly different ($p < 0.05$) from uninfected values by Kruskal-Wallis with Benjamini Hochberg correction and subsequent Dunn's multiple comparisons testing. For exact *p*-values, see Supplementary Table 4. (**F**) Spearman's rank correlation of IDO1 mRNA versus KYN/TRP ratios in spleen.

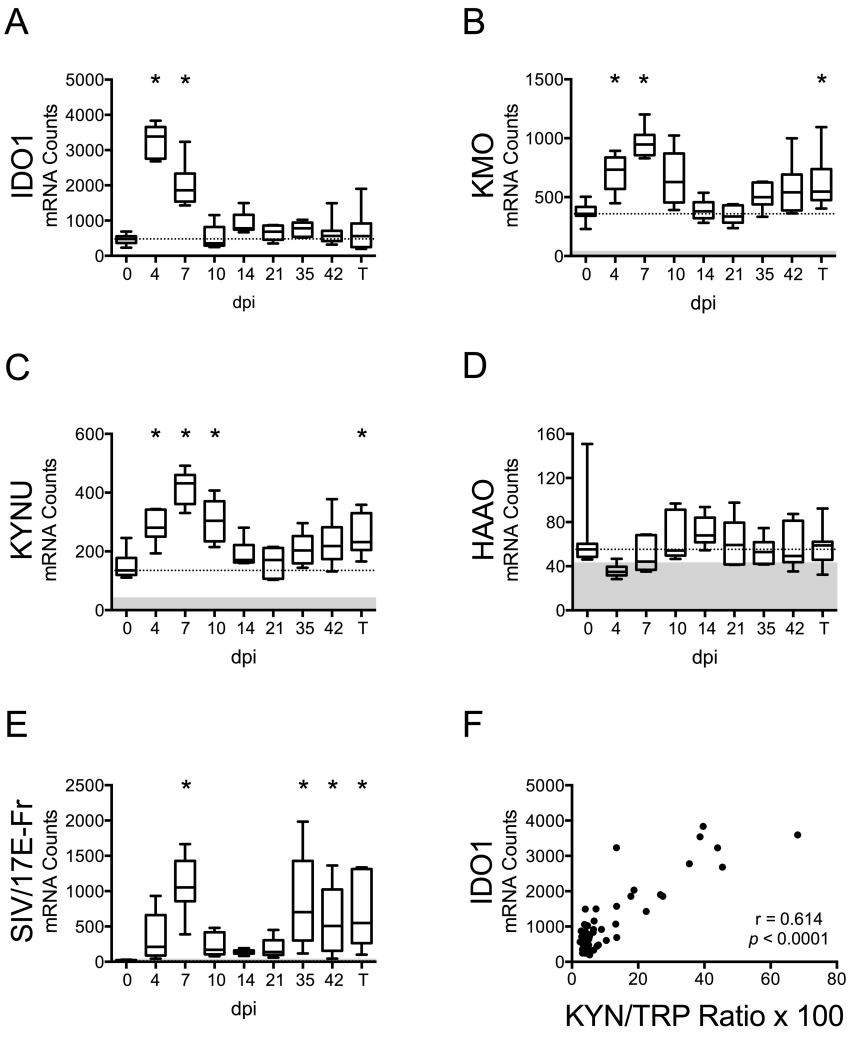
A
IDO1
mRNA Counts
5000
4000
3000
2000
1000
0
0 4 7 10 14 21 35 42 T
dpi
B
KMO
mRNA Counts
1500
1000
500
0
0 4 7 10 14 21 35 42 T
dpi
C
KYNU
mRNA Counts
600
400
200
0
0 4 7 10 14 21 35 42 T
dpi
D
HAAO
mRNA Counts
160
120
80
40
0
0 4 7 10 14 21 35 42 T
dpi
E
SIV/17E-Fr
mRNA Counts
2500
2000
1500
1000
500
0
0 4 7 10 14 21 35 42 T
dpi
F
IDO1
mRNA Counts
5000
4000
3000
2000
1000
0
r = 0.614
p < 0.0001
0 20 40 60 80
KYN/TRP Ratio x 100

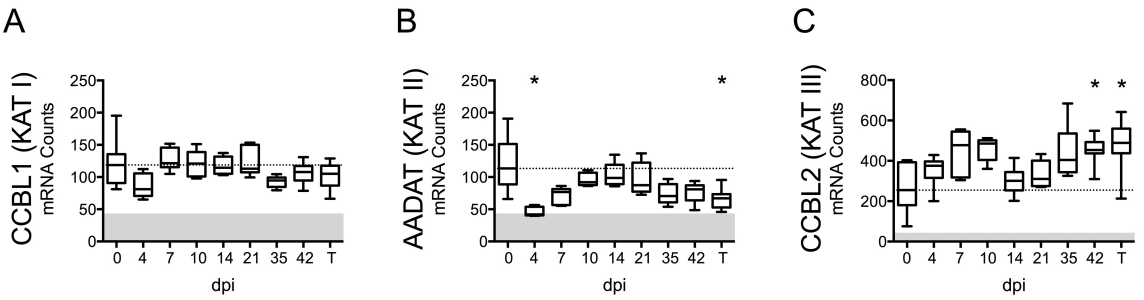

Figure 7. KAT II mRNA expression decreases while KAT III expression increases during SIV infection in spleen. mRNA from archived spleen samples were analyzed by Nanostring nCounter assay. (**A-C**) The expression levels of 3 kynurenine aminotransferases (KATs) responsible for conversion of KYN to KYNA in spleen are shown: *CCBL1* (*KAT I*), *AADAT* (*KAT II*), and *CCBL2* (*KAT III*). The dotted lines in all graphs represent the medians of uninfected controls. The shaded regions represent background thresholds of the assay, as determined by the average + 2SD of 8 spiked-in negative controls. Asterisks (*) represent timepoints that are significantly different ($p < 0.05$) from uninfected values by Kruskal-Wallis with Benjamini Hochberg correction and subsequent Dunn's multiple comparisons testing. For exact *p*-values, see Supplementary Table 4.

Figure 8. mDCs express the highest levels of *IDO1* and *Mx* mRNA in SIV-infected macaque spleen. Cells were teased out of spleen tissue from 2 animals at 84 days p.i., then sorted by FACS to separate pure populations of pDCs, mDCs, CD14+ monocyte/macrophages, CD4+ T cells, and CD8+ T cells. mRNA was extracted from the isolated cells and analyzed for *IDO1* and *Mx* expression levels. All data were normalized to internal *GAPDH* housekeeping mRNA and then to the highest expressing cell type, which were the mDCs in both data sets, by the ΔΔCt method. Fold change data were transformed to a percentage of the mDC values for IDO1 and Mx. Similar results were obtained with normalization to 18s ribosomal RNA. (**A**) Representative FACS gating for isolation of pDCs, mDCs, and CD14+ monocytes/macrophages (mons/macs) from spleen tissue. pDCs are BDCA-2+/CD123+; mDCs are BDCA-1+/CD20-; and mons/macs are CD20-/CD3-/CD14+/BDCA-1-. (**B**) Representative FACS gating for isolation of CD4+ and CD8+ T cells from spleen tissue. (**C**) Comparison of *IDO1* mRNA expression in various cell types. (**D**) Comparison of *Mx* mRNA expression in various cell types.

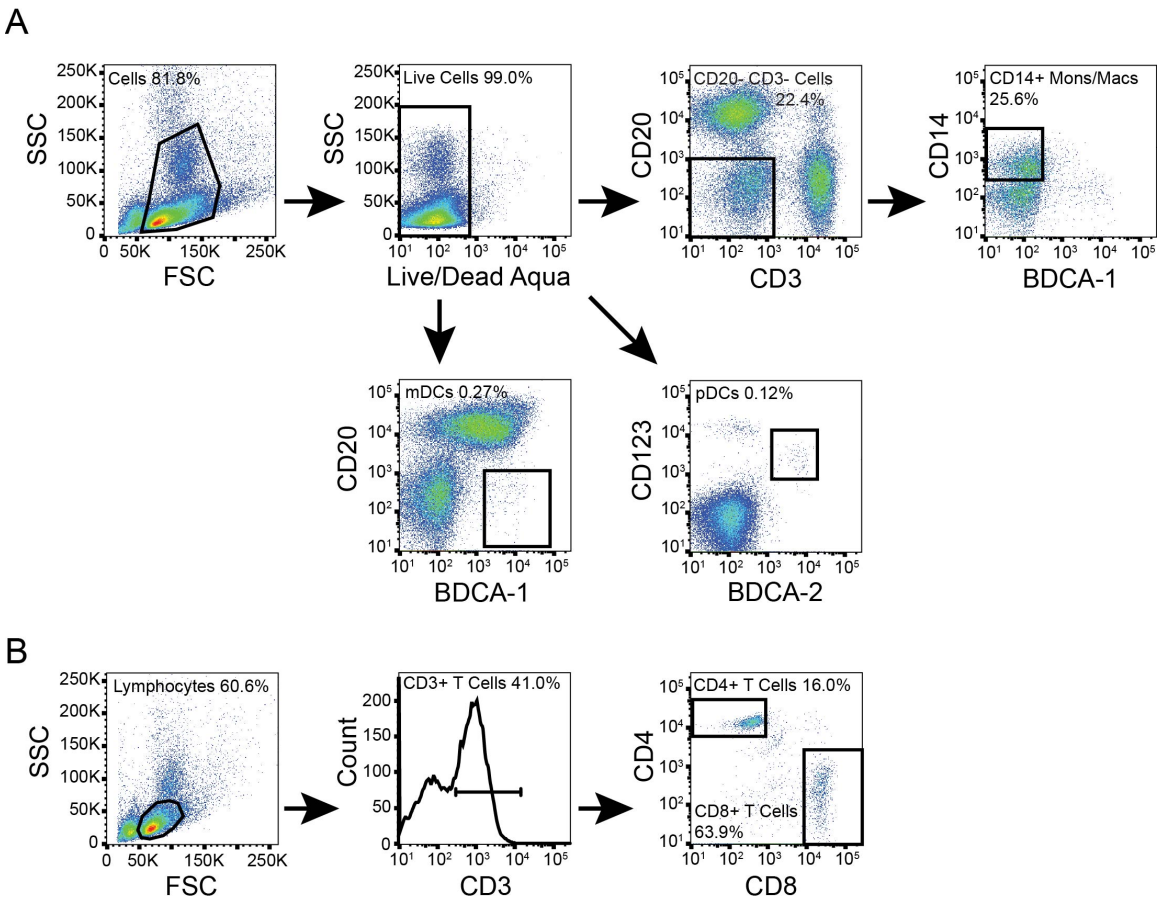
A
Cells 81.8%
SSC
FSC
Live Cells 99.0%
Live/Dead Aqua
CD20- CD3- Cells
22.4%
CD20
CD3
CD14+ Mons/Macs
25.6%
CD14
BDCA-1
mDCs 0.27%
CD20
BDCA-1
pDCs 0.12%
CD123
BDCA-2
B
Lymphocytes 60.6%
SSC
FSC
CD3+ T Cells 41.0%
Count
CD3
CD4+ T Cells 16.0%
CD4
CD8+ T Cells
63.9%
CD8

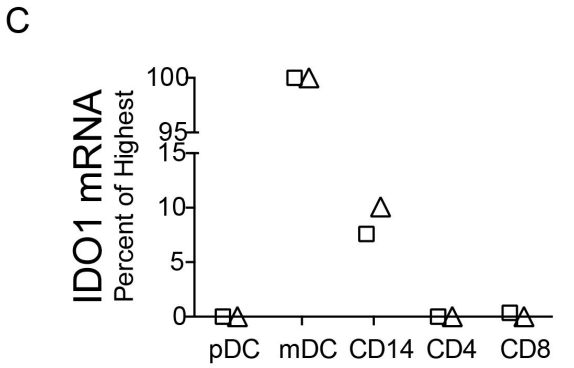
C
IDO1 mRNA
Percent of Highest
pDC
mDC
CD14
CD4
CD8

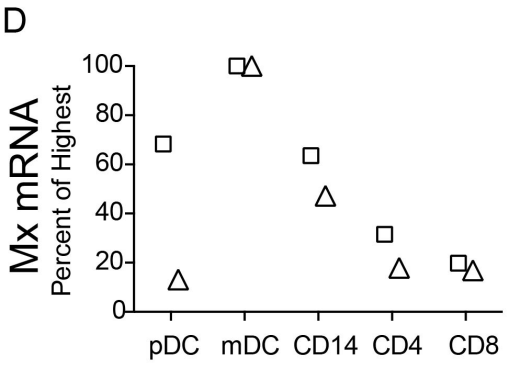
D
Mx mRNA
Percent of Highest
pDC
mDC
CD14
CD4
CD8

Analyte	Overall K-W p-value	Uninfected versus: 4 dpi	7 dpi	10 dpi	14 dpi	21 dpi	35 dpi	42 dpi	56 dpi	T
TRP	< 0.0001	ns	ns	ns	ns	ns	ns	ns	ns	ns
KYN	< 0.0001	ns	ns	ns	ns	ns	ns	ns	ns	ns
3HK	0.0003	ns	ns	ns	ns	ns	ns	ns	ns	ns
QUIN	< 0.0001	ns	< 0.01	ns	ns	ns	ns	ns	ns	ns
KYN/TRP Ratio	< 0.0001	ns	ns	ns	ns	ns	ns	ns	ns	ns

Supplementary Table 1. Kruskal-Wallis (K-W) with Dunn's post-test for longitudinal spleen metabolites.

Analyte	Friedman *p*-value	Uninfected versus: 7 dpi	10 dpi	14 dpi	21 dpi	28 dpi	42 dpi	56 dpi	70 dpi	T
TRP	0.006	ns	ns	ns	ns	ns	ns	ns	ns	ns
KYN	0.003	< 0.01	ns	ns	ns	ns	ns	< 0.05	ns	ns
3HK	0.003	ns	ns	ns	ns	ns	< 0.05	ns	ns	ns
QUIN	0.0008	< 0.001	ns	< 0.05	ns	ns	ns	< 0.05	< 0.05	ns
KYN/TRP Ratio	< 0.0001	< 0.0001	< 0.001	ns	ns	ns	ns	ns	ns	< 0.01

Supplementary Table 2. Friedman's test with Dunn's post-test on raw, longitudinal plasma metabolites.

	Friedman *p*-	Uninfected versus:							
Gene	value	7 dpi	10 dpi	14 dpi	21 dpi	28 dpi	56 dpi	70 dpi	T
IDO1	0.006	< 0.05	ns	ns	ns	ns	ns	ns	< 0.05
Mx	0.011	< 0.001	ns	ns	ns	ns	ns	ns	< 0.05

Supplementary Table 3. Friedman's test with Dunn's post-test for longitudinal PBMC expression data.

Gene	B-H corrected *p*-value	Uninfected versus:							
		4 dpi	7 dpi	10 dpi	14 dpi	21 dpi	35 dpi	42 dpi	T
SIV 17E-Fr	0.0008	ns	< 0.0001	ns	ns	ns	< 0.001	<0.01	< 0.0001
IDO1	0.0008	< 0.001	< 0.01	ns	ns	ns	ns	ns	ns
KMO	0.0008	< 0.05	< 0.001	ns	ns	ns	ns	ns	< 0.05
KYNU	0.0008	< 0.05	< 0.0001	< 0.05	ns	ns	ns	ns	< 0.05
HAAO	0.021	ns	ns	ns	ns	ns	ns	ns	ns
KAT I (CCBL1)	0.007	ns	ns	ns	ns	ns	ns	ns	ns
KAT II (AADAT)	0.0008	< 0.0001	ns	ns	ns	ns	ns	ns	< 0.01
KAT III (CCBL2)	0.0005	ns	ns	ns	ns	ns	ns	< 0.05	< 0.01

Supplementary Table 4. Benjamini-Hochberg (B-H) corrected Kruskal-Wallis with Dunn's post-test on longitudinal gene expression data in spleen.

CHAPTER IV.

Attenuation of pathogenic immune responses during infection with human and simian immunodeficiency virus (HIV/SIV) by the tetracycline derivative minocycline

This chapter has been accepted for publication in the journal PLOS ONE and is currently in the final proofing phase.

Abstract

HIV immune pathogenesis is postulated to involve two major mechanisms: 1) chronic innate immune responses that drive T cell activation and apoptosis and 2) induction of immune regulators that conversely suppress T cell function and proliferation. Both arms are elevated chronically in lymphoid tissues of non-natural hosts, which ultimately develop AIDS, but are not elevated chronically in natural hosts of SIV infection that avert immune pathogenesis despite similarly high viral loads. In this study we investigated whether minocycline could modulate these pathogenic anti-viral responses in non-natural hosts of HIV and SIV. We found that minocycline attenuated *in vitro* induction of type I interferon (IFN) and the IFN-stimulated genes indoleamine 2,3-dioxygenase (IDO1) and TNF-related apoptosis inducing ligand (TRAIL) in human plasmacytoid dendritic cells and PBMCs exposed to aldrithiol-2 inactivated HIV or infectious influenza virus. Activation-induced TRAIL and expression of cytotoxic T-lymphocyte antigen 4 (CTLA-4) in isolated CD4+ T cells were also reduced by minocycline. Translation of the *in vitro* findings to *in vivo* effects, however, were mixed as minocycline significantly reduced markers of activation and activation-induced cell death (CD25, Fas, caspase-3) but did not affect expression of IFNβ or the IFN-stimulated genes IDO1, FasL, and Mx in spleens of chronically SIV-infected pigtailed macaques. TRAIL expression, reflecting the mixed effects of minocycline on activation and type I IFN stimuli, was reduced by half, but this change was not significant. These results show that minocycline administered after infection may protect against aspects of activation induced cell death during HIV/SIV immune disease, but that *in vitro* effects of minocycline on type I IFN responses are not recapitulated in an aggressive *in vivo* model.

Introduction

In the absence of antiretroviral therapy, the majority of HIV-infected patients develop chronic immune activation, immunosuppression and eventually AIDS in a disease process representative of non-natural hosts (NNH) of HIV/SIV infection. In contrast, most natural hosts (NH) of SIV such as African green monkeys, gorillas, and sooty mangabeys avert immune pathogenesis despite high viral loads (131-134). One hypothesis for the different outcomes in NH versus NNH focuses on host immune responses to the virus. Documented immune differences include differential induction of type I IFN and IFN-stimulated genes (ISGs) such as TNF-related apoptosis inducing ligand (TRAIL), as well as the immune regulators cytotoxic T-lymphocyte antigen 4 (CTLA-4) and indoleamine 2,3-dioxygenase (IDO), all of which contribute to T cell dysfunction and potentially the development of AIDS (116, 118, 135-140). IDO activity and TRAIL (both soluble and membrane-associated) remain elevated even in patients on suppressive cART (7, 11, 141). In addition to their purported role in chronic HIV/SIV infection, many of these genes are also thought to be involved in the "cytokine storm" that contributes to pervasive inflammation, lymphocytopenia, and apoptosis during highly pathogenic influenza infections (142-145). These immune responses therefore represent potential therapeutic targets for not only HIV infection but also other pathogenic viral infections such as influenza.

In the first arm of HIV pathogenesis, hyperactive innate immune responses that are driven by viral stimulation of Toll-like receptors (TLRs) and other pattern recognition receptors lead to chronic ISG expression, cellular activation, and apoptosis. Type I IFN responses are critical in the control of many viral infections, as ISGs can directly inhibit

viral replication (146) and also stimulate adaptive immune responses (147). Although type I IFN can inhibit HIV replication *in vitro*, administration of exogenous type I IFN has only a moderate effect on HIV viral load and disease progression *in vivo* (148-152). Studies comparing NH and NNH have corroborated the hypothesis that hyperactive innate immune responses contribute to pathogenesis, as both NH and NNH express robust levels of ISGs during acute infection *in vivo* (135-137), but NH control this response within weeks while levels of IFNα mRNA and ISGs remain elevated in NNH throughout chronic infection (135-139). These ISGs include TRAIL and Fas ligand (FasL), which can induce apoptosis of uninfected CD4+ T cells expressing the cognate receptors death receptor 5 (DR5) and Fas, and programmed death ligand 1 (PDL1), which can induce apoptosis or exhaustion of CD8+ T cells expressing the corresponding receptor programmed cell death1 (PD1) (9, 153-155). Thus, despite the need for an early phase of IFN expression to stimulate adaptive immune responses and assist in the control of virus replication, chronic expression of type I IFN and ISGs likely does more harm than good in HIV/SIV infection of NNH (156).

In the second arm of HIV pathogenesis, induction of the immune regulators CTLA-4 and IDO suppresses the ability of T cells to proliferate and respond to antigen, further compromising immune responses already damaged by chronic ISGs. CTLA-4 is expressed on activated CD4+ T cells and CD4+Foxp3+ regulatory T cells (Tregs). These CTLA-4-expressing T cells convert DCs into regulatory DCs by ligating with B7 molecules and inducing IDO expression (157, 158). IDO also can be upregulated in plasmacytoid DCs (pDCs) by stimulation with pro-inflammatory cytokines such as IFNα, β, and γ, TNFα, or directly by HIV (27). Alternatively, long-term, chronic expression of

IDO in regulatory pDCs may be mediated by the anti-inflammatory cytokine TGFβ (30, 159). IDO-expressing pDCs mediate suppressive effects on T cells via 1) degradation/depletion of local tryptophan which prevents T cell proliferation and 2) generation of kynurenine and downstream metabolites that block T cell proliferation (52), induce T cell apoptosis (55, 160), and convert naïve CD4+ cells and Th17 cells into Tregs (53, 161). Thus, CTLA-4 and IDO work in tandem to increase the number and regulatory function of suppressive DCs and Tregs in lymphoid tissues. Notably, NNH with progressive infections have higher levels of CTLA-4, Foxp3, and IDO mRNA in their lymphoid tissues compared to non-progressors and uninfected individuals (116, 118, 140). These data suggest that CTLA-4+Foxp3+ Tregs accumulate in lymphoid tissues during progressive infection of NNH, where they can influence the function of DCs and other T cells, and thereby represent an important therapeutic target in preventing immune suppression in HIV (120).

Minocycline, a semi-synthetic tetracycline derivative, ameliorates the severity of a number of inflammatory diseases, including rheumatoid arthritis (162) and animal models of multiple sclerosis (163), amyotrophic lateral sclerosis (164), Huntington's disease (165), Parkinson's disease (166), allergy/asthma (167, 168), Japanese encephalitis virus (169), and SIV-associated neurological disease (60, 170). Minocycline's effects have been primarily attributed to its ability to decrease activation of a variety of immune cell types, including monocytes/macrophages, microglia, and T cells (62, 171-173). Additionally, many inflammatory cytokines can be downregulated by minocycline, including IL-6 (170, 174-176), IL-1β (175), TNFα (174-177), and IFNγ (176-178).

However, minocycline's effects on type I IFN responses and IDO have not been explored.

Here we show that minocycline prevented the pathogenic upregulation of type I IFN and IDO in pDCs following *in vitro* exposure to aldrithiol-2-inactivated (AT-2) HIV and prevented activation of CD4+ T cells after exposure to anti-CD3 and type I IFN, culminating in decreased surface TRAIL expression on both cell types. The AT-2 inactivated form of HIV was used in order to dissociate innate immune signaling from factors associated with productive infection because pDCs can be infected by HIV. Reductions in type I IFN and TRAIL with minocycline treatment were also observed in PBMCs exposed to either AT-2 HIV or infectious influenza virus. A trend towards reduced TRAIL expression was also seen in spleens from minocycline treated, SIV-infected pigtailed macaques and was accompanied by downregulation of the cellular activation marker CD25 and the apoptosis-promoting genes Fas and caspase-3. Notably, these changes in CD25, Fas, and caspase-3 upon minocycline treatment were not significantly different from the changes seen in animals treated with combination antiretroviral therapy (cART). However, minocycline did not reduce expression of ISGs in the SIV-infected spleens. Taken together, our data suggest that minocycline is capable of attenuating aspects of pathogenic immune responses during HIV/SIV infection and may be of use as an adjunct immunotherapy against hyperactive immune responses in diverse viral infections.

Materials & Methods

Ethics statement on human subjects

For *in vitro* experiments, blood was drawn from healthy human donors following their informed oral consent in accordance with the Johns Hopkins Medicine Institutional Review Board protocol NA 00014329 or via anonymous donor leukopaks from the Johns Hopkins University Outpatient Center or New York Blood Bank. The Johns Hopkins Medicine Institutional Review Board approved all experiments involving healthy human donors and approved the use of informed oral consent in place of written consent.

Ethics statement on animal subjects

All animal studies were approved by the Johns Hopkins Animal Care and Use Committee (IACUC protocol #PR12M310); all animals were humanely treated in accordance with federal guidelines and institutional policies. A total of thirty-four pigtailed macaques (*Macaca nemestrina*) were studied. Of the 34 animals, 7 were used as uninfected controls and 27 were inoculated intravenously with SIV/DeltaB670 and SIV/17E-Fr, as previously described (59). All animals were male with the exception of 2 procedural controls that were female. Eleven of the SIV-infected macaques received no drug treatment. Eleven of the SIV-infected macaques received minocycline at a dose of 4 mg/kg per day divided over two doses and administered orally starting at 21 days p.i. as previously described (60). No adverse effects due to minocycline treatment were observed in these animals. Five of the SIV-infected macaques received combination antiretroviral therapy (cART) beginning at day 12 p.i. which suppressed plasma viremia to <100 SIV RNA copy eq./mL by day 70 p.i. (63). The 4-drug cART regimen consisted

of 270 mg/kg of the protease inhibitor atazanavir (Bristol-Myers Squibb), 10 mg/kg of the integrase inhibitor L-870812 (Merck), and 205 mg/kg of the protease inhibitor saquinavir (Roche) administered orally twice/day; as well as 30 mg/kg of the nucleotide reverse transcriptase inhibitor PMPA (Gilead) administered subcutaneously once daily.

Macaques were housed in Johns Hopkins University facilities that are fully accredited by the association for the Assessment and Accreditation of Laboratory Animal Care, International, (AALAC). All housing met or exceeded guidelines of the National Institutes of Health "Guide for the Care and Use of Laboratory Animals" and the United States Department of Agriculture Animal Welfare Act. Macaques were fed a balanced, commercial macaque chow (Purina Mills, Gray Summit, MO, USA) once a day supplemented with a variety of food enrichment. Water was provided *ad libitum*. Macaques were provided with environmental enrichment including manipulanda, novel foodstuffs and movies/radio under the supervision of an enrichment specialist. Macaques were observed 1-2 times daily by trained laboratory and/or veterinary staff, and attitude, appetite and fecal consistency noted; macaques were weighed and plasma and CSF viral loads monitored at least once every two weeks. If abnormalities were noted, veterinary personnel were consulted and treatment initiated if necessary. Euthanasia was performed under veterinary supervision using an overdose of intravenous sodium pentobarbital while under deep ketamine sedation (10 mg/kg intramuscular), followed by perfusion with 1X PBS prior to tissue harvest. All infected, untreated macaques were euthanized during late-stage infection at approximately 84 days p.i., a timepoint at which the majority of infected animals develop encephalitis (179), or prior to this timepoint if macaques presented with clinical symptoms as previously described (101). Minocycline-

treated animals were also euthanized at approximately 84 days p.i.. cART-treated animals were euthanized at approximately 180 days p.i. after approximately 100 days of plasma virus suppression.

Minocycline dosage in vitro

A dose of 20 μM minocycline was chosen based on *in vitro* dose-response testing on pDC viability as well as a review of pharmacokinetic studies of patients given a commonly prescribed dose of minocycline (oral 200 mg/day), where plasma concentrations of minocycline reached 3.0 – 3.6 mg/L, roughly equivalent to 6-7 μM (180). Since minocycline is absorbed into tissues at a high rate (up to 10 times the amount in plasma) (181), an *in vitro* dose of 20 μM minocycline is a physiologically relevant concentration that could be feasibly obtained in tissue microenvironments.

PBMC isolation

Whole blood from healthy human donors was obtained in accordance with the Johns Hopkins IRB protocol NA 00014329 or via leukopaks from the Johns Hopkins University Outpatient Center or New York Blood Bank. PBMCs were isolated from whole blood via Ficoll-Hypaque density gradient centrifugation and red blood cell lysis (10 minute incubation at 37°C with 1X solution of the following 10X buffer: 4.15g NH_4Cl, 0.5g $KHCO_3$, 0.15 g EDTA dissolved in water and adjusted to pH 7.2-7.3 in a final volume of 500 mL). PBMCs were subsequently washed with HBSS with EDTA before further use.

pDC isolation and culture

pDCs were isolated from healthy human PBMCs via the Diamond pDC Isolation Kit (Miltenyi). Purity was consistently >95% as determined by BDCA-2 and CD123 flow cytometry staining. pDCs were plated at a density of 50,000 cells/well in flat-bottom 96-well plates in 150 µL RPMI 1640 supplemented with 10% FBS, 2 mM L-glutamine, 1 mM HEPES buffer, and 1% Pen-Strep (Invitrogen; final concentration 100 U/mL penicillin and 100 µg/mL streptomycin). Ten ng/mL IL-3 (R&D Systems) was added to the media daily. pDCs were co-treated with 20 µM minocycline hydrochloride (Sigma) dissolved in warm media and 300 ng/mL p24 equivalents of AT-2 HIV-1_{MN} (X4-tropic, strain P3935, AIDS and Cancer Vaccine Program, SAIC-Frederick, a gift of Dr. Jeffery Lifson and Julian Bess). After 18 hours, cell-free supernatants were collected and stored at -80°C and cells were either analyzed by flow cytometry or lysed for RNA extraction.

CD4+ T cell isolation and culture

CD4+ T cells were isolated from PBMCs by the Dynabeads FlowComp Human CD4 kit (Invitrogen). Purity was consistently >95% of live cells as determined by CD3 and CD4 staining by flow cytometry. CD4+ T cells were grown in 96-well plates or anti-CD3 coated 96-well plates (BD) with or without 20 µM minocycline hydrochloride (Sigma) in 100 µl RPMI 1640 supplemented with 10% FBS, 2 mM L-glutamine, 1 mM HEPES buffer, and 2 mg/mL gentamicin. After 24 hours, a 50 µL aliquot containing 60 µM minocycline was added to replenish minocycline at a final concentration of 20 µM in the 150 µL well volume. Some wells were also stimulated with 1,000 U/mL each of

IFNα-2a and IFNβ-1a (PBL). All wells had a final volume of 150 μL and were cultured for an additional 24 hours (total 48 hours) before flow cytometry analysis.

PBMC treatment with virus and minocycline

PBMCs were seeded in 24-well plates at a density of 4-5 million/mL in RPMI 1640 supplemented with 10% FBS, 2 mM L-glutamine, 1 mM HEPES buffer, and 10 U/mL recombinant IL-2 (BD Biosciences). Cells were treated with varying doses of minocycline hydrochloride (Sigma; 0, 20, or 40 μM) dissolved in warm media for two hours before adding varying doses of either AT-2 HIV (AIDS and Cancer Vaccine Program, SAIC-Frederick, a gift of Dr. Jeffery Lifson and Julian Bess) or infectious influenza virus (A/Hong Kong/68-X-31 (H3N2)). AT-2 HIV concentrations are shown as ng/mL p24 equivalents while influenza concentrations are shown as ng/mL nucleoprotein, as measured by the Influenza A Nucleoprotein Antigen Capture ELISA (Virusys). After overnight culture, cells were harvested for flow cytometry.

Flow cytometry

Cells were removed from plates with gentle pipetting, washed with 1 x PBS, and stained for 1 hour at room temperature in the dark. PBMCs were stained with TRAIL antibody and gated on lymphocytes by forward and side scatter profiles. Isolated pDCs were stained with Annexin V, TRAIL, and 7AAD antibodies to discriminate viable cells. Isolated CD4+ T cells were stained with CD3 and TRAIL antibodies and gated on the lymphocyte morphology gate as determined by forward and side scatter. All antibodies were from BD. Samples were washed with 1 x PBS to remove excess antibodies and run

on a BD FACSCalibur machine (pDC, CD4+ T cell experiments) with appropriate isotype controls or on a BD LSRFortessa (PBMC experiments). Data were analyzed by FlowJo software.

IFN ELISAs

Cell-free supernatants from pDCs were analyzed by ELISAs for IFNα (PBL Interferon Source #41100, which primarily recognizes 7/16 subtypes) and IFNβ (Invitrogen, with an extended initial incubation of 18 hours shaking at 4°C instead of 1 hour). Cell-free supernatants from PBMCs were analyzed by ELISAs for IFNα (PBL Interferon Source) and IFNβ (PBL Interferon Source). All plates were read on a microplate reader (BioRad) at the recommended wavelengths for each respective ELISA assay.

RNA extraction from pDCs

RNA from human pDCs was isolated using the RNeasy Plus kit (Qiagen) followed by treatment with RQ1 DNase (Promega) for 30 min at 37°C and inactivation with Stop Solution (Promega) for 10 min at 65°C.

RNA extraction from macaque spleen

RNA was harvested from 25 mg of snap-frozen macaque spleen tissue by RNA STAT-60 (Isotex Diagnostics) extraction, DNase treatment with RQ1 DNase (Promega) for 1 hour at 37°C, and finally purification with miRVana Kit (Invitrogen). RNA concentration was determined by NanoDrop (ThermoFisher) and subsequently diluted to

40 ng/μL for Nanostring nCounter gene expression analysis. All samples underwent RNA integrity testing, and samples with RNA integrity scores less than 5 were excluded.

qRT-PCR

RNA was reverse transcribed into cDNA with SuperScript III (Invitrogen). PCR amplification of cDNA was performed in a Chromo4 or CFX96 thermal cycler (both from BioRad) with Multiplex NoRox PCR Mix (Qiagen) and gene-specific primers and probes. Results were analyzed via the ΔΔCt method (182) with normalization to both 18S rRNA and negative controls. The following primers and probes were used for the *in vitro* human samples: IDO1 (5'- TGCTTTGACGTCCTGCTGG, 5'- TTCCTGTGAGCTGGTGGCA, and 5'- TXR - ATGCTGCTCAGTTCCTCCAGGACA - IAbRQs); Mx (5'- AGGAGTTGCCCTTCCCAGA, 5'- TCGTTCACAAGTTTCTTCAGTTTCA, and 5'- Hex - ACCAGCGGGCATCTGGTCACGA - BHQ1); 18S rRNA (5'- TAGAGGGACAAGTGGCGTTC, 5'- CGCTGAGCCAGTCAGTGT, and 5'- Cy5 - AGCAATAACAGGTCTGTGATG - BHQ2 or Crimson); IFNβ (5'- GCCTCAAGGACAGGATGAACTT, 5'- GCGTCCTCCTTCTGGAACTG, and 5'- Cy5 - CATCCCTGAGGAAATTAAGCAGCCGC - BHQ2). For some *in vitro* human samples, negative controls for IFNβ and IDO1 mRNA were not detectable and were assigned a Ct of 45 (limit of detection). The above sequences for IFNβ, Mx, and 18S as well as identical thermal cycling conditions were used for analysis of pigtailed macaque spleen RNA. Because IFNβ is an intronless gene, RNA samples underwent an additional DNase step with Turbo DNase (Invitrogen Life Technologies) for 30 min at 37°C to

eliminate any residual genomic DNA immediately prior to IFNβ testing. A subset of the macaque samples were normalized in a second reaction to the lymphocyte gene CD2 (Invitrogen Life Technologies TaqMan Assay Rh02839718_m1), which was one of the most stable transcripts in the Nanostring nCounter assay across the samples used in this study. Normalization to CD2 yielded similar results to those from 18S normalization.

Nanostring nCounter gene expression analysis

Nanostring analysis allows for the highly sensitive and reproducible detection of mRNA molecules without the need for enzymatic amplification (106). As part of a larger collaborative project, a CodeSet for 116 macaque genes (including the 7 transcripts analyzed in this manuscript as well as 11 putative housekeeping genes) for 96 samples were designed according to NanoString specifications based on rhesus macaque (*Macaca mulata*) and human sequences. Two hundred ng of each RNA sample were hybridized for 16 hours with the CodeSet, and genes were quantitated using the nCounter Digital Analyzer. Thirty-four of the 96 samples were examined in this study; the rest were excluded from the present analysis. Data were first normalized by the geometric mean of six spiked positive controls to correct for assay efficiency. Background was assessed as the average of eight spiked negative controls plus two standard deviations following positive control correction. Any genes with values below this threshold of 30 counts were excluded from the present analysis, with the exception of SIV 17E-Fr for which below threshold values were expected and obtained for uninfected and cART-treated animals. As no single housekeeping gene has been proven to be consistently expressed across different cell types, cell maturation states, tissue types, or disease models (107-111), we

used the Kruskal-Wallis non-parametric analysis of variance (ANOVA) test on all positive control normalized genes to find the three most stably expressed genes across our spleen samples (107, 112). We found that the lymphocyte markers CD7, CD2, and CD5 were the least varying genes between infection groups (p-values = 0.953, 0.937, 0.828, respectively). The geometric mean of these three genes was used to normalize the positive control corrected data (111). Alternative normalization to lymphocyte genes such as CD4 in HIV/SIV infected lymphoid tissue has been used in other studies as well (116-118). Similar results were obtained when our data was normalized to the most stably expressed housekeeping gene, ribosomal gene RPS9 (Supp. Fig. 1). All other traditional housekeeping genes in our panel (ACTB, B2M, GAPDH, HPRT1, HMBS, RPL13A, SDHA, TBP, UBC, and YWHAZ) had Kruskal-Wallis p-values < 0.100. Trends in SIV viral load and IDO1 mRNA expression in spleen have been independently verified for subsets of the animals by qRT-PCR and kynurenine/tryptophan metabolite ratios, respectively (data not shown).

Statistics

TRAIL and CTLA-4 in isolated pDCs and CD4+ T cells passed the Kolmogorov-Smirnov test for Gaussian distribution and were analyzed by paired t-test. ELISAs were analyzed by Wilcoxon paired t-test for nonparametric data. qRT-PCR data on *in vitro* experiments were analyzed by Wilcoxon paired t-test to compare different treatments. PBMC data on dose-response curves of minocycline with either AT-2 HIV or influenza were analyzed by two-way repeated measures ANOVA. *In vivo* spleen RNA data were

analyzed by the Mann-Whitney test for nonparametric, unpaired data. All tests were performed with Prism software (version 5 or 6).

Results

Minocycline attenuated IFN responses in pDCs

As diagrammed in Figure 1A, the elevated expression of type I IFNs and downstream ISGs such as TRAIL, FasL, and PDL1 in chronic infection of NNH compared to NH suggests that IFN responses are a point of divergence between pathogenic and nonpathogenic HIV/SIV infection and represent a potential target for immunotherapy (135-139). To test whether minocycline could modulate these hyperactive innate immune responses, we first exposed plasmacytoid dendritic cells (pDCs) to aldrithiol-2 inactivated HIV (AT-2 HIV) in the presence or absence of 20 μM minocycline. pDCs are the body's professional type I IFN-producing cells, and although their number and function in chronic HIV/SIV infection is controversial (183-186), during acute HIV/SIV infection pDCs are known to be recruited to lymphoid tissues where they contribute to the innate immune response (122, 187, 188). Because pDCs can be productively infected with HIV, we used AT-2 HIV to separate innate immune signaling from factors associated with productive infection (189).

Minocycline treatment prevented secretion of both IFNα (Fig. 1B; $p = 0.031$) and IFNβ (Fig. 1C; $p = 0.031$, respectively) by pDCs in response to AT-2 HIV stimulation, maintaining type I IFNs in the supernatant at nearly undetectable levels. We also examined IFNβ mRNA levels and found that minocycline-treated, AT-2 HIV-exposed cells exhibited significantly lower levels of IFNβ mRNA than cells exposed to virus alone (Fig. 1D; $p = 0.031$), indicating at least a partial block of the type I IFN response at the transcriptional level.

We also measured the expression of the ISGs myxovirus resistance A (Mx) and TRAIL in virus-exposed pDCs. Minocycline treatment reduced the median Mx mRNA expression to approximately half that induced by virus alone. However, this decrease in Mx was not significant (Fig. 1E; $p = 0.094$) despite reductions in 5 of 6 donors. Although there was incomplete suppression of Mx by minocycline, the ISG TRAIL was significantly downregulated by minocycline even in control samples without virus stimulation (Fig. 1F; $p = 0.048$). Minocycline also suppressed TRAIL (Fig. 1F; $p = 0.001$) to control levels in samples exposed to AT-2 HIV. The dosage of minocycline used in these studies (20 μM) did not affect pDC viability (Fig. 1G; $p = 0.563$, virus alone compared to virus + MC). These data confirm that minocycline inhibits IFN responses in isolated pDCs, decreasing their expression of TRAIL, which potentially inhibits their ability to cause TRAIL-mediated bystander T cell apoptosis.

Minocycline prevented activation-induced TRAIL expression on CD4+ T cells

Because TRAIL upregulation in T cells can be mediated by type I IFN and/or activation through the TCR (190), we stimulated isolated CD4+ T cells from healthy human donors with anti-CD3 alone or in combination with type I IFNs (IFNα-2a and IFNβ-1a) in the presence or absence of minocycline. TRAIL was upregulated on CD4+ T cells after 48 hours of activation with anti-CD3 alone (Fig. 1H; $p = 0.054$) and with anti-CD3 plus IFNα and β ($p = 0.002$) when compared to unstimulated controls. Minocycline prevented upregulation of TRAIL in response to both anti-CD3 alone and anti-CD3 with exogenous IFN ($p = 0.015$, $p = 0.020$, respectively). These data suggest that minocycline

can attenuate TRAIL upregulation *in vitro* via both inhibition of IFN signaling in pDCs and inhibition of activation signals through the TCR in CD4+ T cells.

Representative flow cytometry gating of isolated pDCs and CD4+ T cells

Representative flow cytometry gating for the purity of isolated pDCs and CD4+ T cells is shown in Figure 1I-J. The purity of isolated pDCs (Fig. 1I) was tested by first gating on general cells (which excludes debris) by forward scatter (FSC) and side scatter (SSC), then by dual labeling for CD123 and BDCA-2 according to the manufacturer's instructions to specifically identify pDCs from blood cell populations. The purity of isolated CD4+ T cells (Fig. 1J) was tested by using FSC and SSC gating for general cells (excluding cell debris), then for dual labeling with CD3 and CD4.

Representative flow cytometry gating on pDCs and CD4+ T cells following cell culture are shown in Fig. 1K-L. After 18 hours in culture, viability of the pDCs was examined by exclusion staining for Annexin V and 7AAD, markers for apoptosing and dead cells, respectively (Fig. 1K). TRAIL expression was then examined on the viable cell population (Annexin V-/7AAD-). A representative histogram of TRAIL expression in negative controls and AT-2 HIV stimulated cells with or without minocycline is also shown. pDC expression of TRAIL was high for all conditions examined; as a result, TRAIL data in Figure 1F was expressed as a percent change rather than percent positive. TRAIL expression on isolated CD4+ T cells following culture for 48 hours was analyzed by gating on lymphocyte morphology by FSC and SSC, then by the percentage of CD3+ T cells expressing TRAIL (Fig. 1L).

Minocycline attenuated HIV- and influenza-mediated type I IFN responses in PBMCs

We next investigated whether minocycline could inhibit type I IFN responses in PBMCs by treating healthy human PBMCs with 0, 20, or 40 μM minocycline and increasing amounts of AT-2 HIV. Cells were analyzed after 18 hours for TRAIL surface expression by flow cytometry, and levels of IFNα and IFNβ in the supernatants were measured by ELISA. AT-2 HIV stimulated the production and secretion of IFNα (Fig. 2A; $p < 0.0001$) and IFNβ (Fig. 2B; $p < 0.0001$) by PBMCs in a dose-dependent manner, culminating in upregulation of TRAIL surface expression on lymphocytes (Fig. 2C; $p < 0.0001$) that peaked with 300 ng/mL AT-2 HIV. Minocycline treatment decreased the production of IFNα (Fig. 2A; $p < 0.0001$) and IFNβ (Fig. 2B; $p < 0.0001$) and attenuated TRAIL upregulation in response to AT-2 HIV (Fig. 2C; $p = 0.006$).

To determine whether this effect was HIV-specific, and given the similarities in cytokine responses between HIV-1 and influenza, we stimulated PBMCs with varying doses of influenza virus with or without minocycline treatment. Influenza, like AT-2 HIV, induced robust IFNα (Fig. 2D; $p < 0.0001$), IFNβ (Fig. 2E; $p < 0.0001$), and TRAIL production (Fig. 2F; $p < 0.0001$) in the PBMCs. Minocycline treatment tempered this response, yielding significantly lower levels of IFNα (Fig. 2D; $p = 0.0004$) and IFNβ (Fig. 2E; $p = 0.0003$), which suggests that minocycline has a broad inhibitory effect on anti-viral IFN signaling in PBMCs. Minocycline also prevented influenza-mediated TRAIL induction on lymphocytes in the PBMCs in a dose-dependent manner (Fig. 2F; $p = 0.0003$), again suggesting that this effect is not specific to HIV.

Representative flow cytometry gating of TRAIL expression on lymphocytes in a PBMC culture is shown in Figure 2G for AT2-HIV stimulation and Figure 2H for

influenza (FLU) stimulation. In both cases, lymphocytes were gated on by FSC and SSC morphology. Flow cytometry scatter plots are representative of 4 experiments with AT-2 HIV and 3 experiments with influenza.

Minocycline prevented upregulation of CTLA-4 and IDO in CD4+ T cells and pDCs

As diagrammed in Fig. 3A, in the second arm of HIV/SIV pathogenesis CTLA-4 and IDO work in tandem to increase the number of suppressive DCs and Tregs in lymphoid tissues, further compromising immune responses already damaged by chronic ISGs (120). Because CTLA-4-expressing T cells can induce IDO in pDCs, we examined whether minocycline could modulate CTLA-4 expression *in vitro* by activating CD4+ T cells with anti-CD3 in the presence or absence of minocycline (Fig. 3B). Minocycline maintained CTLA-4 at very low levels after exposure to anti-CD3 compared to anti-CD3 stimulation alone ($p = 0.006$). These data are in agreement with previous studies that demonstrated that minocycline attenuates CTLA-4 expression (191) and other markers of CD4+ T cell activation (171, 172). However, IDO can also be induced in pDCs directly by virus or by cytokines such as type I IFN (27, 28). Therefore, we stimulated pDCs with AT-2 HIV in the presence or absence of minocycline and analyzed IDO1 mRNA expression. pDCs that were treated with virus and minocycline expressed significantly less IDO1 mRNA than with virus alone ($p = 0.031$). IDO2, a variant of IDO1 that also catabolizes tryptophan, was not detected in any of the samples (data not shown).

Representative flow cytometry gating of CTLA-4 expression on isolated CD4+ T cells for all four treatment conditions is shown in Fig. 3D. Cells were gated on by FSC and SSC morphology.

Minocycline downregulated activation-induced genes Fas, CD25, and caspase-3 but not IFN-stimulated genes in spleens of chronically SIV-infected pigtailed macaques

To determine whether our *in vitro* findings could be recapitulated *in vivo*, we examined whether minocycline had an effect on IFN, IDO, and apoptosis-inducing factors TRAIL, FasL, and Fas in archived spleen samples from SIV-infected pigtailed macaques (59). RNA was harvested from spleen from uninfected macaques, SIV-infected macaques in late stage infection, or SIV-infected macaques treated with either minocycline or cART and analyzed for viral RNA and various markers of immune activation.

We first measured the viral loads in the spleen because minocycline has previously been shown to reduce viral replication both *in vitro* and *in vivo* (60, 170) and can also inhibit HIV reactivation from latency (192). Minocycline reduced median viral loads in the spleens of SIV-infected animals by 50%, but this decrease was not significant (Fig. 4A; $p = 0.240$). Despite high levels of virus in the chronically SIV-infected animals, IFNβ expression in spleen was not significantly elevated above uninfected controls during chronic infection (Fig. 4B; $p = 0.157$, Uninf vs. SIV). This may have been due to the wide spread of IFNβ expression, with one control animal in particular having very high levels. Though IFNβ was not significantly increased during chronic infection, we also measured the ISG Mx as a surrogate marker of total type I IFN responses because even small amounts of type I IFN can induce robust downstream responses. Mx was significantly elevated in chronically SIV infected animals compared to uninfected controls (Fig. 4B; $p < 0.0001$). Minocycline treatment had no effect on IFNβ (Fig. 4B; $p = 0.638$) or Mx (Fig. 4C; $p > 0.999$) transcriptional expression compared to SIV alone.

Similarly, minocycline did not significantly reduce expression of IDO1 (Fig. 4D; p = 0.552) or the death ligands TRAIL (Fig. 4E; p = 0.170) and FasL (Fig 4F; p = 0.881) *in vivo*.

In contrast to the lack of effect on the death ligands TRAIL and FasL, minocycline potently downregulated expression of the death receptor Fas (Fig 4G; p = 0.003). Minocycline also significantly downregulated expression of the activation marker CD25 (Fig. 4H; p = 0.040) in the SIV-infected spleens. Finally, we examined expression of caspase-3, an important molecule in both extrinsic and intrinsic apoptosis signaling pathways, because several studies in a variety of disease models have demonstrated that minocycline alters caspase-3 transcription and activation (165, 193-195). In our SIV-infected macaques minocycline potently reduced caspase-3 mRNA levels (Fig. 4I; p = 0.003).

Comparison of minocycline with combination antiretroviral therapy (cART)

Given the significant effects of minocycline on various markers of activation-induced cell death in the spleens of SIV-infected macaques, we next determined how minocycline treatment compared to cART, the standard of care for HIV-infected individuals. cART treatment reduced the median expression levels of all genes back to uninfected levels, with the exception of IFNβ and FasL which were unchanged with either minocycline or cART treatment compared to spleens from SIV infected animals. As expected, cART treatment was significantly more effective than minocycline at reducing SIV viral load and the ISGs Mx and TRAIL in the macaque spleens (Fig. 4; MC vs. cART, p = 0.0005 for SIV, p = 0.0005 for Mx, p = 0.027 for TRAIL). Although

cART medians were consistently lower than minocycline's across all inflammatory genes, cART was not significantly more effective than minocycline at reducing expression of IDO1 (Fig. 4D; $p = 0.171$), FasL (Fig. 4F; $p = 0.908$), Fas (Fig. 4G; $p = 0.208$), CD25 (Fig. 4H; $p = 0.110$), or caspase-3 (Fig. 4I; $p = 0.411$).

Discussion

Differences between NH and NNH suggest that chronic induction of the IFN and IDO pathways are at the root of immune pathogenesis seen in HIV infection (120). In this study, minocycline had potent activity against IFN, IDO, and activation pathways in an acute model of HIV infection *in vitro,* which culminated in reductions in TRAIL expression on both pDCs and CD4+ T cells. We also observed reductions in IFN responses and TRAIL expression in minocycline-treated PBMCs exposed to either infectious influenza virus or AT-2 HIV. However, in spleens from chronically SIV-infected pigtailed macaques, minocycline did not affect IFNβ, Mx, IDO, TRAIL, or FasL but did significantly reduce activation-induced genes Fas, CD25, and caspase-3. Overall, these data suggest that minocycline attenuates markers of activation-induced cell death, a major component of HIV pathogenesis, but that testing of inhibition of type I IFN responses is more complex than can be discerned from our *in vitro* model.

In our *in vitro* model of acute infection, minocycline blocked both IFN- and activation-induced TRAIL, as seen by inhibition of AT-2 HIV-triggered IFNα and IFNβ responses in pDCs as well as prevention of TRAIL upregulation on CD4+ T cells activated with αCD3 antibody. The suppression of pDC IFN production could also be linked to modulation of pDC activation by minocycline; this will need to be confirmed in future studies. Importantly, minocycline also prevented TRAIL upregulation on CD4+ T cells stimulated with both αCD3 antibody and exogenous IFNα and IFNβ. These data showed that minocycline suppressed TRAIL even in a complex immune environment consisting of both TCR activation and IFN signals and led us to examine TRAIL in the chronically infected spleens.

Minocycline reduced TRAIL expression in the SIV-infected spleens by 50% but this change was not significant. This partial inhibition of TRAIL is consistent with our data that showed minocycline blocked only one of the two modes of TRAIL induction *in vivo*; i.e., minocycline reduced cellular activation (Fas and CD25) but did not reduce type I IFN responses (neither IFNβ nor the ISG Mx). Mechanistically, TRAIL upregulation on T cells through TCR activation/signaling is dependent on protein kinase C (PKC) translocation and Ca^{2+} mobilization (196). Minocycline has previously been shown to inhibit these two mechanisms in other cell types and in isolated mitochondria (197-199), suggesting that the effects we observed on activation-induced TRAIL in T cells might be due to inhibition of PKC and/or Ca^{2+} mobilization by minocycline.

Despite not finding evidence for blockade of type I IFN signaling in the SIV-infected spleens, our experiments with influenza virus showed that minocycline's inhibitory effects on type I IFN and TRAIL in *in vitro* PBMCs were not specific for inactivated viruses nor were they specific for HIV. These results are compelling because a cytokine storm is widely associated with influenza pathogenesis. Additionally, two groups recently reported that pDCs may participate in the cytokine storm observed in pathogenic influenza infections (142, 200), which posits a need for therapeutics that could modulate pDC cytokine responses in pathogenic influenza as well as HIV infection. Future studies must address whether minocycline's inhibition of influenza-induced IFN responses *in vitro* can be recapitulated in an *in vivo* model or suffer from the same pitfalls as translation of HIV-induced IFN responses from *in vitro* to *in vivo*.

In contrast to the lack of an effect on type I IFN responses in the SIV-infected spleens, minocycline treatment showed a trend towards reduced SIV RNA levels in

spleen compared to infected, untreated animals, reducing viral loads by approximately 50%. Previous studies from our group and others have demonstrated that minocycline reduces viral replication in macaques and a humanized mouse model of HIV infection, as well as *in vitro* in human and macaque primary macrophages and lymphocytes (60, 170, 191, 192). However, in a recent pilot study of seven HIV-infected individuals not on anti-retroviral therapy, viral loads in both CSF and plasma were unchanged with an eight-week course of minocycline treatment (201). Thus our findings of a trend towards reduction of viral loads in the spleens of SIV-infected animals may reflect a broader picture that is emerging of a more marginal effect of minocycline on viral loads during chronic infection, particularly in patients, than previously proposed.

Given the trend towards reduced splenic viral loads *in vivo* and minocycline's robust inhibition of type I IFN responses in our *in vitro* model of acute infection, our finding that minocycline had no effect on IFNβ, Mx, or IDO transcript levels in the chronically infected spleen samples was surprising. IDO is induced by several other cytokines, including IFNγ and TFNα, but these have also been shown to be reduced by minocycline in *in vitro* studies (174, 175, 178, 202) as well as in a mouse model of vaginal mucosal inflammation (177). However, in a pilot study in HIV-infected patients, minocycline did not affect plasma or CSF levels of neopterin, a marker of macrophage/microglial activation that is also induced by IFNγ (201). It is possible that a higher dose of minocycline would be required to recapitulate *in vitro* findings for IFN and ISGs such as IDO *in vivo*.

Alternatively, it was recently reported that HIV-infected cells may serve as a more potent stimulator of type I IFN in PBMCs than cell-free virions (203). It is

conceivable that minocycline may not have as strong of an effect on IFN signaling mediated through contact with infected cells as opposed to free virus. In a pilot experiment with three donors using HIV-infected peripheral blood leukocytes co-cultured with autologous target PBMCs, minocycline inhibited TRAIL induction in pDCs but not in T cells as examined by flow cytometry (unpublished data). In contrast, minocycline reduced TRAIL induction in both pDCs and T cells from the same three donors after exposure to the toll-like receptor (TLR) 3 agonist poly I:C, suggesting that minocycline's efficacy against type I IFN signaling may be dependent on both the cell type and source of immune stimuli.

Additionally, there may be differences in the mechanisms for IFN and ISG production during acute versus chronic SIV/HIV infection. For example, while pDCs are known to be major contributors to IFN responses in acute infection (122, 187, 188), their number and function in chronic infection is controversial, with some studies reporting higher numbers and/or higher IFN-producing capabilities of pDCs in chronically infected tissues (122, 183-185, 204), while others have reported depletion and/or dysfunction of pDCs in chronically infected tissues (186, 205). Chronically infected animals also tend to have a smaller type I IFN fold induction compared to acutely infected animals (206-208), perhaps in part because of pDC dysfunction. In addition to different cellular sources of IFN, other variables potentially explaining the discordant findings on minocycline's effectiveness against type I IFN responses *in vitro* versus *in vivo* include tissue selection, stage of disease, virus subtype, noncanonical IFN signaling (209) or alternative signaling pathways leading to ISG expression such as the TGFβ/IDO axis (30, 210).

We focused on TRAIL, a TNF family death ligand, as a representative downstream interferon effector molecule (Fig. 1A) in this study because it is consistently elevated in SIV/HIV infection of NNH (6, 9, 139, 211-214). However, there is controversy over the expression of TRAIL's death receptors, DR4 and DR5. Stary *et al.* and Kim *et al.* reported elevated DR4, but not DR5, by flow cytometry of circulating CD4+ T cells from HIV-infected patients (9) and SIV-infected rhesus macaques (214). Herbeuval *et al.* demonstrated elevated DR5 mRNA expression in tonsillar lymphoid tissues from HIV progressors compared to nonprogressors (139). In contrast, Chehimi *et al.* were unable to detect significant changes in DR5 by flow cytometry of CD4+ T cells from viremic individuals (7).

Because of these controversies surrounding DR4 and DR5 expression, we also examined expression of Fas and FasL in the SIV-infected spleens. Similar to TRAIL induction, Fas and FasL are highly regulated at the transcriptional level by either TCR activation or type I IFN signaling (196, 208, 215, 216), although *in vivo* data in mice suggests that FasL expression is more susceptible to IFN signaling than Fas (217). We found that minocycline potently suppressed Fas ($p = 0.003$) but did not change FasL expression, consistent with our findings that minocycline reduced activation genes such as CD25 but not type I IFN *in vivo*. These data also support a greater role for IFN in the induction of death ligands than death receptors as others have found (217).

Finally, we also examined expression of caspase-3, a downstream mediator of both intrinsic and extrinsic apoptosis pathways that has been shown to be elevated in HIV/SIV infection (10, 218). Additionally, minocycline's protective effects against apoptosis in neurodegenerative diseases (164, 165) and fulminant hepatitis (193) have

recently been attributed, in part, to reductions in caspase-3 expression and activation (165, 193-195). We reproduced those findings in SIV-infected pigtailed macaques, demonstrating that minocycline-treated animals had significantly lower caspase-3 expression than infected, untreated animals ($p = 0.003$). By inhibiting caspase-3 expression, minocycline may attenuate not only TRAIL-mediated apoptosis but also other mechanisms of cell death. However, caspase-3 is also regulated at the protein level, and minocycline treatment did not completely reduce caspase-3 expression to uninfected control levels, so some degree of apoptosis could continue.

In comparison to minocycline, cART-treated animals consistently had lower expression of inflammatory and apoptotic genes, although only SIV 17E-Fr, Mx, and TRAIL mRNA levels were significantly different between the two treatments. The difference between splenic viral loads is not surprising ($p = 0.0005$, MC vs cART), because cART inhibits virus replication directly, whereas minocycline mediates its anti-viral effects indirectly by reducing cellular activation and thereby reducing the susceptibility of cells to infection. However, minocycline did reduce Fas, CD25, and caspase-3 to levels that were not significantly different from those of cART-treated animals. The overall modulation of the genes in this study, combined with other published mechanisms in HIV/SIV models (60-62, 170, 191, 192, 219, 220), suggests that immunomodulatory drugs such as minocycline might provide an important adjunct to cART (192).

However, despite the promising results obtained with minocycline in several animal models of inflammatory disorders, pilot studies in HIV-infected individuals have yet to yield significant changes in inflammatory markers such as neopterin, CCL2, or

cognitive impairment (201, 221, 222). Longer trials and perhaps earlier dosing with minocycline may be necessary, as the importance of early versus late initiation of minocycline treatment has been previously demonstrated (61). In the present study, minocycline treatment was initiated at 21 days p.i., an asymptomatic timepoint occurring after the acute phase of infection but before the establishment of chronic infection and emergence of clinical symptoms. This is in contrast to the recent clinical trials, in which treatment was given to patients already displaying evidence of advanced, chronic infection (indicated by low CD4 counts, time since HIV diagnosis, and/or presence of neurocognitive impairment) (201, 221, 222). Thus, particular attention should be paid towards whether minocycline can *prevent* immune pathogenesis as compared to reversing it. Future studies should also determine which of the myriad properties of minocycline are critical for its beneficial effects on HIV/SIV pathogenesis in animal models; these findings could then assist in discovery of drugs with enhanced pharmacological properties to improve efficacy in human trials.

The need for an adjunct for cART stems from evidence that, despite robust suppression of viral replication, small elevations in genes such as TRAIL (6-8), DR4 (8, 9), DR5 (6), Fas (6), FasL (6), caspase-3 (10), and IDO activity (11) persist in patients on cART, although these differences are not always significant and vary between cell and tissue types examined. Remarkably, in this study we found that cART treatment restored inflammatory gene expression back to uninfected control levels in spleen, with the exception of IFNβ (which was not significantly different between uninfected animals and chronically infected animals) and FasL. Additionally, despite viral suppression, one of the five cART treated animals consistently had higher gene activation than the rest of his

group and may have been a candidate for adjunct therapy. The lingering immune activation seen in this animal may be analogous to the residual immune activation seen in some patients on cART, activation that is thought to contribute to comorbidities such as HIV-associated neurological disease. We propose the further study of immunomodulatory agents as adjuncts to cART, with the goal of reducing chronic immune activation back to uninfected control levels and improving the quality of life of HIV-infected individuals. Finally, our results with influenza, in conjunction with a recent report on the protective anti-inflammatory effects of doxycycline during influenza-associated pneumonia in mice (223), suggest that the tetracycline class of compounds may be useful in other viral diseases as well in which robust inflammatory cytokine responses and immune hyperactivation are associated with pathogenesis.

Figure 1. Minocycline prevents TRAIL upregulation in pDCs and CD4+ T cells by attenuating anti-viral IFN and activation responses. (**A**) pDCs become activated in response to TLR7/9 stimulation by HIV and secrete type I IFN, which in turn upregulates ISGs on leukocytes, including the TNF family members TRAIL and FasL and the B7 family member PDL1. These ligands induce apoptosis and/or exhaustion on target cells expressing the cognate death receptors (TRAIL/DR5; FasL/Fas; PDL1/PD1). (**B - G**) pDCs were isolated from blood of healthy human donors and exposed to 300 ng p24 eq./mL of AT-2 HIV with or without 20 μM minocycline for 18 hours (n = 6 different donors). (**B**, **C**) IFNα and IFNβ protein from pDC supernatants were measured by ELISA. (**D**) IFNβ mRNA was measured by qRT-PCR. (**E**) Mx mRNA and (**F**) TRAIL were measured as examples of ISGs by qRT-PCR and flow cytometry, respectively. (**G**) Viability of pDCs was determined by Annexin V/7AAD staining. (**H**) CD4+ T cells were isolated from blood of healthy human donors and activated with anti-CD3 with or without 20 μM minocycline (n = 6 different donors). After 24 hours, minocycline was replenished and some wells were additionally stimulated with IFNα and IFNβ. TRAIL was measured by flow cytometry after an additional 24 hours. (**I**) Representative flow cytometry gating of pDC purity by BDCA2+/CD123+ double staining immediately following isolation. (**J**) Representative gating of CD4+ T cell purity immediately following isolation by CD4+/CD3+ double staining. (**K**) Representative gating of pDC viability (Annexin V-/7AAD-) and TRAIL expression after 18 hours of stimulation in culture with virus and/or minocycline. (**L**) Representative gating of TRAIL expression in CD4+ T cells following 48 hours in culture.

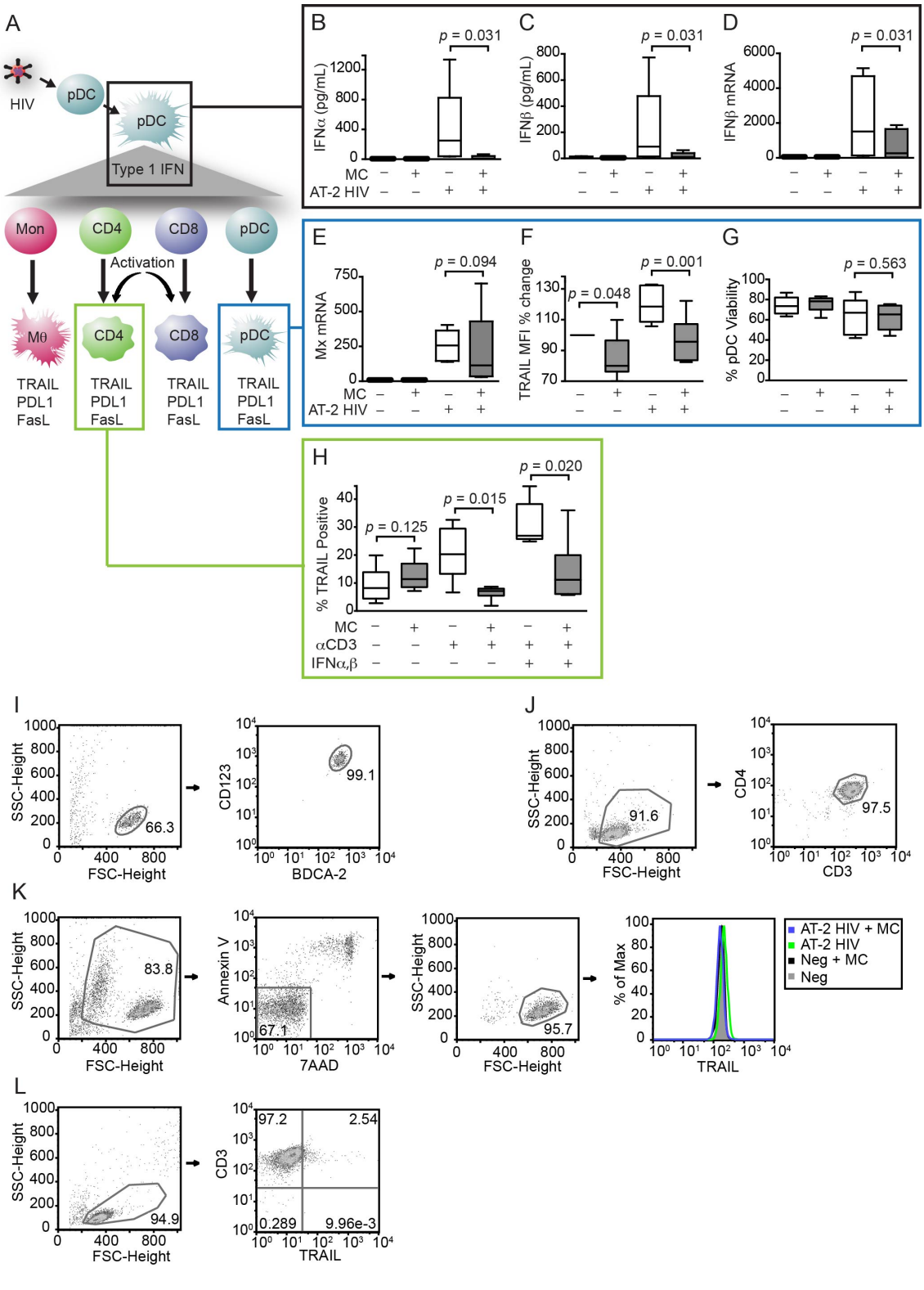
A
HIV
pDC
pDC
Type 1 IFN
Mon
CD4
CD8
pDC
Activation
Mθ
CD4
CD8
pDC
TRAIL
PDL1
FasL
B
p = 0.031
IFNα (pg/mL)
C
p = 0.031
IFNβ (pg/mL)
D
p = 0.031
IFNβ mRNA
MC
AT-2 HIV
E
p = 0.094
Mx mRNA
F
p = 0.048
p = 0.001
TRAIL MFI % change
G
p = 0.563
% pDC Viability
H
p = 0.125
p = 0.015
p = 0.020
% TRAIL Positive
αCD3
IFNα,β
I
SSC-Height
FSC-Height
66.3
CD123
BDCA-2
99.1
J
SSC-Height
FSC-Height
91.6
CD4
CD3
97.5
K
SSC-Height
FSC-Height
83.8
Annexin V
7AAD
67.1
SSC-Height
FSC-Height
95.7
% of Max
TRAIL
AT-2 HIV + MC
AT-2 HIV
Neg + MC
Neg
L
SSC-Height
FSC-Height
94.9
CD3
TRAIL
97.2
2.54
0.289
9.96e-3

Figure 2. Minocycline attenuates type I IFN production and TRAIL expression in lymphocytes. PBMCs were isolated from the blood of healthy human donors, pretreated for two hours *in vitro* with 0, 20, or 40 μM minocycline, and exposed to increasing amounts of either AT-2 inactivated HIV (n = 4 different donors) or infectious influenza virus (n = 3 different donors). After overnight culture, supernatants were analyzed for secreted IFNα (**A**, **D**) and IFNβ protein (**B**, **E**) by ELISA. (**C**, **F**) Lymphocytes were analyzed by flow cytometry for TRAIL expression. (**G**) Representative flow cytometry gating of lymphocyte TRAIL expression in PBMC mixed cultures following AT-2 HIV stimulation. (**H**) Representative gating of lymphocyte TRAIL expression in PBMC mixed cultures following influenza stimulation. A two-way repeated measures ANOVA was used to compare the effect of different doses of minocycline (p-value shown on graph) and varying levels of AT-2 HIV or influenza on levels of TRAIL, IFNα, and IFNβ.

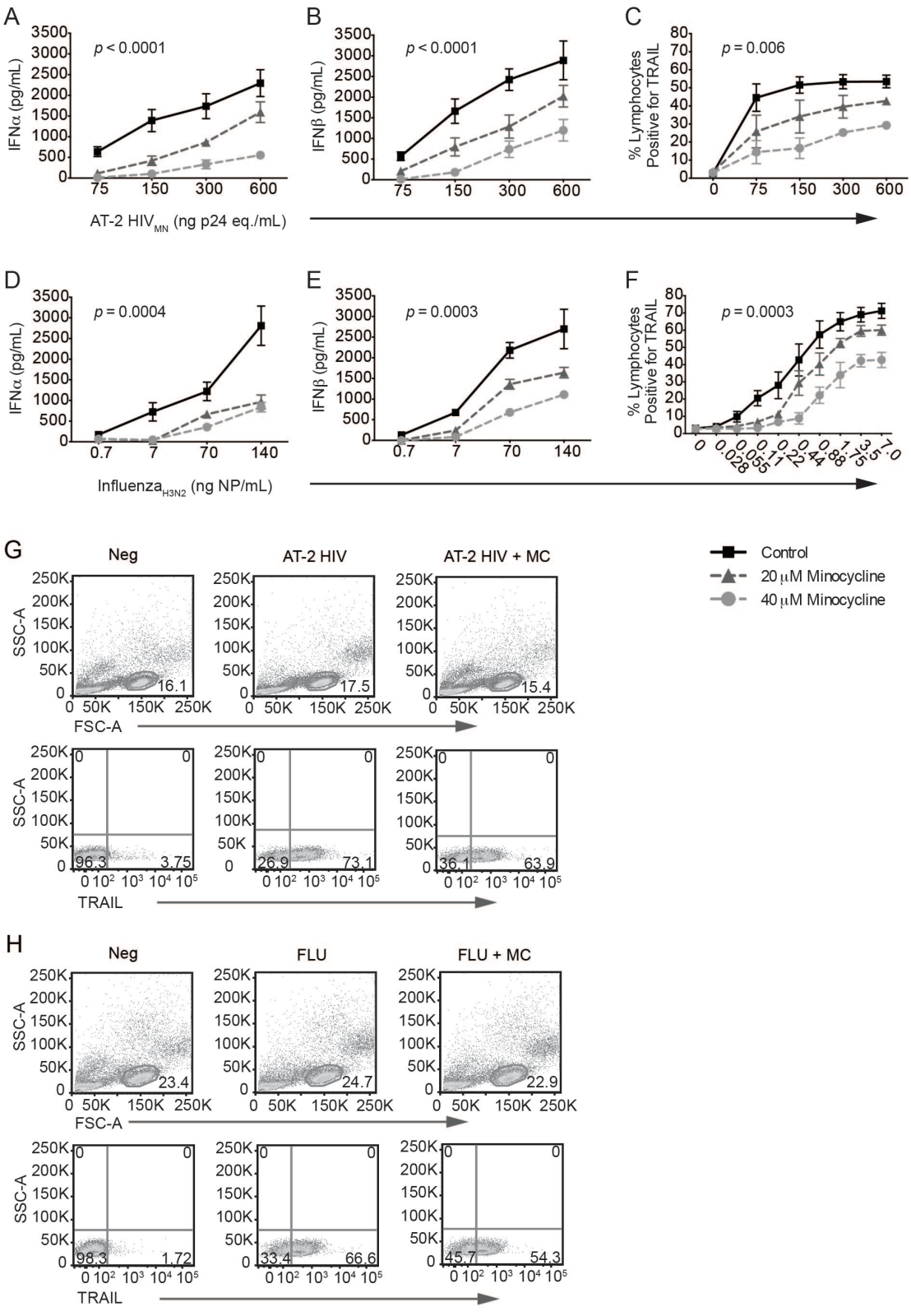
A
B
C
D
E
F
G
H
IFNα (pg/mL)
IFNβ (pg/mL)
% Lymphocytes Positive for TRAIL
p < 0.0001
p < 0.0001
p = 0.006
p = 0.0004
p = 0.0003
p = 0.0003
AT-2 HIV$_{MN}$ (ng p24 eq./mL)
Influenza$_{H3N2}$ (ng NP/mL)
Control
20 μM Minocycline
40 μM Minocycline
Neg
AT-2 HIV
AT-2 HIV + MC
FLU
FLU + MC
SSC-A
FSC-A
TRAIL
16.1
17.5
15.4
96.3
3.75
26.9
73.1
36.1
63.9
23.4
24.7
22.9
98.3
1.72
33.4
66.6
45.7
54.3

Figure 3. Minocycline prevents CTLA-4 and IDO expression in CD4+ T cells and pDCs. (**A**) IDO can be induced in pDCs by engagement of B7 receptors with CTLA-4 on CD4+ T cells or by stimulation with IFNα, β, γ, TNFα, TGFβ, or HIV. IDO converts the amino acid tryptophan (TRP) into L-formylkynurenine, initiating the production of a cascade of TRP metabolites that block T cell proliferation, induce T cell apoptosis, and convert CD4+ cells into Tregs. KYN: kynurenine; PIC: picolinic acid; TRP: tryptophan; 3HAA: 3-hydroxy anthranilic acid. (**B**) CD4+ T cells were isolated from blood of healthy human donors and activated with anti-CD3 with or without 20 μM minocycline (n = 6 different donors). After 24 hours minocycline was replenished and some wells were stimulated with IFNα and IFNβ. After 48 hours total cells were analyzed by flow cytometry for CTLA-4. (**C**) pDCs were isolated from blood of healthy human donors and exposed to AT-2 HIV with or without 20 μM minocycline (n = 6 different donors). After 18 hours RNA was harvested for IDO1 qRT-PCR. CTLA-4 data were analyzed by paired t-test. IDO mRNA was analyzed by Wilcoxon signed-rank test. (**D**) Representative flow cytometry gating of CTLA-4 expression on isolated CD4+ T cells.

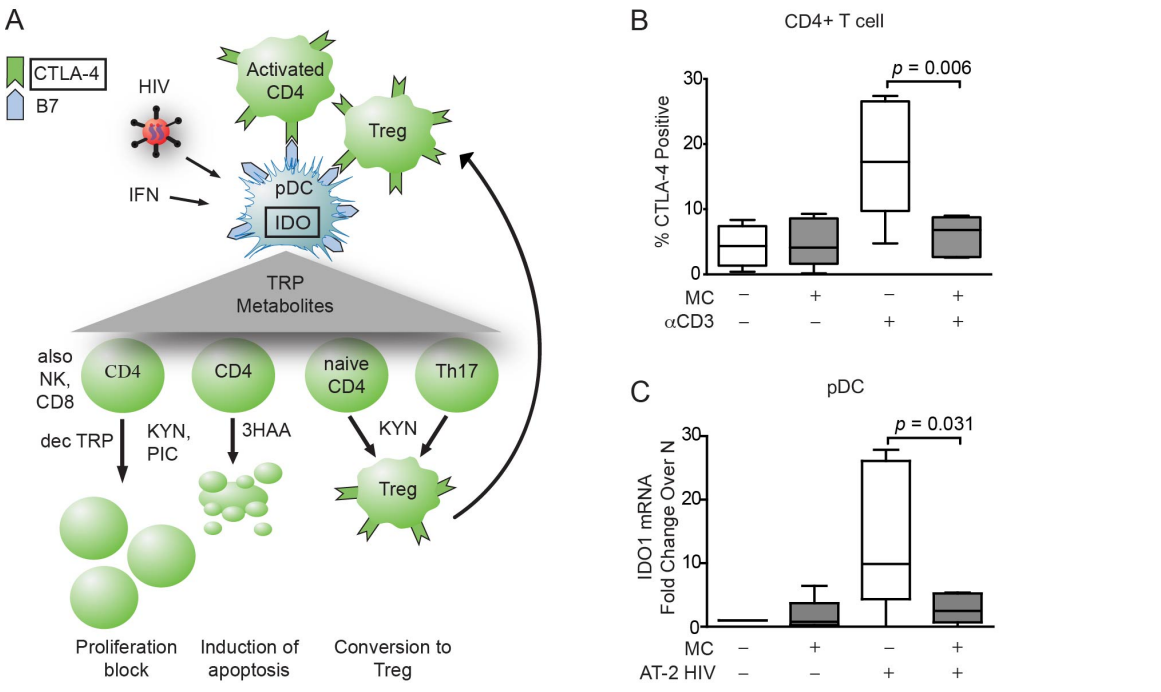
A
CTLA-4
B7
HIV
Activated CD4
Treg
IFN
pDC
IDO
TRP Metabolites
also NK, CD8
CD4
CD4
naive CD4
Th17
dec TRP
KYN, PIC
3HAA
KYN
Treg
Proliferation block
Induction of apoptosis
Conversion to Treg
B
CD4+ T cell
p = 0.006
% CTLA-4 Positive
MC
αCD3
C
pDC
p = 0.031
IDO1 mRNA Fold Change Over N
MC
AT-2 HIV

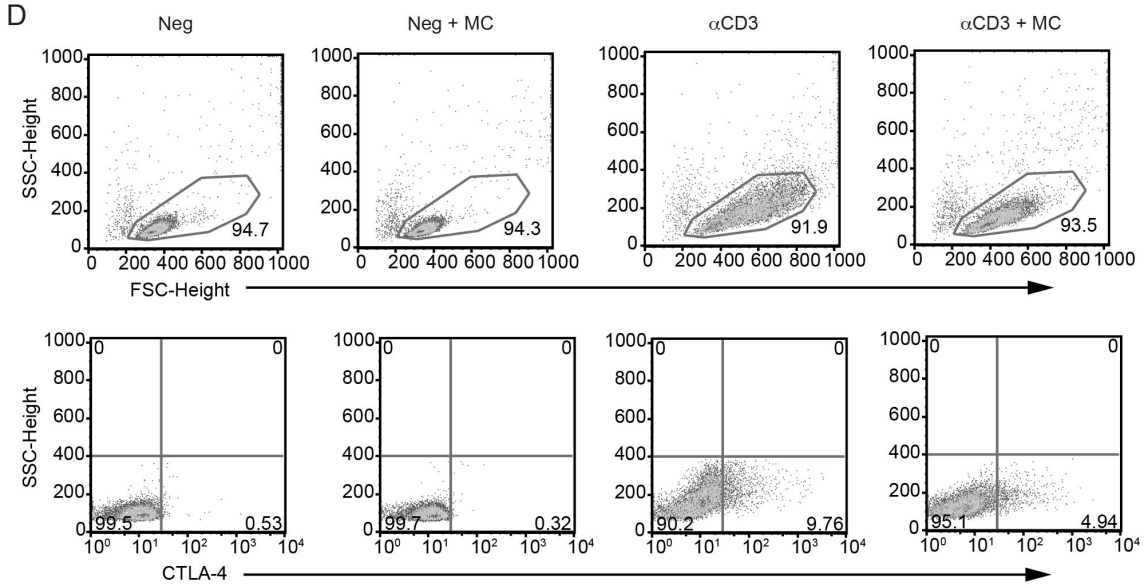
D
Neg
Neg + MC
αCD3
αCD3 + MC
SSC-Height
FSC-Height
94.7
94.3
91.9
93.5
CTLA-4
99.5
0.53
99.7
0.32
90.2
9.76
95.1
4.94

Figure 4. Minocycline attenuates activation but not IFN responses in spleens of SIV-infected pigtailed macaques. (**A**-**I**) The RNA expression of virus and 8 genes putatively involved in HIV/SIV pathogenesis were analyzed in RNA from archived spleens of uninfected controls (Uninf; *n* = 7), chronically SIV-infected pigtailed macaques (SIV; *n* = 11), chronically SIV-infected pigtailed macaques treated with minocycline starting at day 21 p.i. (MC; *n* = 11), and SIV-infected pigtailed macaques treated with cART starting at day 12 p.i. (cART; *n* = 5). All genes were analyzed by Nanostring nCounter analysis with the exception of IFNβ (**B**) and Mx (**C**), which were analyzed by qRT-PCR. Nanostring data are represented as counts; qRT-PCR data are represented as fold change over the median of 7 uninfected animals, although statistics were performed on delta Ct values prior to transformation. Solid lines denote medians; dashed lines represent the medians of uninfected controls. Data were analyzed by Mann-Whitney test.

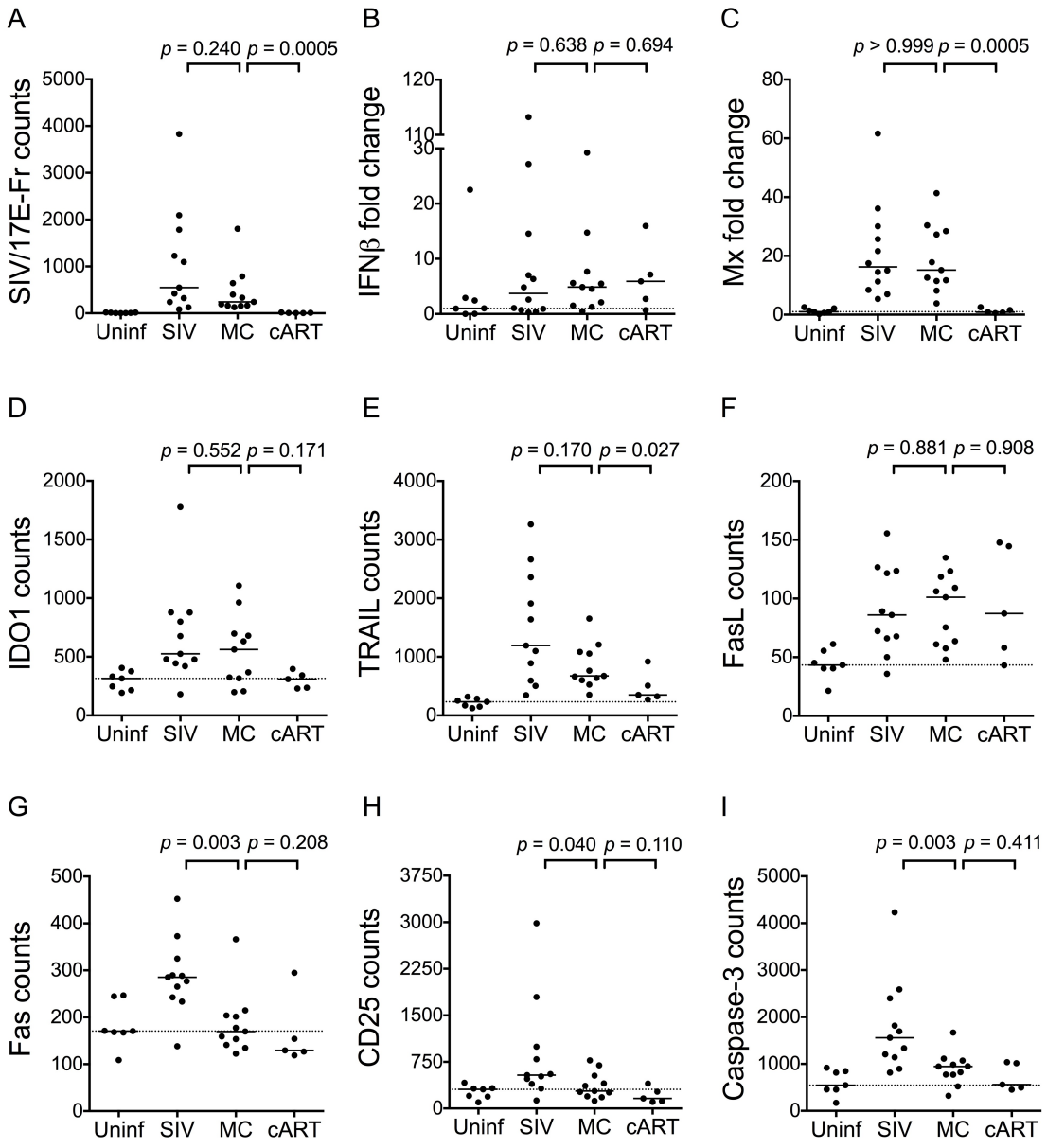
A
p = 0.240 p = 0.0005
SIV/17E-Fr counts
5000
4000
3000
2000
1000
0
Uninf SIV MC cART
B
p = 0.638 p = 0.694
IFNβ fold change
120
110
30
20
10
0
Uninf SIV MC cART
C
p > 0.999 p = 0.0005
Mx fold change
80
60
40
20
0
Uninf SIV MC cART
D
p = 0.552 p = 0.171
IDO1 counts
2000
1500
1000
500
0
Uninf SIV MC cART
E
p = 0.170 p = 0.027
TRAIL counts
4000
3000
2000
1000
0
Uninf SIV MC cART
F
p = 0.881 p = 0.908
FasL counts
200
150
100
50
0
Uninf SIV MC cART
G
p = 0.003 p = 0.208
Fas counts
500
400
300
200
100
0
Uninf SIV MC cART
H
p = 0.040 p = 0.110
CD25 counts
3750
3000
2250
1500
750
0
Uninf SIV MC cART
I
p = 0.003 p = 0.411
Caspase-3 counts
5000
4000
3000
2000
1000
0
Uninf SIV MC cART

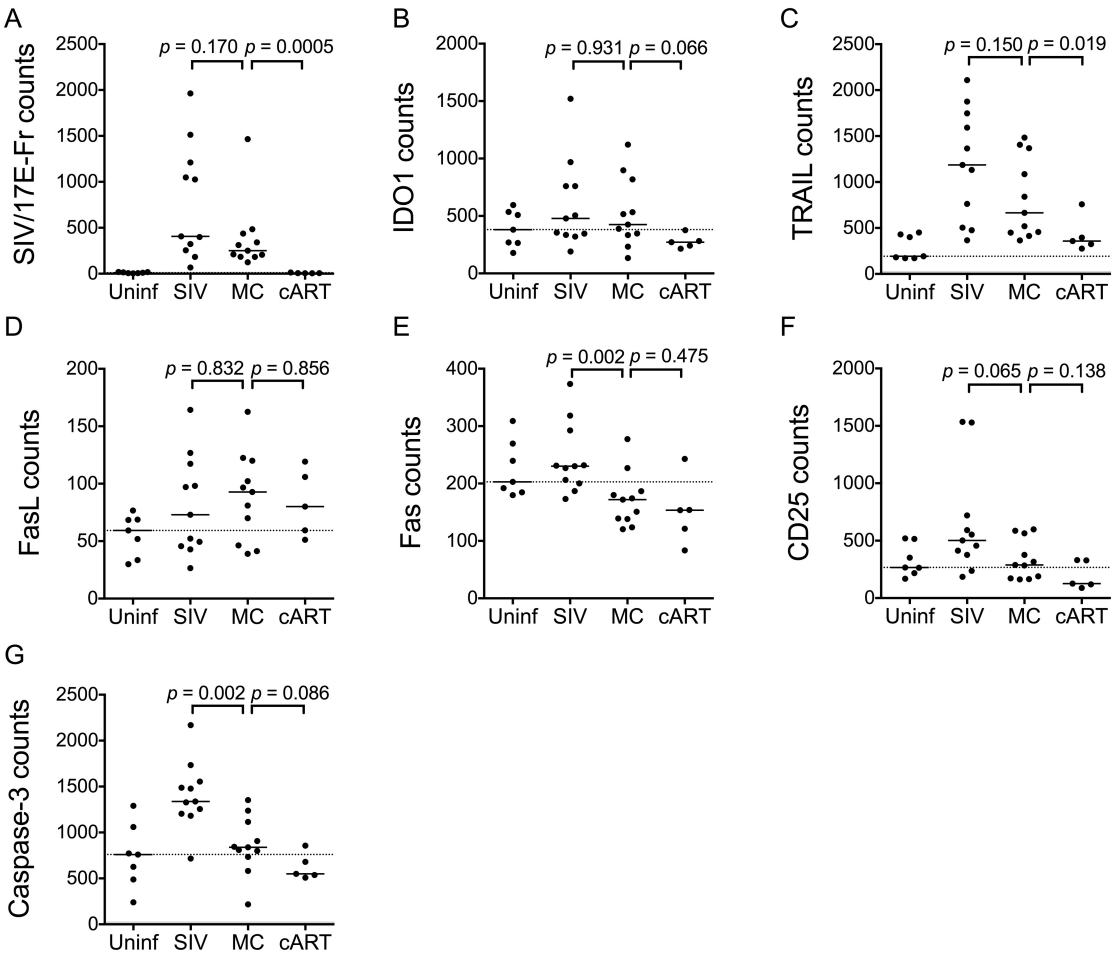

Supplementary Figure 1. *In vivo* spleen data normalized to RPS9 housekeeping gene. In an alternative analysis to the one shown in Figure 4, spleen Nanostring nCounter data were normalized to the geometric mean of positive controls and then against the ribosomal gene RPS9, which was the traditional housekeeping gene that showed the least variance in expression between groups of animals.

CHAPTER V.

Summary & Future Directions

The findings presented in this dissertation provide key insights into the neurotoxic and immunomodulatory contributions of the KYN pathway to HIV/SIV pathogenesis. We examined the ability of two disparate therapeutic strategies – the anti-viral activities of cART and the anti-inflammatory activities of minocycline – to attenuate KYN pathway activation and found that neither was sufficient to normalize KYN pathway activation. We also demonstrated that while KYN pathway metabolites were elevated to neurotoxic and immunomodulatory concentrations, TRP was not significantly depleted in the tissues. However, this preservation of TRP in the CNS may have come at the expense of reduced serotonin synthesis. Finally, given the need for a biomarker of ongoing neurological and immunological dysfunction in the cART era, we also examined the utility of circulating KYN pathway metabolites as biomarkers of tissue disease and identified QUIN/TRP ratios as a novel, early predictive biomarker of neurological disease.

Previously published work from the Retrovirus laboratory demonstrated that cART does not normalize IDO expression to uninfected control levels in the brains of SIV-infected macaques (92). This led us to hypothesize that the ongoing neurological disease seen in patients on cART might be due in part to sustained upregulation of neurotoxic KYN pathway metabolites. Indeed, we found that levels of the metabolites KYN, 3HK, and QUIN all remained significantly above uninfected control levels in the brains of cART-treated animals. While high concentrations of these metabolites are required in order to induce acute toxicity in neurons, several studies have established that chronic exposure of neurons to small elevations in QUIN can cause phenotypic changes in neurons *in vitro* (43, 44). Our finding of elevated metabolites in brain tissue despite

cART is the first study of its kind and emphasizes the importance of finding brain-penetrant cART therapies or adjunct therapies that can reduce neuroinflammation.

To this end, we also examined the potential for minocycline to attenuate IDO activation in SIV-infected macaques in the hopes that minocycline could be an important adjunct to cART. We found that minocycline was able to potently inhibit type I IFN and IDO induction *in vitro* in pDCs, a cell type that has been implicated in HIV/SIV pathogenesis of non-natural hosts. Following these promising results, we then compared minocycline side by side with cART-treated animals and examined markers of immune dysfunction in the spleens of SIV-infected macaques. Interestingly, even though cART had not normalized levels of IDO expression in the brain (92), cART therapy did normalize IDO expression to control levels in the spleen, which is likely due to enhanced spleen tissue penetration as compared to the brain with this non-CNS penetrant cART regimen. In contrast, we found no beneficial effect of minocycline on IDO expression in the spleen. We also did not find evidence for inhibition of type I IFN responses in the spleen by minocycline. We hypothesized that the discordance between the *in vitro* and *in vivo* results with minocycline may have been a result of several factors including insufficient drug concentrations in the tissue, differential effects of minocycline on various cell types, and subversion of minocycline's effects on IFN signaling by direct infected cell-to-cell signaling. However, minocycline did attenuate other aspects of immune disease in the spleen, including the activation marker CD25 and markers involved in activation-induced cell death, Fas and caspase-3.

Overall these pharmacotherapeutic studies suggest that an adjunct therapy or a better CNS-penetrant cART regimen may be necessary in order to supplement the effects

of cART, and that minocycline may be useful against some, but not all, aspects of HIV/SIV immune pathogenesis.

An ongoing debate in immunology questions whether induction of IDO can result in depletion of TRP to levels low enough to cause suppression of T cell responses. In Chapters II and III of this dissertation, we reported that TRP was not significantly depleted in either the brain or spleen, and was certainly not depleted to the low micromolar levels necessary to prevent T cell proliferation (37). We also showed in Chapter III that monocyte-derived macrophages were similarly capable of maintaining intracellular TRP levels despite profound KYN pathway activation and depletion of TRP in supernatants *in vitro*. These data suggest that the immunomodulatory effects of the KYN pathway are likely mediated by KYN metabolites rather than TRP starvation in the context of HIV/SIV infection.

However, we did find that serotonin levels were reduced in the brains of SIV-infected macaques. This reduction in serotonin did not appear to be a result of decreased levels of the enzymes that synthesize serotonin from TRP, as expression of both tryptophan hydroxylases *TPH1* and *TPH2* in the brain remained stable during infection. Additionally, we found that TRP levels were profoundly reduced in the CSF. Taken together, the reductions in brain serotonin and CSF TRP suggest that the preservation of TRP levels in the brain takes priority over synthesis of serotonin, and also results in reduced drainage of TRP into the CSF. Overall this indicates that KYN pathway induction in the brain results in significant changes in the way that TRP is utilized in the CNS, even if overt TRP levels remain unchanged in the brain.

Although changes in TRP in the circulation did not mimic changes (or lack thereof) occurring in the tissues, we found that circulating KYN and QUIN levels closely reflected their tissue counterparts. In addition to being reflective of tissue levels, CSF QUIN has previously been shown to differentiate between HIV-infected individuals with or without dementia (78), with or without functional impairments in motor-skill learning and reaction time (224), and is higher in SIV-infected macaques with encephalitis as compared to those without encephalitis (225). Elevations in QUIN are also specific to inflammatory (e.g., HIV encephalitis) as compared to non-inflammatory neurological disorders (e.g., Alzheimer's, Huntington's, etc.) (93). However, none of these studies examined QUIN levels longitudinally in order to determine whether CSF QUIN could predict the development of encephalitis, nor did they examine milder versions of neurological impairment.

To enhance the sensitivity of QUIN as a potential biomarker in our model and in the cART era where milder manifestations of neurological disease are becoming more prevalent, we normalized QUIN to TRP levels since TRP was reduced in the CSF. Levels of QUIN/TRP ratios in the CSF were then able to predict whether an animal would develop moderate to severe encephalitis at euthanasia by day 28 p.i., a remarkably early timepoint during asymptomatic infection. Given the promising leads but continued absence of a validated, clinical biomarker (e.g., CD4+ T cell nadir, IL-6, neopterin, CSF viremia, etc., as reviewed in Morris *et al.*) (226), validating our findings on QUIN/TRP ratios in patient cohorts is a critical future aim. Importantly, we also recommend that since no single biomarker may be able to identify all HIV-infected individuals at risk of

developing neurological disease, incorporation of QUIN/TRP ratios into a biomarker panel that includes other promising analytes may prove to be the most salient solution.

Thus, important future directions include the validation of QUIN/TRP ratios as a predictive biomarker of mild CNS disease in patients and identification of cART regimens or adjunct therapies that can normalize KYN pathway activation in both the CNS and in the periphery.

REFERENCES

1. Palmer, S., F. Maldarelli, A. Wiegand, B. Bernstein, G. J. Hanna, S. C. Brun, D. J. Kempf, J. W. Mellors, J. M. Coffin, and M. S. King. 2008. Low-level viremia persists for at least 7 years in patients on suppressive antiretroviral therapy. *Proc Natl Acad Sci U S A* 105:3879-3884.

2. Maldarelli, F., S. Palmer, M. S. King, A. Wiegand, M. A. Polis, J. Mican, J. A. Kovacs, R. T. Davey, D. Rock-Kress, R. Dewar, S. Liu, J. A. Metcalf, C. Rehm, S. C. Brun, G. J. Hanna, D. J. Kempf, J. M. Coffin, and J. W. Mellors. 2007. ART suppresses plasma HIV-1 RNA to a stable set point predicted by pretherapy viremia. *PLoS Pathog* 3:e46.

3. Langford, D., J. Marquie-Beck, S. de Almeida, D. Lazzaretto, S. Letendre, I. Grant, J. A. McCutchan, E. Masliah, and R. J. Ellis. 2006. Relationship of antiretroviral treatment to postmortem brain tissue viral load in human immunodeficiency virus-infected patients. *J Neurovirol* 12:100-107.

4. Ramratnam, B., R. Ribeiro, T. He, C. Chung, V. Simon, J. Vanderhoeven, A. Hurley, L. Zhang, A. S. Perelson, D. D. Ho, and M. Markowitz. 2004. Intensification of antiretroviral therapy accelerates the decay of the HIV-1 latent reservoir and decreases, but does not eliminate, ongoing virus replication. *J Acquir Immune Defic Syndr* 35:33-37.

5. Tan, I. L., and J. C. McArthur. 2012. HIV-associated neurological disorders: a guide to pharmacotherapy. *CNS drugs* 26:123-134.

6. Herbeuval, J. P., J. Nilsson, A. Boasso, A. W. Hardy, M. Vaccari, V. Cecchinato, V. Valeri, G. Franchini, J. Andersson, and G. M. Shearer. 2009. HAART reduces

death ligand but not death receptors in lymphoid tissue of HIV-infected patients and simian immunodeficiency virus-infected macaques. *AIDS* 23:35-40.

7. Chehimi, J., E. Papasavvas, C. Tomescu, B. Gekonge, S. Abdulhaqq, A. Raymond, A. Hancock, K. Vinekar, C. Carty, G. Reynolds, M. Pistilli, K. Mounzer, J. Kostman, and L. J. Montaner. 2010. Inability of plasmacytoid dendritic cells to directly lyse HIV-infected autologous CD4+ T cells despite induction of tumor necrosis factor-related apoptosis-inducing ligand. *J Virol* 84:2762-2773.

8. Hansjee, N., G. R. Kaufmann, C. Strub, R. Weber, M. Battegay, and P. Erb. 2004. Persistent apoptosis in HIV-1-infected individuals receiving potent antiretroviral therapy is associated with poor recovery of CD4 T lymphocytes. *J Acquir Immune Defic Syndr* 36:671-677.

9. Stary, G., I. Klein, S. Kohlhofer, F. Koszik, T. Scherzer, L. Mullauer, H. Quendler, N. Kohrgruber, and G. Stingl. 2009. Plasmacytoid dendritic cells express TRAIL and induce CD4+ T-cell apoptosis in HIV-1 viremic patients. *Blood* 114:3854-3863.

10. Ronquillo, R. E., S. N. Desai, P. J. Norris, E. T. Golub, R. M. Greenblatt, S. J. Gange, and A. L. Landay. 2010. Elevated caspase-3 expression and T-cell activation in elite suppressors. *J Acquir Immune Defic Syndr* 54:110-111.

11. Jenabian, M. A., M. Patel, I. Kema, C. Kanagaratham, D. Radzioch, P. Thebault, R. Lapointe, C. Tremblay, N. Gilmore, P. Ancuta, and J. P. Routy. 2013. Distinct tryptophan catabolism and Th17/Treg balance in HIV progressors and elite controllers. *PLoS One* 8:e78146.

12. Aiuti, F., and I. Mezzaroma. 2006. Failure to reconstitute CD4+ T-cells despite suppression of HIV replication under HAART. *AIDS Rev* 8:88-97.

13. McArthur, J. C., J. Steiner, N. Sacktor, and A. Nath. 2010. Human immunodeficiency virus-associated neurocognitive disorders: Mind the gap. *Ann Neurol* 67:699-714.

14. Kaul, M., and S. A. Lipton. 2006. Mechanisms of neuronal injury and death in HIV-1 associated dementia. *Curr HIV Res* 4:307-318.

15. Antinori, A., G. Arendt, J. T. Becker, B. J. Brew, D. A. Byrd, M. Cherner, D. B. Clifford, P. Cinque, L. G. Epstein, K. Goodkin, M. Gisslen, I. Grant, R. K. Heaton, J. Joseph, K. Marder, C. M. Marra, J. C. McArthur, M. Nunn, R. W. Price, L. Pulliam, K. R. Robertson, N. Sacktor, V. Valcour, and V. E. Wojna. 2007. Updated research nosology for HIV-associated neurocognitive disorders. *Neurology* 69:1789-1799.

16. Ances, B. M., and R. J. Ellis. 2007. Dementia and neurocognitive disorders due to HIV-1 infection. *Seminars in neurology* 27:86-92.

17. Heaton, R. K., D. R. Franklin, R. J. Ellis, J. A. McCutchan, S. L. Letendre, S. Leblanc, S. H. Corkran, N. A. Duarte, D. B. Clifford, S. P. Woods, A. C. Collier, C. M. Marra, S. Morgello, M. R. Mindt, M. J. Taylor, T. D. Marcotte, J. H. Atkinson, T. Wolfson, B. B. Gelman, J. C. McArthur, D. M. Simpson, I. Abramson, A. Gamst, C. Fennema-Notestine, T. L. Jernigan, J. Wong, I. Grant, C. Group, and H. Group. 2011. HIV-associated neurocognitive disorders before and during the era of combination antiretroviral therapy: differences in rates, nature, and predictors. *J Neurovirol* 17:3-16.

18. Ciesla, J. A., and J. E. Roberts. 2001. Meta-analysis of the relationship between HIV infection and risk for depressive disorders. *The American journal of psychiatry* 158:725-730.

19. Braganca, M., and A. Palha. 2011. Depression and neurocognitive performance in Portuguese patients infected with HIV. *AIDS and behavior* 15:1879-1887.

20. Fernandes Filho, S. M., and H. R. de Melo. 2012. Frequency and risk factors for HIV-associated neurocognitive disorder and depression in older individuals with HIV in northeastern Brazil. *International psychogeriatrics / IPA* 24:1648-1655.

21. Grohmann, U., F. Fallarino, and P. Puccetti. 2003. Tolerance, DCs and tryptophan: much ado about IDO. *Trends in immunology* 24:242-248.

22. Danesch, U., B. Gloss, W. Schmid, G. Schutz, R. Schule, and R. Renkawitz. 1987. Glucocorticoid induction of the rat tryptophan oxygenase gene is mediated by two widely separated glucocorticoid-responsive elements. *EMBO J* 6:625-630.

23. Wichers, M. C., G. H. Koek, G. Robaeys, R. Verkerk, S. Scharpe, and M. Maes. 2005. IDO and interferon-alpha-induced depressive symptoms: a shift in hypothesis from tryptophan depletion to neurotoxicity. *Molecular psychiatry* 10:538-544.

24. O'Connor, J. C., C. Andre, Y. Wang, M. A. Lawson, S. S. Szegedi, J. Lestage, N. Castanon, K. W. Kelley, and R. Dantzer. 2009. Interferon-gamma and tumor necrosis factor-alpha mediate the upregulation of indoleamine 2,3-dioxygenase and the induction of depressive-like behavior in mice in response to bacillus Calmette-Guerin. *J Neurosci* 29:4200-4209.

25. Smith, D. G., G. J. Guillemin, L. Pemberton, S. Kerr, A. Nath, G. A. Smythe, and B. J. Brew. 2001. Quinolinic acid is produced by macrophages stimulated by platelet activating factor, Nef and Tat. *J Neurovirol* 7:56-60.

26. Fujigaki, H., K. Saito, S. Fujigaki, M. Takemura, K. Sudo, H. Ishiguro, and M. Seishima. 2006. The signal transducer and activator of transcription 1alpha and interferon regulatory factor 1 are not essential for the induction of indoleamine 2,3-dioxygenase by lipopolysaccharide: involvement of p38 mitogen-activated protein kinase and nuclear factor-kappaB pathways, and synergistic effect of several proinflammatory cytokines. *Journal of biochemistry* 139:655-662.

27. Boasso, A., J. P. Herbeuval, A. W. Hardy, S. A. Anderson, M. J. Dolan, D. Fuchs, and G. M. Shearer. 2007. HIV inhibits CD4+ T-cell proliferation by inducing indoleamine 2,3-dioxygenase in plasmacytoid dendritic cells. *Blood* 109:3351-3359.

28. Mellor, A. L., B. Baban, P. R. Chandler, A. Manlapat, D. J. Kahler, and D. H. Munn. 2005. Cutting edge: CpG oligonucleotides induce splenic CD19+ dendritic cells to acquire potent indoleamine 2,3-dioxygenase-dependent T cell regulatory functions via IFN Type 1 signaling. *J Immunol* 175:5601-5605.

29. Connor, T. J., N. Starr, J. B. O'Sullivan, and A. Harkin. 2008. Induction of indolamine 2,3-dioxygenase and kynurenine 3-monooxygenase in rat brain following a systemic inflammatory challenge: a role for IFN-gamma? *Neurosci Lett* 441:29-34.

30. Pallotta, M. T., C. Orabona, C. Volpi, C. Vacca, M. L. Belladonna, R. Bianchi, G. Servillo, C. Brunacci, M. Calvitti, S. Bicciato, E. M. Mazza, L. Boon, F. Grassi,

M. C. Fioretti, F. Fallarino, P. Puccetti, and U. Grohmann. 2011. Indoleamine 2,3-dioxygenase is a signaling protein in long-term tolerance by dendritic cells. *Nat Immunol* 12:870-878.

31. Chen, W. 2011. IDO: more than an enzyme. *Nat Immunol* 12:809-811.

32. Krishnan, V., and E. J. Nestler. 2008. The molecular neurobiology of depression. *Nature* 455:894-902.

33. Ruhe, H. G., N. S. Mason, and A. H. Schene. 2007. Mood is indirectly related to serotonin, norepinephrine and dopamine levels in humans: a meta-analysis of monoamine depletion studies. *Molecular psychiatry* 12:331-359.

34. Kumar, A. M., J. R. Berger, C. Eisdorfer, J. B. Fernandez, K. Goodkin, and M. Kumar. 2001. Cerebrospinal fluid 5-hydroxytryptamine and 5-hydroxyindoleacetic acid in HIV-1 infection. *Neuropsychobiology* 44:13-18.

35. Reynolds, G. P., and A. M. Sardar. 1996. 5-Hydroxytryptamine deficits in the caudate nucleus in AIDS. *AIDS* 10:1303-1304.

36. Pfefferkorn, E. R. 1984. Interferon gamma blocks the growth of Toxoplasma gondii in human fibroblasts by inducing the host cells to degrade tryptophan. *Proc Natl Acad Sci U S A* 81:908-912.

37. Munn, D. H., M. D. Sharma, B. Baban, H. P. Harding, Y. Zhang, D. Ron, and A. L. Mellor. 2005. GCN2 kinase in T cells mediates proliferative arrest and anergy induction in response to indoleamine 2,3-dioxygenase. *Immunity* 22:633-642.

38. Goldstein, L. E., M. C. Leopold, X. Huang, C. S. Atwood, A. J. Saunders, M. Hartshorn, J. T. Lim, K. Y. Faget, J. A. Muffat, R. C. Scarpa, L. T. Chylack, Jr., E. F. Bowden, R. E. Tanzi, and A. I. Bush. 2000. 3-Hydroxykynurenine and 3-

hydroxyanthranilic acid generate hydrogen peroxide and promote alpha-crystallin cross-linking by metal ion reduction. *Biochemistry* 39:7266-7275.

39. Okuda, S., N. Nishiyama, H. Saito, and H. Katsuki. 1998. 3-Hydroxykynurenine, an endogenous oxidative stress generator, causes neuronal cell death with apoptotic features and region selectivity. *J Neurochem* 70:299-307.

40. Platenik, J., P. Stopka, M. Vejrazka, and S. Stipek. 2001. Quinolinic acid-iron(ii) complexes: slow autoxidation, but enhanced hydroxyl radical production in the Fenton reaction. *Free radical research* 34:445-459.

41. Guillemin, G. J., J. Croitoru-Lamoury, D. Dormont, P. J. Armati, and B. J. Brew. 2003. Quinolinic acid upregulates chemokine production and chemokine receptor expression in astrocytes. *Glia* 41:371-381.

42. Stone, T. W. 1993. Neuropharmacology of quinolinic and kynurenic acids. *Pharmacological reviews* 45:309-379.

43. Whetsell, W. O., Jr., and R. Schwarcz. 1989. Prolonged exposure to submicromolar concentrations of quinolinic acid causes excitotoxic damage in organotypic cultures of rat corticostriatal system. *Neurosci Lett* 97:271-275.

44. Kerr, S. J., P. J. Armati, G. J. Guillemin, and B. J. Brew. 1998. Chronic exposure of human neurons to quinolinic acid results in neuronal changes consistent with AIDS dementia complex. *AIDS* 12:355-363.

45. Schwarcz, R., W. O. Whetsell, Jr., and R. M. Mangano. 1983. Quinolinic acid: an endogenous metabolite that produces axon-sparing lesions in rat brain. *Science* 219:316-318.

46. Schwarcz, R., J. P. Bruno, P. J. Muchowski, and H. Q. Wu. 2012. Kynurenines in the mammalian brain: when physiology meets pathology. *Nature reviews. Neuroscience* 13:465-477.

47. Rassoulpour, A., H. Q. Wu, S. Ferre, and R. Schwarcz. 2005. Nanomolar concentrations of kynurenic acid reduce extracellular dopamine levels in the striatum. *J Neurochem* 93:762-765.

48. Berger, J. R., and G. Arendt. 2000. HIV dementia: the role of the basal ganglia and dopaminergic systems. *Journal of psychopharmacology* 14:214-221.

49. Munn, D. H., M. Zhou, J. T. Attwood, I. Bondarev, S. J. Conway, B. Marshall, C. Brown, and A. L. Mellor. 1998. Prevention of allogeneic fetal rejection by tryptophan catabolism. *Science* 281:1191-1193.

50. Miki, T., H. Sun, Y. Lee, A. Tandin, A. M. Kovscek, V. Subbotin, J. J. Fung, and L. A. Valdivia. 2001. Blockade of tryptophan catabolism prevents spontaneous tolerogenicity of liver allografts. *Transplant Proc* 33:129-130.

51. Friberg, M., R. Jennings, M. Alsarraj, S. Dessureault, A. Cantor, M. Extermann, A. L. Mellor, D. H. Munn, and S. J. Antonia. 2002. Indoleamine 2,3-dioxygenase contributes to tumor cell evasion of T cell-mediated rejection. *Int J Cancer* 101:151-155.

52. Frumento, G., R. Rotondo, M. Tonetti, G. Damonte, U. Benatti, and G. B. Ferrara. 2002. Tryptophan-derived catabolites are responsible for inhibition of T and natural killer cell proliferation induced by indoleamine 2,3-dioxygenase. *J Exp Med* 196:459-468.

53. Favre, D., J. Mold, P. W. Hunt, B. Kanwar, P. Loke, L. Seu, J. D. Barbour, M. M. Lowe, A. Jayawardene, F. Aweeka, Y. Huang, D. C. Douek, J. M. Brenchley, J. N. Martin, F. M. Hecht, S. G. Deeks, and J. M. McCune. 2010. Tryptophan catabolism by indoleamine 2,3-dioxygenase 1 alters the balance of TH17 to regulatory T cells in HIV disease. *Sci Transl Med* 2:32ra36.

54. Mezrich, J. D., J. H. Fechner, X. Zhang, B. P. Johnson, W. J. Burlingham, and C. A. Bradfield. 2010. An interaction between kynurenine and the aryl hydrocarbon receptor can generate regulatory T cells. *J Immunol* 185:3190-3198.

55. Lee, S. M., Y. S. Lee, J. H. Choi, S. G. Park, I. W. Choi, Y. D. Joo, W. S. Lee, J. N. Lee, I. Choi, and S. K. Seo. 2010. Tryptophan metabolite 3-hydroxyanthranilic acid selectively induces activated T cell death via intracellular GSH depletion. *Immunol Lett* 132:53-60.

56. Hiramatsu, R., T. Hara, H. Akimoto, O. Takikawa, T. Kawabe, K. Isobe, and F. Nagase. 2008. Cinnabarinic acid generated from 3-hydroxyanthranilic acid strongly induces apoptosis in thymocytes through the generation of reactive oxygen species and the induction of caspase. *Journal of cellular biochemistry* 103:42-53.

57. Yan, Y., G. X. Zhang, B. Gran, F. Fallarino, S. Yu, H. Li, M. L. Cullimore, A. Rostami, and H. Xu. 2010. IDO upregulates regulatory T cells via tryptophan catabolite and suppresses encephalitogenic T cell responses in experimental autoimmune encephalomyelitis. *J Immunol* 185:5953-5961.

58. Opitz, C. A., U. M. Litzenburger, F. Sahm, M. Ott, I. Tritschler, S. Trump, T. Schumacher, L. Jestaedt, D. Schrenk, M. Weller, M. Jugold, G. J. Guillemin, C.

L. Miller, C. Lutz, B. Radlwimmer, I. Lehmann, A. von Deimling, W. Wick, and M. Platten. 2011. An endogenous tumour-promoting ligand of the human aryl hydrocarbon receptor. *Nature* 478:197-203.

59. Zink, M. C., K. Suryanarayana, J. L. Mankowski, A. Shen, M. Piatak, Jr., J. P. Spelman, D. L. Carter, R. J. Adams, J. D. Lifson, and J. E. Clements. 1999. High viral load in the cerebrospinal fluid and brain correlates with severity of simian immunodeficiency virus encephalitis. *J Virol* 73:10480-10488.

60. Zink, M. C., J. Uhrlaub, J. DeWitt, T. Voelker, B. Bullock, J. Mankowski, P. Tarwater, J. Clements, and S. Barber. 2005. Neuroprotective and anti-human immunodeficiency virus activity of minocycline. *JAMA* 293:2003-2011.

61. Meulendyke, K. A., M. V. Pletnikov, E. L. Engle, P. M. Tarwater, D. R. Graham, and M. C. Zink. 2012. Early minocycline treatment prevents a decrease in striatal dopamine in an SIV model of HIV-associated neurological disease. *Journal of neuroimmune pharmacology : the official journal of the Society on NeuroImmune Pharmacology* 7:454-464.

62. Follstaedt, S. C., S. A. Barber, and M. C. Zink. 2008. Mechanisms of minocycline-induced suppression of simian immunodeficiency virus encephalitis: inhibition of apoptosis signal-regulating kinase 1. *J Neurovirol* 14:376-388.

63. Dinoso, J. B., S. A. Rabi, J. N. Blankson, L. Gama, J. L. Mankowski, R. F. Siliciano, M. C. Zink, and J. E. Clements. 2009. A simian immunodeficiency virus-infected macaque model to study viral reservoirs that persist during highly active antiretroviral therapy. *J Virol* 83:9247-9257.

64. Gibbie, T., A. Mijch, S. Ellen, J. Hoy, C. Hutchison, E. Wright, P. Chua, and F. Judd. 2006. Depression and neurocognitive performance in individuals with HIV/AIDS: 2-year follow-up. *HIV Med* 7:112-121.

65. Heaton, R. K., D. B. Clifford, D. R. Franklin, Jr., S. P. Woods, C. Ake, F. Vaida, R. J. Ellis, S. L. Letendre, T. D. Marcotte, J. H. Atkinson, M. Rivera-Mindt, O. R. Vigil, M. J. Taylor, A. C. Collier, C. M. Marra, B. B. Gelman, J. C. McArthur, S. Morgello, D. M. Simpson, J. A. McCutchan, I. Abramson, A. Gamst, C. Fennema-Notestine, T. L. Jernigan, J. Wong, and I. Grant. 2010. HIV-associated neurocognitive disorders persist in the era of potent antiretroviral therapy: CHARTER Study. *Neurology* 75:2087-2096.

66. Israelski, D. M., D. E. Prentiss, S. Lubega, G. Balmas, P. Garcia, M. Muhammad, S. Cummings, and C. Koopman. 2007. Psychiatric co-morbidity in vulnerable populations receiving primary care for HIV/AIDS. *AIDS Care* 19:220-225.

67. Robertson, K. R., M. Smurzynski, T. D. Parsons, K. Wu, R. J. Bosch, J. Wu, J. C. McArthur, A. C. Collier, S. R. Evans, and R. J. Ellis. 2007. The prevalence and incidence of neurocognitive impairment in the HAART era. *AIDS* 21:1915-1921.

68. Leserman, J. 2003. HIV disease progression: depression, stress, and possible mechanisms. *Biol Psychiatry* 54:295-306.

69. Leserman, J., J. M. Petitto, H. Gu, B. N. Gaynes, J. Barroso, R. N. Golden, D. O. Perkins, J. D. Folds, and D. L. Evans. 2002. Progression to AIDS, a clinical AIDS condition and mortality: psychosocial and physiological predictors. *Psychological medicine* 32:1059-1073.

70. Larsson, M., L. Hagberg, G. Norkrans, and A. Forsman. 1989. Indole amine deficiency in blood and cerebrospinal fluid from patients with human immunodeficiency virus infection. *J Neurosci Res* 23:441-446.

71. Launay, J. M., L. Copel, J. Callebert, N. Corvaia, E. Lepage, F. Bricaire, F. Saal, and J. Peries. 1988. Decreased whole blood 5-hydroxytryptamine (serotonin) in AIDS patients. *J Acquir Immune Defic Syndr* 1:324-325.

72. Fuchs, D., A. A. Moller, G. Reibnegger, E. Stockle, E. R. Werner, and H. Wachter. 1990. Decreased serum tryptophan in patients with HIV-1 infection correlates with increased serum neopterin and with neurologic/psychiatric symptoms. *J Acquir Immune Defic Syndr* 3:873-876.

73. Fuchs, D., A. A. Moller, G. Reibnegger, E. R. Werner, G. Werner-Felmayer, M. P. Dierich, and H. Wachter. 1991. Increased endogenous interferon-gamma and neopterin correlate with increased degradation of tryptophan in human immunodeficiency virus type 1 infection. *Immunol Lett* 28:207-211.

74. Fuchs, D., A. Forsman, L. Hagberg, M. Larsson, G. Norkrans, G. Reibnegger, E. R. Werner, and H. Wachter. 1990. Immune activation and decreased tryptophan in patients with HIV-1 infection. *J Interferon Res* 10:599-603.

75. Sardar, A. M., and G. P. Reynolds. 1995. Frontal cortex indoleamine-2,3-dioxygenase activity is increased in HIV-1-associated dementia. *Neurosci Lett* 187:9-12.

76. Burudi, E. M., M. C. Marcondes, D. D. Watry, M. Zandonatti, M. A. Taffe, and H. S. Fox. 2002. Regulation of indoleamine 2,3-dioxygenase expression in simian immunodeficiency virus-infected monkey brains. *J Virol* 76:12233-12241.

77. Heyes, M. P., D. Rubinow, C. Lane, and S. P. Markey. 1989. Cerebrospinal fluid quinolinic acid concentrations are increased in acquired immune deficiency syndrome. *Ann Neurol* 26:275-277.

78. Heyes, M. P., B. J. Brew, A. Martin, R. W. Price, A. M. Salazar, J. J. Sidtis, J. A. Yergey, M. M. Mouradian, A. E. Sadler, J. Keilp, and et al. 1991. Quinolinic acid in cerebrospinal fluid and serum in HIV-1 infection: relationship to clinical and neurological status. *Ann Neurol* 29:202-209.

79. Christen, S., E. Peterhans, and R. Stocker. 1990. Antioxidant activities of some tryptophan metabolites: possible implication for inflammatory diseases. *Proc Natl Acad Sci U S A* 87:2506-2510.

80. Hardeland, R., B. K. Zsizsik, B. Poeggeler, B. Fuhrberg, S. Holst, and A. Coto-Montes. 1999. Indole-3-pyruvic and -propionic acids, kynurenic acid, and related metabolites as luminophores and free-radical scavengers. *Adv Exp Med Biol* 467:389-395.

81. Lugo-Huitron, R., T. Blanco-Ayala, P. Ugalde-Muniz, P. Carrillo-Mora, J. Pedraza-Chaverri, D. Silva-Adaya, P. D. Maldonado, I. Torres, E. Pinzon, E. Ortiz-Islas, T. Lopez, E. Garcia, B. Pineda, M. Torres-Ramos, A. Santamaria, and V. P. La Cruz. 2011. On the antioxidant properties of kynurenic acid: free radical scavenging activity and inhibition of oxidative stress. *Neurotoxicology and teratology* 33:538-547.

82. Martinez, P., A. C. Tsai, C. Muzoora, A. Kembabazi, S. D. Weiser, Y. Huang, J. E. Haberer, J. N. Martin, D. R. Bangsberg, and P. W. Hunt. 2013. Reversal of the

Kynurenine Pathway of Tryptophan Catabolism May Improve Depression in ART-treated HIV-infected Ugandans. *J Acquir Immune Defic Syndr*.

83. Gendelman, H. E., J. Zheng, C. L. Coulter, A. Ghorpade, M. Che, M. Thylin, R. Rubocki, Y. Persidsky, F. Hahn, J. Reinhard, Jr., and S. Swindells. 1998. Suppression of inflammatory neurotoxins by highly active antiretroviral therapy in human immunodeficiency virus-associated dementia. *J Infect Dis* 178:1000-1007.

84. Kumar, A. M., I. Borodowsky, B. Fernandez, L. Gonzalez, and M. Kumar. 2007. Human immunodeficiency virus type 1 RNA Levels in different regions of human brain: quantification using real-time reverse transcriptase-polymerase chain reaction. *J Neurovirol* 13:210-224.

85. McArthur, J. C., B. J. Brew, and A. Nath. 2005. Neurological complications of HIV infection. *Lancet Neurol* 4:543-555.

86. Perkins, M. N., and T. W. Stone. 1983. Pharmacology and regional variations of quinolinic acid-evoked excitations in the rat central nervous system. *J Pharmacol Exp Ther* 226:551-557.

87. de Carvalho, L. P., P. Bochet, and J. Rossier. 1996. The endogenous agonist quinolinic acid and the non endogenous homoquinolinic acid discriminate between NMDAR2 receptor subunits. *Neurochem Int* 28:445-452.

88. Macaya, A., F. Munell, R. M. Gubits, and R. E. Burke. 1994. Apoptosis in substantia nigra following developmental striatal excitotoxic injury. *Proc Natl Acad Sci U S A* 91:8117-8121.

89. Heyes, M. P., K. Saito, A. Lackner, C. A. Wiley, C. L. Achim, and S. P. Markey. 1998. Sources of the neurotoxin quinolinic acid in the brain of HIV-1-infected patients and retrovirus-infected macaques. *FASEB J* 12:881-896.

90. Witwer, K. W., L. Gama, M. Li, C. M. Bartizal, S. E. Queen, J. J. Varrone, A. K. Brice, D. R. Graham, P. M. Tarwater, J. L. Mankowski, M. C. Zink, and J. E. Clements. 2009. Coordinated regulation of SIV replication and immune responses in the CNS. *PLoS One* 4:e8129.

91. Guillemin, G. J., S. J. Kerr, G. A. Smythe, D. G. Smith, V. Kapoor, P. J. Armati, J. Croitoru, and B. J. Brew. 2001. Kynurenine pathway metabolism in human astrocytes: a paradox for neuronal protection. *J Neurochem* 78:842-853.

92. Zink, M. C., A. K. Brice, K. M. Kelly, S. E. Queen, L. Gama, M. Li, R. J. Adams, C. Bartizal, J. Varrone, S. A. Rabi, D. R. Graham, P. M. Tarwater, J. L. Mankowski, and J. E. Clements. 2010. Simian immunodeficiency virus-infected macaques treated with highly active antiretroviral therapy have reduced central nervous system viral replication and inflammation but persistence of viral DNA. *J Infect Dis* 202:161-170.

93. Heyes, M. P., K. Saito, J. S. Crowley, L. E. Davis, M. A. Demitrack, M. Der, L. A. Dilling, J. Elia, M. J. Kruesi, A. Lackner, and et al. 1992. Quinolinic acid and kynurenine pathway metabolism in inflammatory and non-inflammatory neurological disease. *Brain* 115 (Pt 5):1249-1273.

94. Mankowski, J. L., S. E. Queen, J. E. Clements, and M. C. Zink. 2004. Cerebrospinal fluid markers that predict SIV CNS disease. *J Neuroimmunol* 157:66-70.

95. Hammoud, D. A., C. J. Endres, E. Hammond, O. Uzuner, A. Brown, A. Nath, A. I. Kaplin, and M. G. Pomper. 2010. Imaging serotonergic transmission with [11C]DASB-PET in depressed and non-depressed patients infected with HIV. *Neuroimage* 49:2588-2595.

96. O'Connor, J. C., M. A. Lawson, C. Andre, M. Moreau, J. Lestage, N. Castanon, K. W. Kelley, and R. Dantzer. 2009. Lipopolysaccharide-induced depressive-like behavior is mediated by indoleamine 2,3-dioxygenase activation in mice. *Molecular psychiatry* 14:511-522.

97. Pocivavsek, A., H. Q. Wu, M. C. Potter, G. I. Elmer, R. Pellicciari, and R. Schwarcz. 2011. Fluctuations in endogenous kynurenic acid control hippocampal glutamate and memory. *Neuropsychopharmacology : official publication of the American College of Neuropsychopharmacology* 36:2357-2367.

98. Amori, L., H. Q. Wu, M. Marinozzi, R. Pellicciari, P. Guidetti, and R. Schwarcz. 2009. Specific inhibition of kynurenate synthesis enhances extracellular dopamine levels in the rodent striatum. *Neuroscience* 159:196-203.

99. MacKenzie, C. R., K. Heseler, A. Muller, and W. Daubener. 2007. Role of indoleamine 2,3-dioxygenase in antimicrobial defence and immuno-regulation: tryptophan depletion versus production of toxic kynurenines. *Curr Drug Metab* 8:237-244.

100. Braidy, N., G. J. Guillemin, and R. Grant. 2011. Effects of Kynurenine Pathway Inhibition on NAD Metabolism and Cell Viability in Human Primary Astrocytes and Neurons. *International journal of tryptophan research : IJTR* 4:29-37.

101. Weed, M. R., R. D. Hienz, J. V. Brady, R. J. Adams, J. L. Mankowski, J. E. Clements, and M. C. Zink. 2003. Central nervous system correlates of behavioral deficits following simian immunodeficiency virus infection. *J Neurovirol* 9:452-464.

102. Mankowski, J. L., S. E. Queen, P. M. Tarwater, K. J. Fox, and V. H. Perry. 2002. Accumulation of beta-amyloid precursor protein in axons correlates with CNS expression of SIV gp41. *J Neuropathol Exp Neurol* 61:85-90.

103. Clements, J. E., J. L. Mankowski, L. Gama, and M. C. Zink. 2008. The accelerated simian immunodeficiency virus macaque model of human immunodeficiency virus-associated neurological disease: from mechanism to treatment. *J Neurovirol* 14:309-317.

104. Notarangelo, F. M., H. Q. Wu, A. Macherone, D. R. Graham, and R. Schwarcz. 2012. Gas chromatography/tandem mass spectrometry detection of extracellular kynurenine and related metabolites in normal and lesioned rat brain. *Anal Biochem* 421:573-581.

105. Eckstein, J. A., G. M. Ammerman, J. M. Reveles, and B. L. Ackermann. 2008. Simultaneous profiling of multiple neurochemical pathways from a single cerebrospinal fluid sample using GC/MS/MS with electron capture detection. *J Mass Spectrom* 43:782-790.

106. Geiss, G. K., R. E. Bumgarner, B. Birditt, T. Dahl, N. Dowidar, D. L. Dunaway, H. P. Fell, S. Ferree, R. D. George, T. Grogan, J. J. James, M. Maysuria, J. D. Mitton, P. Oliveri, J. L. Osborn, T. Peng, A. L. Ratcliffe, P. J. Webster, E. H.

Davidson, L. Hood, and K. Dimitrov. 2008. Direct multiplexed measurement of gene expression with color-coded probe pairs. *Nat Biotechnol* 26:317-325.

107. Lee, P. D., R. Sladek, C. M. Greenwood, and T. J. Hudson. 2002. Control genes and variability: absence of ubiquitous reference transcripts in diverse mammalian expression studies. *Genome Res* 12:292-297.

108. Chege, D., Y. Chai, S. Huibner, L. McKinnon, C. Wachihi, M. Kimani, W. Jaoko, J. Kimani, T. B. Ball, F. A. Plummer, R. Kaul, and A. Rebbapragada. 2010. Evaluation of a quantitative real-time PCR assay to measure HIV-specific mucosal CD8+ T cell responses in the cervix. *PLoS One* 5:e13077.

109. Harman, A. N., J. Wilkinson, C. R. Bye, L. Bosnjak, J. L. Stern, M. Nicholle, J. Lai, and A. L. Cunningham. 2006. HIV induces maturation of monocyte-derived dendritic cells and Langerhans cells. *J Immunol* 177:7103-7113.

110. Radonic, A., S. Thulke, I. M. Mackay, O. Landt, W. Siegert, and A. Nitsche. 2004. Guideline to reference gene selection for quantitative real-time PCR. *Biochem Biophys Res Commun* 313:856-862.

111. Vandesompele, J., K. De Preter, F. Pattyn, B. Poppe, N. Van Roy, A. De Paepe, and F. Speleman. 2002. Accurate normalization of real-time quantitative RT-PCR data by geometric averaging of multiple internal control genes. *Genome Biol* 3:RESEARCH0034.

112. Gubern, C., O. Hurtado, R. Rodriguez, J. R. Morales, V. G. Romera, M. A. Moro, I. Lizasoain, J. Serena, and J. Mallolas. 2009. Validation of housekeeping genes for quantitative real-time PCR in in-vivo and in-vitro models of cerebral ischaemia. *BMC Mol Biol* 10:57.

113. Twisk, J., and W. de Vente. 2002. Attrition in longitudinal studies. How to deal with missing data. *J Clin Epidemiol* 55:329-337.

114. Kelley, C. F., C. M. Kitchen, P. W. Hunt, B. Rodriguez, F. M. Hecht, M. Kitahata, H. M. Crane, J. Willig, M. Mugavero, M. Saag, J. N. Martin, and S. G. Deeks. 2009. Incomplete peripheral CD4+ cell count restoration in HIV-infected patients receiving long-term antiretroviral treatment. *Clin Infect Dis* 48:787-794.

115. Metz, R., C. Smith, J. B. Duhadaway, P. Chandler, B. Baban, L. M. Merlo, E. Pigott, M. P. Keough, S. Rust, A. L. Mellor, L. Mandik-Nayak, A. J. Muller, and G. C. Prendergast. 2014. IDO2 is critical for IDO1-mediated T-cell regulation and exerts a non-redundant function in inflammation. *Int Immunol*.

116. Boasso, A., M. Vaccari, A. Hryniewicz, D. Fuchs, J. Nacsa, V. Cecchinato, J. Andersson, G. Franchini, G. M. Shearer, and C. Chougnet. 2007. Regulatory T-cell markers, indoleamine 2,3-dioxygenase, and virus levels in spleen and gut during progressive simian immunodeficiency virus infection. *J Virol* 81:11593-11603.

117. Andersson, J., A. Boasso, J. Nilsson, R. Zhang, N. J. Shire, S. Lindback, G. M. Shearer, and C. A. Chougnet. 2005. The prevalence of regulatory T cells in lymphoid tissue is correlated with viral load in HIV-infected patients. *J Immunol* 174:3143-3147.

118. Nilsson, J., A. Boasso, P. A. Velilla, R. Zhang, M. Vaccari, G. Franchini, G. M. Shearer, J. Andersson, and C. Chougnet. 2006. HIV-1-driven regulatory T-cell accumulation in lymphoid tissues is associated with disease progression in HIV/AIDS. *Blood* 108:3808-3817.

119. Eriksson, T., and L. Lidberg. 1996. Decreased plasma ratio of tryptophan to competing large neutral amino acids in human immunodeficiency virus type 1 infected subjects: possible implications for development of neuro-psychiatric disorders. *Journal of neural transmission* 103:157-164.

120. Boasso, A., and G. M. Shearer. 2008. Chronic innate immune activation as a cause of HIV-1 immunopathogenesis. *Clin Immunol* 126:235-242.

121. Wonderlich, E. R., M. Kader, V. Wijewardana, and S. M. Barratt-Boyes. 2011. Dissecting the role of dendritic cells in simian immunodeficiency virus infection and AIDS. *Immunol Res* 50:228-234.

122. Malleret, B., B. Maneglier, I. Karlsson, P. Lebon, M. Nascimbeni, L. Perie, P. Brochard, B. Delache, J. Calvo, T. Andrieu, O. Spreux-Varoquaux, A. Hosmalin, R. Le Grand, and B. Vaslin. 2008. Primary infection with simian immunodeficiency virus: plasmacytoid dendritic cell homing to lymph nodes, type I interferon, and immune suppression. *Blood* 112:4598-4608.

123. Murray, M. F. 2003. Tryptophan depletion and HIV infection: a metabolic link to pathogenesis. *Lancet Infect Dis* 3:644-652.

124. Huengsberg, M., J. B. Winer, M. Gompels, R. Round, J. Ross, and M. Shahmanesh. 1998. Serum kynurenine-to-tryptophan ratio increases with progressive disease in HIV-infected patients. *Clin Chem* 44:858-862.

125. Boasso, A., J. P. Herbeuval, A. W. Hardy, C. Winkler, and G. M. Shearer. 2005. Regulation of indoleamine 2,3-dioxygenase and tryptophanyl-tRNA-synthetase by CTLA-4-Fc in human CD4+ T cells. *Blood* 105:1574-1581.

126. Carlin, J. M., E. C. Borden, P. M. Sondel, and G. I. Byrne. 1989. Interferon-induced indoleamine 2,3-dioxygenase activity in human mononuclear phagocytes. *J Leukoc Biol* 45:29-34.

127. Orabona, C., M. T. Pallotta, C. Volpi, F. Fallarino, C. Vacca, R. Bianchi, M. L. Belladonna, M. C. Fioretti, U. Grohmann, and P. Puccetti. 2008. SOCS3 drives proteasomal degradation of indoleamine 2,3-dioxygenase (IDO) and antagonizes IDO-dependent tolerogenesis. *Proc Natl Acad Sci U S A* 105:20828-20833.

128. Moutsopoulos, N. M., N. Vazquez, T. Greenwell-Wild, I. Ecevit, J. Horn, J. Orenstein, and S. M. Wahl. 2006. Regulation of the tonsil cytokine milieu favors HIV susceptibility. *J Leukoc Biol* 80:1145-1155.

129. Akhtar, L. N., H. Qin, M. T. Muldowney, L. L. Yanagisawa, O. Kutsch, J. E. Clements, and E. N. Benveniste. 2010. Suppressor of cytokine signaling 3 inhibits antiviral IFN-beta signaling to enhance HIV-1 replication in macrophages. *J Immunol* 185:2393-2404.

130. Lim, C. K., M. M. Yap, S. J. Kent, G. Gras, B. Samah, J. C. Batten, R. De Rose, B. Heng, B. J. Brew, and G. J. Guillemin. 2013. Characterization of the kynurenine pathway and quinolinic Acid production in macaque macrophages. *International journal of tryptophan research : IJTR* 6:7-19.

131. Kraus, G., A. Werner, M. Baier, D. Binniger, F. J. Ferdinand, S. Norley, and R. Kurth. 1989. Isolation of human immunodeficiency virus-related simian immunodeficiency viruses from African green monkeys. *Proc Natl Acad Sci U S A* 86:2892-2896.

132. Chahroudi, A., S. E. Bosinger, T. H. Vanderford, M. Paiardini, and G. Silvestri. 2012. Natural SIV hosts: showing AIDS the door. *Science* 335:1188-1193.

133. Rey-Cuille, M. A., J. L. Berthier, M. C. Bomsel-Demontoy, Y. Chaduc, L. Montagnier, A. G. Hovanessian, and L. A. Chakrabarti. 1998. Simian immunodeficiency virus replicates to high levels in sooty mangabeys without inducing disease. *J Virol* 72:3872-3886.

134. Silvestri, G., D. L. Sodora, R. A. Koup, M. Paiardini, S. P. O'Neil, H. M. McClure, S. I. Staprans, and M. B. Feinberg. 2003. Nonpathogenic SIV infection of sooty mangabeys is characterized by limited bystander immunopathology despite chronic high-level viremia. *Immunity* 18:441-452.

135. Jacquelin, B., V. Mayau, B. Targat, A. S. Liovat, D. Kunkel, G. Petitjean, M. A. Dillies, P. Roques, C. Butor, G. Silvestri, L. D. Giavedoni, P. Lebon, F. Barre-Sinoussi, A. Benecke, and M. C. Muller-Trutwin. 2009. Nonpathogenic SIV infection of African green monkeys induces a strong but rapidly controlled type I IFN response. *J Clin Invest* 119:3544-3555.

136. Harris, L. D., B. Tabb, D. L. Sodora, M. Paiardini, N. R. Klatt, D. C. Douek, G. Silvestri, M. Muller-Trutwin, I. Vasile-Pandrea, C. Apetrei, V. Hirsch, J. Lifson, J. M. Brenchley, and J. D. Estes. 2010. Downregulation of robust acute type I interferon responses distinguishes nonpathogenic simian immunodeficiency virus (SIV) infection of natural hosts from pathogenic SIV infection of rhesus macaques. *J Virol* 84:7886-7891.

137. Bosinger, S. E., Q. Li, S. N. Gordon, N. R. Klatt, L. Duan, L. Xu, N. Francella, A. Sidahmed, A. J. Smith, E. M. Cramer, M. Zeng, D. Masopust, J. V. Carlis, L.

Ran, T. H. Vanderford, M. Paiardini, R. B. Isett, D. A. Baldwin, J. G. Else, S. I. Staprans, G. Silvestri, A. T. Haase, and D. J. Kelvin. 2009. Global genomic analysis reveals rapid control of a robust innate response in SIV-infected sooty mangabeys. *J Clin Invest* 119:3556-3572.

138. Herbeuval, J. P., J. C. Grivel, A. Boasso, A. W. Hardy, C. Chougnet, M. J. Dolan, H. Yagita, J. D. Lifson, and G. M. Shearer. 2005. CD4+ T-cell death induced by infectious and noninfectious HIV-1: role of type 1 interferon-dependent, TRAIL/DR5-mediated apoptosis. *Blood* 106:3524-3531.

139. Herbeuval, J. P., J. Nilsson, A. Boasso, A. W. Hardy, M. J. Kruhlak, S. A. Anderson, M. J. Dolan, M. Dy, J. Andersson, and G. M. Shearer. 2006. Differential expression of IFN-alpha and TRAIL/DR5 in lymphoid tissue of progressor versus nonprogressor HIV-1-infected patients. *Proc Natl Acad Sci U S A* 103:7000-7005.

140. Bandera, A., G. Ferrario, M. Saresella, I. Marventano, A. Soria, F. Zanini, F. Sabbatini, M. Airoldi, G. Marchetti, F. Franzetti, D. Trabattoni, M. Clerici, and A. Gori. 2010. CD4+ T cell depletion, immune activation and increased production of regulatory T cells in the thymus of HIV-infected individuals. *PLoS One* 5:e10788.

141. Hansjee, N., G. R. Kaufmann, C. Strub, R. Weber, M. Battegay, P. Erb, and H. I. V. C. S. Swiss. 2004. Persistent apoptosis in HIV-1-infected individuals receiving potent antiretroviral therapy is associated with poor recovery of CD4 T lymphocytes. *J Acquir Immune Defic Syndr* 36:671-677.

142. Sandbulte, M. R., A. C. Boon, R. J. Webby, and J. M. Riberdy. 2008. Analysis of cytokine secretion from human plasmacytoid dendritic cells infected with H5N1 or low-pathogenicity influenza viruses. *Virology* 381:22-28.

143. Peiris, J. S., C. Y. Cheung, C. Y. Leung, and J. M. Nicholls. 2009. Innate immune responses to influenza A H5N1: friend or foe? *Trends in immunology* 30:574-584.

144. Geiler, J., M. Michaelis, P. Sithisarn, and J. Cinatl, Jr. 2011. Comparison of pro-inflammatory cytokine expression and cellular signal transduction in human macrophages infected with different influenza A viruses. *Med Microbiol Immunol* 200:53-60.

145. Wurzer, W. J., C. Ehrhardt, S. Pleschka, F. Berberich-Siebelt, T. Wolff, H. Walczak, O. Planz, and S. Ludwig. 2004. NF-kappaB-dependent induction of tumor necrosis factor-related apoptosis-inducing ligand (TRAIL) and Fas/FasL is crucial for efficient influenza virus propagation. *J Biol Chem* 279:30931-30937.

146. Samuel, C. E. 2001. Antiviral actions of interferons. *Clin Microbiol Rev* 14:778-809, table of contents.

147. Gonzalez-Navajas, J. M., J. Lee, M. David, and E. Raz. 2012. Immunomodulatory functions of type I interferons. *Nat Rev Immunol* 12:125-135.

148. Fernandez-Cruz, E., J. M. Lang, J. Frissen, V. Furner, M. Chateauvert, C. A. Boucher, P. Dowd, and J. Stevens. 1995. Zidovudine plus interferon-alpha versus zidovudine alone in HIV-infected symptomatic or asymptomatic persons with CD4+ cell counts > 150 x 10(6)/L: results of the Zidon trial. Zidon Study Group. *AIDS* 9:1025-1035.

149. Lane, H. C., V. Davey, J. A. Kovacs, J. Feinberg, J. A. Metcalf, B. Herpin, R. Walker, L. Deyton, R. T. Davey, Jr., J. Falloon, and et al. 1990. Interferon-alpha in patients with asymptomatic human immunodeficiency virus (HIV) infection. A randomized, placebo-controlled trial. *Ann Intern Med* 112:805-811.

150. Rivero, J., M. Limonta, A. Aguilera, M. Fraga, and P. Lopez Saura. 1994. Use of recombinant interferon-alpha in human immunodeficiency virus (HIV)-infected individuals. *Biotherapy* 8:23-31.

151. Skillman, D. R., J. L. Malone, C. F. Decker, K. F. Wagner, R. L. Mapou, M. J. Liao, D. Testa, and M. S. Meltzer. 1996. Phase I trial of interferon alfa-n3 in early-stage human immunodeficiency virus type 1 disease: evidence for drug safety, tolerance, and antiviral activity. *J Infect Dis* 173:1107-1114.

152. Katabira, E. T., N. K. Sewankambo, R. D. Mugerwa, E. M. Belsey, F. X. Mubiru, C. Othieno, P. Kataaha, M. Karam, M. Youle, J. H. Perriens, and J. M. Lange. 1998. Lack of efficacy of low dose oral interferon alfa in symptomatic HIV-1 infection: a randomised, double blind, placebo controlled trial. *Sex Transm Infect* 74:265-270.

153. Jeremias, I., I. Herr, T. Boehler, and K. M. Debatin. 1998. TRAIL/Apo-2-ligand-induced apoptosis in human T cells. *Eur J Immunol* 28:143-152.

154. Dockrell, D. H., A. D. Badley, A. Algeciras-Schimnich, M. Simpson, R. Schut, D. H. Lynch, and C. V. Paya. 1999. Activation-induced CD4+ T cell death in HIV-positive individuals correlates with Fas susceptibility, CD4+ T cell count, and HIV plasma viral copy number. *AIDS Res Hum Retroviruses* 15:1509-1518.

155. Meier, A., A. Bagchi, H. K. Sidhu, G. Alter, T. J. Suscovich, D. G. Kavanagh, H. Streeck, M. A. Brockman, S. LeGall, J. Hellman, and M. Altfeld. 2008. Upregulation of PD-L1 on monocytes and dendritic cells by HIV-1 derived TLR ligands. *AIDS* 22:655-658.

156. Herbeuval, J. P., and G. M. Shearer. 2007. HIV-1 immunopathogenesis: how good interferon turns bad. *Clin Immunol* 123:121-128.

157. Grohmann, U., C. Orabona, F. Fallarino, C. Vacca, F. Calcinaro, A. Falorni, P. Candeloro, M. L. Belladonna, R. Bianchi, M. C. Fioretti, and P. Puccetti. 2002. CTLA-4-Ig regulates tryptophan catabolism in vivo. *Nat Immunol* 3:1097-1101.

158. Munn, D. H., M. D. Sharma, and A. L. Mellor. 2004. Ligation of B7-1/B7-2 by human CD4+ T cells triggers indoleamine 2,3-dioxygenase activity in dendritic cells. *J Immunol* 172:4100-4110.

159. Belladonna, M. L., C. Orabona, U. Grohmann, and P. Puccetti. 2009. TGF-beta and kynurenines as the key to infectious tolerance. *Trends Mol Med* 15:41-49.

160. Fallarino, F., U. Grohmann, C. Vacca, R. Bianchi, C. Orabona, A. Spreca, M. C. Fioretti, and P. Puccetti. 2002. T cell apoptosis by tryptophan catabolism. *Cell Death Differ* 9:1069-1077.

161. Fallarino, F., U. Grohmann, S. You, B. C. McGrath, D. R. Cavener, C. Vacca, C. Orabona, R. Bianchi, M. L. Belladonna, C. Volpi, P. Santamaria, M. C. Fioretti, and P. Puccetti. 2006. The combined effects of tryptophan starvation and tryptophan catabolites down-regulate T cell receptor zeta-chain and induce a regulatory phenotype in naive T cells. *J Immunol* 176:6752-6761.

162. Tilley, B. C., G. S. Alarcon, S. P. Heyse, D. E. Trentham, R. Neuner, D. A. Kaplan, D. O. Clegg, J. C. Leisen, L. Buckley, S. M. Cooper, H. Duncan, S. R. Pillemer, M. Tuttleman, and S. E. Fowler. 1995. Minocycline in rheumatoid arthritis. A 48-week, double-blind, placebo-controlled trial. MIRA Trial Group. *Ann Intern Med* 122:81-89.

163. Brundula, V., N. B. Rewcastle, L. M. Metz, C. C. Bernard, and V. W. Yong. 2002. Targeting leukocyte MMPs and transmigration: minocycline as a potential therapy for multiple sclerosis. *Brain* 125:1297-1308.

164. Zhu, S., I. G. Stavrovskaya, M. Drozda, B. Y. Kim, V. Ona, M. Li, S. Sarang, A. S. Liu, D. M. Hartley, D. C. Wu, S. Gullans, R. J. Ferrante, S. Przedborski, B. S. Kristal, and R. M. Friedlander. 2002. Minocycline inhibits cytochrome c release and delays progression of amyotrophic lateral sclerosis in mice. *Nature* 417:74-78.

165. Chen, M., V. O. Ona, M. Li, R. J. Ferrante, K. B. Fink, S. Zhu, J. Bian, L. Guo, L. A. Farrell, S. M. Hersch, W. Hobbs, J. P. Vonsattel, J. H. Cha, and R. M. Friedlander. 2000. Minocycline inhibits caspase-1 and caspase-3 expression and delays mortality in a transgenic mouse model of Huntington disease. *Nat Med* 6:797-801.

166. Du, Y., Z. Ma, S. Lin, R. C. Dodel, F. Gao, K. R. Bales, L. C. Triarhou, E. Chernet, K. W. Perry, D. L. Nelson, S. Luecke, L. A. Phebus, F. P. Bymaster, and S. M. Paul. 2001. Minocycline prevents nigrostriatal dopaminergic neurodegeneration in the MPTP model of Parkinson's disease. *Proc Natl Acad Sci U S A* 98:14669-14674.

167. Naura, A. S., H. Kim, J. Ju, P. C. Rodriguez, J. Jordan, A. D. Catling, B. M. Rezk, Z. Y. Abd Elmageed, K. Pyakurel, A. F. Tarhuni, M. Q. Abughazleh, Y. Errami, M. Zerfaoui, A. C. Ochoa, and A. H. Boulares. 2013. Minocycline blocks asthma-associated inflammation in part by interfering with the t cell receptor-nuclear factor kappaB-GATA-3-IL-4 axis without a prominent effect on poly(ADP-ribose) polymerase. *J Biol Chem* 288:1458-1468.

168. Joks, R., T. Smith-Norowitz, M. Nowakowski, M. H. Bluth, and H. G. Durkin. 2010. Tetracycline-mediated IgE isotype-specific suppression of ongoing human and murine IgE responses in vivo and murine memory IgE responses induced in vitro. *Int Immunol* 22:281-288.

169. Dutta, K., K. L. Kumawat, A. Nazmi, M. K. Mishra, and A. Basu. 2010. Minocycline differentially modulates viral infection and persistence in an experimental model of Japanese encephalitis. *Journal of neuroimmune pharmacology : the official journal of the Society on NeuroImmune Pharmacology* 5:553-565.

170. Campbell, J. H., T. H. Burdo, P. Autissier, J. P. Bombardier, S. V. Westmoreland, C. Soulas, R. G. Gonzalez, E. M. Ratai, and K. C. Williams. 2011. Minocycline inhibition of monocyte activation correlates with neuronal protection in SIV neuroAIDS. *PLoS One* 6:e18688.

171. Szeto, G. L., J. L. Pomerantz, D. R. Graham, and J. E. Clements. 2011. Minocycline suppresses activation of nuclear factor of activated T cells 1 (NFAT1) in human CD4+ T cells. *J Biol Chem*.

172. Kloppenburg, M., C. L. Verweij, A. M. Miltenburg, A. J. Verhoeven, M. R. Daha, B. A. Dijkmans, and F. C. Breedveld. 1995. The influence of tetracyclines on T cell activation. *Clin Exp Immunol* 102:635-641.

173. Nikodemova, M., I. D. Duncan, and J. J. Watters. 2006. Minocycline exerts inhibitory effects on multiple mitogen-activated protein kinases and IkappaBalpha degradation in a stimulus-specific manner in microglia. *J Neurochem* 96:314-323.

174. Kloppenburg, M., B. M. Brinkman, H. H. de Rooij-Dijk, A. M. Miltenburg, M. R. Daha, F. C. Breedveld, B. A. Dijkmans, and C. Verweij. 1996. The tetracycline derivative minocycline differentially affects cytokine production by monocytes and T lymphocytes. *Antimicrob Agents Chemother* 40:934-940.

175. Pang, T., J. Wang, J. Benicky, and J. M. Saavedra. 2012. Minocycline ameliorates LPS-induced inflammation in human monocytes by novel mechanisms including LOX-1, Nur77 and LITAF inhibition. *Biochim Biophys Acta* 1820:503-510.

176. Tai, K., H. Iwasaki, S. Ikegaya, and T. Ueda. 2012. Minocycline modulates cytokine and chemokine production in lipopolysaccharide-stimulated THP-1 monocytic cells by inhibiting IkappaB kinase alpha/beta phosphorylation. *Translational research : the journal of laboratory and clinical medicine*.

177. Li, L., Y. Ben, Z. Zhu, W. Li, J. Xu, and X. Zhang. 2012. Minocycline down-regulates topical mucosal inflammation during the application of microbicide candidates. *PLoS One* 7:e43211.

178. Enose-Akahata, Y., E. Matsuura, Y. Tanaka, U. Oh, and S. Jacobson. 2012. Minocycline modulates antigen-specific CTL activity through inactivation of

mononuclear phagocytes in patients with HTLV-I associated neurologic disease. *Retrovirology* 9:16.

179. Zink, M. C., and J. E. Clements. 2002. A novel simian immunodeficiency virus model that provides insight into mechanisms of human immunodeficiency virus central nervous system disease. *J Neurovirol* 8 Suppl 2:42-48.

180. Agwuh, K. N., and A. MacGowan. 2006. Pharmacokinetics and pharmacodynamics of the tetracyclines including glycylcyclines. *J Antimicrob Chemother* 58:256-265.

181. Macdonald, H., R. G. Kelly, E. S. Allen, J. F. Noble, and L. A. Kanegis. 1973. Pharmacokinetic studies on minocycline in man. *Clin Pharmacol Ther* 14:852-861.

182. Livak, K. J., and T. D. Schmittgen. 2001. Analysis of relative gene expression data using real-time quantitative PCR and the 2(-Delta Delta C(T)) Method. *Methods* 25:402-408.

183. Reeves, R. K., T. I. Evans, J. Gillis, F. E. Wong, G. Kang, Q. Li, and R. P. Johnson. 2012. SIV infection induces accumulation of plasmacytoid dendritic cells in the gut mucosa. *J Infect Dis* 206:1462-1468.

184. Lehmann, C., M. Lafferty, A. Garzino-Demo, N. Jung, P. Hartmann, G. Fatkenheuer, J. S. Wolf, J. van Lunzen, and F. Romerio. 2010. Plasmacytoid dendritic cells accumulate and secrete interferon alpha in lymph nodes of HIV-1 patients. *PLoS One* 5:e11110.

185. Lehmann, C., J. M. Harper, D. Taubert, P. Hartmann, G. Fatkenheuer, N. Jung, J. van Lunzen, H. J. Stellbrink, R. C. Gallo, and F. Romerio. 2008. Increased

interferon alpha expression in circulating plasmacytoid dendritic cells of HIV-1-infected patients. *J Acquir Immune Defic Syndr* 48:522-530.

186. Brown, K. N., A. Trichel, and S. M. Barratt-Boyes. 2007. Parallel loss of myeloid and plasmacytoid dendritic cells from blood and lymphoid tissue in simian AIDS. *J Immunol* 178:6958-6967.

187. Brown, K. N., V. Wijewardana, X. Liu, and S. M. Barratt-Boyes. 2009. Rapid influx and death of plasmacytoid dendritic cells in lymph nodes mediate depletion in acute simian immunodeficiency virus infection. *PLoS Pathog* 5:e1000413.

188. Kader, M., A. P. Smith, C. Guiducci, E. R. Wonderlich, D. Normolle, S. C. Watkins, F. J. Barrat, and S. M. Barratt-Boyes. 2013. Blocking TLR7- and TLR9-mediated IFN-alpha Production by Plasmacytoid Dendritic Cells Does Not Diminish Immune Activation in Early SIV Infection. *PLoS Pathog* 9:e1003530.

189. Rossio, J. L., M. T. Esser, K. Suryanarayana, D. K. Schneider, J. W. Bess, Jr., G. M. Vasquez, T. A. Wiltrout, E. Chertova, M. K. Grimes, Q. Sattentau, L. O. Arthur, L. E. Henderson, and J. D. Lifson. 1998. Inactivation of human immunodeficiency virus type 1 infectivity with preservation of conformational and functional integrity of virion surface proteins. *J Virol* 72:7992-8001.

190. Kayagaki, N., N. Yamaguchi, M. Nakayama, H. Eto, K. Okumura, and H. Yagita. 1999. Type I Interferons (IFNs) Regulate Tumor Necrosis Factor–related Apoptosis-inducing Ligand (TRAIL) Expression on Human T Cells: A Novel Mechanism for the Antitumor Effects of Type I IFNs. *The Journal of Experimental Medicine* 189:1451-1460.

191. Singh, M., P. Singh, D. Vaira, M. Amand, S. Rahmouni, and M. Moutschen. 2014. Minocycline Attenuates HIV-1 Infection and Suppresses Chronic Immune Activation in Humanized NOD/LtsZ-scidIL-2Rgamma mice. *Immunology*.

192. Szeto, G. L., A. K. Brice, H. C. Yang, S. A. Barber, R. F. Siliciano, and J. E. Clements. 2010. Minocycline attenuates HIV infection and reactivation by suppressing cellular activation in human CD4+ T cells. *J Infect Dis* 201:1132-1140.

193. Chu, H. C., Y. L. Lin, H. K. Sytwu, S. H. Lin, C. L. Liao, and Y. C. Chao. 2005. Effects of minocycline on Fas-mediated fulminant hepatitis in mice. *Br J Pharmacol* 144:275-282.

194. Wei, X., L. Zhao, J. Liu, R. C. Dodel, M. R. Farlow, and Y. Du. 2005. Minocycline prevents gentamicin-induced ototoxicity by inhibiting p38 MAP kinase phosphorylation and caspase 3 activation. *Neuroscience* 131:513-521.

195. Noble, W., C. Garwood, J. Stephenson, A. M. Kinsey, D. P. Hanger, and B. H. Anderton. 2009. Minocycline reduces the development of abnormal tau species in models of Alzheimer's disease. *FASEB J* 23:739-750.

196. Wang, R., L. Zhang, X. Zhang, J. Moreno, X. Luo, M. Tondravi, and Y. Shi. 2001. Differential regulation of the expression of CD95 ligand, receptor activator of nuclear factor-kappa B ligand (RANKL), TNF-related apoptosis-inducing ligand (TRAIL), and TNF-alpha during T cell activation. *J Immunol* 166:1983-1990.

197. Fernandez-Gomez, F. J., M. F. Galindo, M. Gomez-Lazaro, C. Gonzalez-Garcia, V. Cena, N. Aguirre, and J. Jordan. 2005. Involvement of mitochondrial potential

and calcium buffering capacity in minocycline cytoprotective actions. *Neuroscience* 133:959-967.

198. Garcia-Martinez, E. M., S. Sanz-Blasco, A. Karachitos, M. J. Bandez, F. J. Fernandez-Gomez, S. Perez-Alvarez, R. M. de Mera, M. J. Jordan, N. Aguirre, M. F. Galindo, C. Villalobos, A. Navarro, H. Kmita, and J. Jordan. 2010. Mitochondria and calcium flux as targets of neuroprotection caused by minocycline in cerebellar granule cells. *Biochem Pharmacol* 79:239-250.

199. Nikodemova, M., J. J. Watters, S. J. Jackson, S. K. Yang, and I. D. Duncan. 2007. Minocycline down-regulates MHC II expression in microglia and macrophages through inhibition of IRF-1 and protein kinase C (PKC)alpha/betaII. *J Biol Chem* 282:15208-15216.

200. Bel, M., M. Ocana-Macchi, M. Liniger, K. C. McCullough, M. Matrosovich, and A. Summerfield. 2011. Efficient sensing of avian influenza viruses by porcine plasmacytoid dendritic cells. *Viruses* 3:312-330.

201. Ho, E. L., S. S. Spudich, E. Lee, D. Fuchs, E. Sinclair, and R. W. Price. 2011. Minocycline fails to modulate cerebrospinal fluid HIV infection or immune activation in chronic untreated HIV-1 infection: results of a pilot study. *AIDS research and therapy* 8:17.

202. Tai, K., H. Iwasaki, S. Ikegaya, and T. Ueda. 2013. Minocycline modulates cytokine and chemokine production in lipopolysaccharide-stimulated THP-1 monocytic cells by inhibiting IkappaB kinase alpha/beta phosphorylation. *Translational research : the journal of laboratory and clinical medicine* 161:99-109.

203. Lepelley, A., S. Louis, M. Sourisseau, H. K. Law, J. Pothlichet, C. Schilte, L. Chaperot, J. Plumas, R. E. Randall, M. Si-Tahar, F. Mammano, M. L. Albert, and O. Schwartz. 2011. Innate sensing of HIV-infected cells. *PLoS Pathog* 7:e1001284.

204. Campillo-Gimenez, L., M. Laforge, M. Fay, A. Brussel, M. C. Cumont, V. Monceaux, O. Diop, Y. Levy, B. Hurtrel, J. Zaunders, J. Corbeil, C. Elbim, and J. Estaquier. 2010. Nonpathogenesis of simian immunodeficiency virus infection is associated with reduced inflammation and recruitment of plasmacytoid dendritic cells to lymph nodes, not to lack of an interferon type I response, during the acute phase. *J Virol* 84:1838-1846.

205. Reeves, R. K., and P. N. Fultz. 2007. Disparate effects of acute and chronic infection with SIVmac239 or SHIV-89.6P on macaque plasmacytoid dendritic cells. *Virology* 365:356-368.

206. Ravimohan, S., L. Gama, E. L. Engle, M. C. Zink, and J. E. Clements. 2012. Early emergence and selection of a SIV-LTR C/EBP site variant in SIV-infected macaques that increases virus infectivity. *PLoS One* 7:e42801.

207. Abel, K., M. J. Alegria-Hartman, K. Rothaeusler, M. Marthas, and C. J. Miller. 2002. The relationship between simian immunodeficiency virus RNA levels and the mRNA levels of alpha/beta interferons (IFN-alpha/beta) and IFN-alpha/beta-inducible Mx in lymphoid tissues of rhesus macaques during acute and chronic infection. *J Virol* 76:8433-8445.

208. Fraietta, J. A., Y. M. Mueller, G. Yang, A. C. Boesteanu, D. T. Gracias, D. H. Do, J. L. Hope, N. Kathuria, S. E. McGettigan, M. G. Lewis, L. D. Giavedoni, J. M.

Jacobson, and P. D. Katsikis. 2013. Type I Interferon Upregulates Bak and Contributes to T Cell Loss during Human Immunodeficiency Virus (HIV) Infection. *PLoS Pathog* 9:e1003658.

209. Rani, M. R., and R. M. Ransohoff. 2005. Alternative and accessory pathways in the regulation of IFN-beta-mediated gene expression. *J Interferon Cytokine Res* 25:788-798.

210. Manches, O., M. V. Fernandez, J. Plumas, L. Chaperot, and N. Bhardwaj. 2012. Activation of the noncanonical NF-kappaB pathway by HIV controls a dendritic cell immunoregulatory phenotype. *Proc Natl Acad Sci U S A* 109:14122-14127.

211. Barblu, L., K. Machmach, C. Gras, J. F. Delfraissy, F. Boufassa, M. Leal, E. Ruiz-Mateos, O. Lambotte, and J. P. Herbeuval. 2012. Plasmacytoid dendritic cells (pDCs) from HIV controllers produce interferon-alpha and differentiate into functional killer pDCs under HIV activation. *J Infect Dis* 206:790-801.

212. Gasper-Smith, N., D. M. Crossman, J. F. Whitesides, N. Mensali, J. S. Ottinger, S. G. Plonk, M. A. Moody, G. Ferrari, K. J. Weinhold, S. E. Miller, C. F. Reich, 3rd, L. Qin, S. G. Self, G. M. Shaw, T. N. Denny, L. E. Jones, D. S. Pisetsky, and B. F. Haynes. 2008. Induction of plasma (TRAIL), TNFR-2, Fas ligand, and plasma microparticles after human immunodeficiency virus type 1 (HIV-1) transmission: implications for HIV-1 vaccine design. *J Virol* 82:7700-7710.

213. Gibellini, D., M. Borderi, E. De Crignis, R. Cicola, F. Vescini, R. Caudarella, F. Chiodo, and M. C. Re. 2007. RANKL/OPG/TRAIL plasma levels and bone mass loss evaluation in antiretroviral naive HIV-1-positive men. *J Med Virol* 79:1446-1454.

214. Kim, N., A. Dabrowska, R. G. Jenner, and A. Aldovini. 2007. Human and simian immunodeficiency virus-mediated upregulation of the apoptotic factor TRAIL occurs in antigen-presenting cells from AIDS-susceptible but not from AIDS-resistant species. *J Virol* 81:7584-7597.

215. Kaser, A., S. Nagata, and H. Tilg. 1999. Interferon alpha augments activation-induced T cell death by upregulation of Fas (CD95/APO-1) and Fas ligand expression. *Cytokine* 11:736-743.

216. Xu, G., and Y. Shi. 2007. Apoptosis signaling pathways and lymphocyte homeostasis. *Cell research* 17:759-771.

217. Fujikura, D., S. Chiba, D. Muramatsu, M. Kazumata, Y. Nakayama, T. Kawai, S. Akira, H. Kida, and T. Miyazaki. 2013. Type-I interferon is critical for FasL expression on lung cells to determine the severity of influenza. *PLoS One* 8:e55321.

218. Liegler, T. J., W. Yonemoto, T. Elbeik, E. Vittinghoff, S. P. Buchbinder, and W. C. Greene. 1998. Diminished spontaneous apoptosis in lymphocytes from human immunodeficiency virus-infected long-term nonprogressors. *J Infect Dis* 178:669-679.

219. Ratai, E. M., J. P. Bombardier, C. G. Joo, L. Annamalai, T. H. Burdo, J. Campbell, R. Fell, R. Hakimelahi, J. He, P. Autissier, M. R. Lentz, E. F. Halpern, E. Masliah, K. C. Williams, S. V. Westmoreland, and R. G. Gonzalez. 2010. Proton magnetic resonance spectroscopy reveals neuroprotection by oral minocycline in a nonhuman primate model of accelerated NeuroAIDS. *PLoS One* 5:e10523.

220. Si, Q., M. Cosenza, M. O. Kim, M. L. Zhao, M. Brownlee, H. Goldstein, and S. Lee. 2004. A novel action of minocycline: inhibition of human immunodeficiency virus type 1 infection in microglia. *J Neurovirol* 10:284-292.

221. Nakasujja, N., S. Miyahara, S. Evans, A. Lee, S. Musisi, E. Katabira, K. Robertson, A. Ronald, D. B. Clifford, and N. Sacktor. 2013. Randomized trial of minocycline in the treatment of HIV-associated cognitive impairment. *Neurology* 80:196-202.

222. Sacktor, N., S. Miyahara, L. Deng, S. Evans, G. Schifitto, B. A. Cohen, R. Paul, K. Robertson, B. Jarocki, K. Scarsi, R. W. Coombs, M. C. Zink, A. Nath, E. Smith, R. J. Ellis, E. Singer, J. Weihe, S. McCarthy, L. Hosey, D. B. Clifford, and A. A. team. 2011. Minocycline treatment for HIV-associated cognitive impairment: results from a randomized trial. *Neurology* 77:1135-1142.

223. Ng, H. H., T. Narasaraju, M. C. Phoon, M. K. Sim, J. E. Seet, and V. T. Chow. 2012. Doxycycline treatment attenuates acute lung injury in mice infected with virulent influenza H3N2 virus: involvement of matrix metalloproteinases. *Experimental and molecular pathology* 92:287-295.

224. Martin, A., M. P. Heyes, A. M. Salazar, W. A. Law, and J. Williams. 1993. Impaired motor-skill learning, slowed reaction time, and elevated cerebrospinal-fluid quinolinic acid in a subgroup of HIV-infected individuals. *Neuropsychology* 7:149-157.

225. Heyes, M. P., E. K. Jordan, K. Lee, K. Saito, J. A. Frank, P. J. Snoy, S. P. Markey, and M. Gravell. 1992. Relationship of neurologic status in macaques

infected with the simian immunodeficiency virus to cerebrospinal fluid quinolinic acid and kynurenic acid. *Brain Res* 570:237-250.

226. Morris, K. A., N. W. Davies, and B. J. Brew. 2010. A guide to interpretation of neuroimmunological biomarkers in the combined antiretroviral therapy-era of HIV central nervous system disease. *Neurobehavioral HIV medicine* 2:59-72.

CURRICULUM VITAE

CURRICULUM VITAE

The Johns Hopkins University School of Medicine

Julia L. Drewes March 23, 2014

EDUCATION

Johns Hopkins University School of Medicine (Fall 2007 – Spring 2014)

- Ph.D. in Cellular and Molecular Medicine, expected May 2014
- Doctoral thesis: "Immunosuppression and neurotoxicity: How IDO contributes to pathogenesis of SIV infection"

Stanford University (Fall 2003 – Spring 2007)

- B.S. in Biological Sciences
- Honors thesis: "Intracellular localization of reporter constructs containing *miR-122* binding sites in liver cells"

Oxford University, Corpus Christi College, Stanford in Oxford Program (January 2006 – March 2006)

- Immunology tutorial with Dr. Kathleen F. Nolan: an intensive 8-week reading and writing course tailored to specific topics in immunology and virology with one-on-one discussions of reading material

RESEARCH EXPERIENCE

Doctoral thesis, Cellular & Molecular Medicine graduate program, Department of Molecular & Comparative Pathobiology, Johns Hopkins University School of Medicine (Fall 2007 – Spring 2014)

- Research advisor: Dr. M. Christine Zink
- Showed that the basal ganglia preserves tryptophan levels at the expense of serotonin following induction of the indoleamine 2,3-dioxygenase (IDO) driven pathway of tryptophan catabolism in the CNS of SIV-infected macaques
- Demonstrated that kynurenine metabolites are increased to both neurotoxic and immunomodulatory levels in tissues, while circulating levels are useful biomarkers of disease progression
- Gained expertise in the fields of gas chromatography mass spectrometry, molecular biology, and flow cytometry
- Collaborated on several multidisciplinary projects with outside labs

Undergraduate honors thesis, Microbiology and Immunology Department, Stanford University (Fall 2005 - Spring 2007)

- Research advisor: Dr. Peter Sarnow
- Found that fluorescent reporter constructs containing *mir-122* binding sites localized to the nucleus rather than the cytoplasm in liver cells, suggesting that *miR-122* does not target mRNA transcripts to cytoplasmic P-bodies as other miRNAs have been shown to do
- Gained practical knowledge of molecular biology and fluorescent and confocal microscopy

Student research intern, DuPont Agriculture Research and Development, Newark, DE (Summer 2005)

- Research advisor: Dr. Yong Tao
- Learned basic molecular biology techniques while overexpressing and harvesting proteins in *E. coli* for downstream applications

Student research intern, Inorganic Chemistry Department, University of Delaware (Summer 2004)

- Research advisor: Dr. Charles Riordan
- Gained exposure to inorganic chemistry techniques while synthesizing 1,3-disubstituted carbanamines

LEADERSHIP EXPERIENCE

Fall Clubs Chairperson, Baltimore Field Hockey Association, est. 1923, Baltimore, MD (Spring 2011 – present)

- Coordinated team designations, schedules, facility rentals, and referees for the fall season
- Oversaw and delegated responsibilities to fall co-chairs
- Coordinated with marketing, social, and tournament committees for outside events including the 90th anniversary celebration of BFHA in 2013

Intramural sports coach/captain (Summer 2010 – present)

- Co-captained several championship intramural sports through Baltimore Beach and Baltimore Sports and Social Club

Lunch with Cellular and Molecular Medicine Co-Organizer, Graduate Program in Cellular and Molecular Medicine, Johns Hopkins School of Medicine (Fall 2009 – Spring 2012)

- Coordinated student-led seminars
- Expanded the seminar series to include outside speakers from a variety of scientific career disciplines including academia, science writing, and public policy
- Initiated the invitation of Cellular and Molecular Medicine alumni speakers to facilitate networking within the program

Community Service Co-Chair (Fall 2005 – Spring 2007); field hockey team representative (Fall 2003 – Spring 2007), Cardinal Council Student Athlete Advisory Committee, Stanford University

- Acted as a liaison between Stanford athletes, the Stanford athletics department, Stanford University, and the NCAA in order to protect the welfare of the student athlete community, foster communication between the various athletic teams, and promote a positive image for student athletes
- As Co-Chair of the Community Service Committee, I helped coordinate student athlete volunteers for 3 major annual events: the Special Olympics of Northern California, the student-athlete-run Stanford Olympics for underprivileged middle school students, and the student-athlete-run Athlete Date Auction charity event
- Attended the PAC-10 (now the PAC-12) SAAC conference in 2004 on behalf of Stanford Athletics

PUBLICATIONS

Drewes, J.L., Szeto, G.L., Engle, E.L., Liao, Z., Shearer, G.M., Zink, M.C., Graham, D.R. Attenuation of pathogenic immune responses during infection with human and simian immunodeficiency virus (HIV/SIV) by the tetracycline derivative minocycline. *PLOS One (accepted March 2014)*.

Meulendyke, K.A., Ubaida-Mohien, C., **Drewes, J.L.**, Liao, Z., Gama, L., Witwer, K.W., Graham, D.R., Zink, M.C. Monoamine oxidase contributes to neuropathogenesis of SIV and HIV infection. *J. Infect. Dis. (accepted March 2014*)

Tovar-y-Romo, L.B., Kolson, D.L., Bandaru, V.V.R., **Drewes, J.L.**, Graham, D.R., and Haughey, N.J. (2013) Adenosine triphosphate released from HIV-infected macrophages regulates glutamatergic tone and dendritic spine density on neurons. *J. Neuroimmune Pharmacol*.

MANUSCRIPTS IN PREPARATION OR UNDER REVIEW

Drewes, J.L., Meulendyke, K.A., Liao, Z., Li, M., Witwer, K.W., Gama, L., Ubaida-Mohien, C., Notarangelo, F.M., Schwarcz, R., Graham, D.R., Zink, M.C. Sustained upregulation of neurotoxic kynurenine pathway metabolites in cART-treated SIV-infected pigtailed macaques: Impact on neuroinflammation and serotonin metabolism. (*in preparation*)

Drewes, J.L., Croteau, J.D., Engle, E.L., Graham, D.R., Zink, M.C. Maintenance of tissue tryptophan levels despite kynurenine pathway activation in the spleens of SIV-infected pigtailed macaques. (*in preparation*)

Sacktor, N., Miyahara, S., Evans, S., Schifitto, G., Cohen, B., Haughey, N., **Drewes, J.L.**, Graham, D., Zink, M.C., Anderson, C., Nath, A., Pardo, C.A., McCarthy, S., Hosey, L., Clifford, D. Impact of minocycline on cerebrospinal fluid markers of oxidative stress, neuronal injury, and inflammation in HIV seropositive individuals with cognitive impairment. (*in preparation*)

INVITED SPEAKER PRESENTATIONS

Zink, M.C., **Drewes, J.L.**, Meulendyke, K.A., Liao, Z., Graham, D.R. (2014). Sustained upregulation of neurotoxic kynurenine pathway metabolites in cART-treated SIV-infected pigtailed macaques: impact on neuroinflammation and serotonin metabolism. Keystone Symposia on HIV Pathogenesis – Virus vs. Host, Banff, Alberta, Canada.

Cohen, R., **Drewes, J.L**, Freeman, Z., Pate, K.M., Hutchinson, E., Graham, D. (2013). Alterations of tryptophan metabolism in macaques with self injurious behavior (SIB). National Meeting for the American Association for Laboratory Animal Science, Baltimore, Maryland, USA.

Zink, M.C., **Drewes, J.L.**, Graham, D.R. (2013). SIV/Macaque model of CNS disease: Longitudinal analysis of the kynurenine pathway. Presentation given to the Viral Oncology seminar series, Department of Oncology, Johns Hopkins University School of Medicine, Baltimore, MD, USA.

Drewes, J.L., Graham, D.R., Zink, M.C. (2012). Longitudinal analysis of tryptophan metabolism in SIV-infected spleens. Presentation given to the laboratory of Dr. Robert Schwarcz, Maryland Psychiatric Research Center, University of Maryland, Catonsville, MD, USA.

Drewes, J.L., *et al*. (2010, 2012, 2013). NeuroAIDS seminar series, Department of Neurology, Johns Hopkins University School of Medicine, Baltimore, MD, USA.

Drewes, J.L., *et al.* (2011, 2012). Molecular and Comparative Pathobiology seminar series, Department of Molecular and Comparative Pathobiology, Johns Hopkins University School of Medicine, Baltimore, MD, USA.

POSTER PRESENTATIONS

Drewes, J.L., Aquino, V., Engle, E., Gama, L., Graham, D.R., and Zink, M.C. (2012). Longitudinal analysis of kynurenine pathway enzymes and metabolites in spleens of SIV-infected pigtailed macaques. Keystone Symposia on Viral Immunity and Host Gene Influence, Keystone, Colorado, USA.

Drewes, J.L., Fuchs, D., Graham, D.R., and Zink, M.C. (2010). Analysis of tryptophan and its metabolites in CSF of SIV-infected pigtail macaques by GCMS/MS. International Symposium on Neurovirology, Milan, Italy.

Drewes, J.L., Szeto, G., Graham, D.R., and Zink, M.C. (2009). Mechanisms of minocycline: effects on the innate and adaptive immune system during HIV/SIV infection and implications for HIV-associated neurological disease. International Symposium on Neurovirology, Miami, Florida, USA.

Meulendyke, K.A., **Drewes, J.L.**, Brice, A., Graham, D.R., and Zink, M.C. (2009). Minocycline's immunomodulatory effects are partly due to calcium chelation. International Symposium on Neurovirology, Miami, Florida, USA.

TEACHING AND MENTORSHIP

Pollard's Scholars Tutor (Spring 2009)
- Provided individual and group tutoring for graduate students in the Cellular and Molecular Medicine program during the Johns Hopkins School of Medicine Immunology course
- Led review sessions

Fundamental Virology Teaching Assistant, Johns Hopkins University School of Public Health (Fall 2009)
- Assisted in designing and grading exam questions
- Provided individual and group tutoring
- Led review sessions

Graduate student mentor (2009 – present)
- Mentor to graduate students and postdocs rotating or working in the Retrovirus Laboratory: Justin Glenn, Greg Laird, Ravi Tharakan, Josh Croteau, Kelly Meulendyke, Rachael Cohen
- Assisted in project design
- Trained students in basic molecular biology techniques and basic scientific practices
- Trained students and postdocs in the conceptual theory behind and practical use of gas chromatography mass spectrometry

AWARDS

Howard Hughes Medical Institute Undergraduate Research Program Major Grant (2006)
- Awarded by Stanford University's Undergraduate Advising and Research program to fund full-time summer research for undergraduate honors theses

Division I National Academic Squad (2003, 2004, 2005, 2006)
- Awarded by the National Field Hockey Coaches Association, based on merit

1st Team All-Norpac Conference Division I (2006)
- Awarded by the Northern Pacific Field Hockey Conference, based on athletic accomplishments

Ford Family Athletic Scholarship (2003-2007)
- Awarded by Stanford University, for Division I athletes